

AD

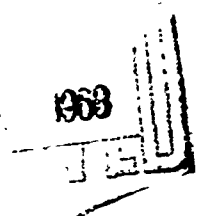
AD 670965

17 MAR 1968
COPY

USAAVLABS TECHNICAL REPORT 68-4
DYNAMIC RESPONSE OF THE XC-142A TILT-WING
V/STOL AIRCRAFT TO IN-FLIGHT CARGO DELIVERY
AT SLOW SPEEDS

By
J. W. Wilson
M. P. Schira
J. S. Beitering

March 1968



U. S. ARMY AVIATION MATERIEL LABORATORIES
FORT EUSTIS, VIRGINIA
CONTRACT DA 44-177-AMC-327(T)
VOUGHT AERONAUTICS DIVISION
LTV AEROSPACE CORPORATION
DALLAS, TEXAS

*This document has been approved
for public release and sale; its
distribution is unlimited.*



Produced by the
CLEARINGHOUSE
for the
Distribution of
Information
Copyright © 1968

AD 670 965

**DYNAMIC RESPONSE OF THE XC-142A TILT-WING V/STOL
AIRCRAFT TO IN-FLIGHT CARGO DELIVERY AT SLOW
SPEEDS**

Jerry W. Wilson, et al

**LTV Aerospace Corporation
Dallas, Texas**

March 1968



DEPARTMENT OF THE ARMY
U. S. ARMY AVIATION MATERIEL LABORATORIES
FORT EUSTIS, VIRGINIA 23604

This report was prepared by the LTV Aerospace Corporation, Vought Aeronautics Division, under the terms of Contract DA 44-177-AMC-327(T). It consists of a mathematical analysis of the dynamics of ground-proximity in-flight delivery of cargo and personnel from XC-142A V/STOL aircraft.

The object of this contractual effort was to explore the low-altitude airdrop capability of the XC-142A V/STOL aircraft in hover and the low-speed flight regime.

Results of the analytical investigation indicate that the stability and control characteristics of the XC-142A aircraft are such that in-flight delivery of cargo is possible with the following exception: flight below an altitude of 26 feet, from 35° to 80° wing incidence configuration (16-35 knots), is prohibited because of a previous flight envelope restriction.

The high-velocity downwash generated by the XC-142A aircraft prohibits aerial delivery of personnel during the hover mode near the ground.

This command concurs in the analytical techniques developed and the conclusions drawn.

Project 1F121401A254
Contract DA 44-177-AMC-327(T)
USAAVIABS Technical Report 68-4
March 1968

DYNAMIC RESPONSE OF THE XC-142A TILT-WING
V/STOL AIRCRAFT TO IN-FLIGHT CARGO DELIVERY
AT SLOW SPEEDS

FINAL REPORT

2-53310/6R-6098

by

J. W. Wilson
M. P. Schira
J. S. Deitering

Prepared by

Vought Aeronautics Division
LTV Aerospace Corporation
Dallas, Texas

for

U. S. ARMY AVIATION MATERIEL LABORATORIES
FORT EUSTIS, VIRGINIA

This document has been approved
for public release and sale;
its distribution is unlimited.

SUMMARY

A study of the dynamics of in-flight delivery of personnel, supplies, and equipment from the XC-142A airplane has been conducted and is presented in this report. The study was partially based on actual air-drop demonstrations and environmental testing at the Naval Air Facility, El Centro, California, and at the Air Force Flight Test Center, Edwards AFB, California. Single cargo loads of up to 3,000 pounds were gravity dropped in hover and at 30 knots, and loads of up to 4,000 pounds were extracted by parachute at 127 knots. Using these flight data to set up a realistic simulation, a mathematical model of the XC-142A airplane and a human pilot was used to examine the aircraft's response with cargo weights up to the airplane's maximum payload of 8,000 pounds in the low-speed portion of transition and 12,000 pounds at a 127-knot flight condition.

Although longitudinal control power available will not statically balance the maximum payload at the aft end of the airplane's cargo ramp at low speeds, this study shows that maximum payload could be successfully dropped with proper pilot technique. A portion of the transition flight envelope that has been restricted because of induced ground effects would, of course, prohibit air drops in this flight region. Environmental testing of personnel in the XC-142A slipstream while in hover flight indicates that there are adverse effects that would prohibit ground delivery of personnel at zero airspeed.

Means of extending the airplane's air-drop capability through the use of special extraction forces and parameters applicable to the air-drop system have been studied and are presented in this report.

FOREWORD

Vought Aeronautics Division (VAD) was authorized by contract DA 44-177-AMC-327(T) with the U. S. Army Aviation Materiel Laboratories, Fort Eustis, Virginia, to study the dynamics of in-flight delivery of personnel, supplies, and equipment from the XC-142A airplane.

The purpose of this program was to study the dynamics of in-flight delivery from the XC-142A V/STOL transport aircraft in the zero to conventional flight speed range, and to identify the relationship between aircraft characteristics and the air-drop sequence. If low-speed delivery of equipment, cargo and personnel was found to be incompatible with current Army air-drop methods, guidelines were to be formed by which air-drop techniques and/or aircraft stability, control and performance characteristics may be changed and/or modified so that the slow speed (hover to conventional flight speeds) air-drop mission may be accomplished.

CONTENTS

	<u>Page</u>
SUMMARY	iii
FOREWORD	v
LIST OF ILLUSTRATIONS	ix
LIST OF SYMBOLS	xv
METHOD OF ANALYSIS	1
SIMULATION TEST PROGRAM	16
RESULTS AND DISCUSSIONS	66
CONCLUSIONS	71
REFERENCES	72
APPENDIXES	
I. Environmental Characteristics of XC-142A Propeller Slipstream in Ground Effects for Hover and Low Transition Flight Speeds	73
II. Root Locus Analysis (O/30 Configuration)	78
III. Photographs of the XC-142A Airplane and Air- Drop Demonstration (No. 4 Aircraft, S.N. 62-5924)	92
DISTRIBUTION	105

LIST OF ILLUSTRATIONS

<u>Figure</u>		<u>Page</u>
1	Variation of Airplane Trim Velocity With Wing Incidence - Landing Flap Program	2
2	Variation of Tail Propeller Required to Trim Versus Velocity and CG Position	4
3	Maximum Cargo Weight That Can Be Carried on the Airplane Cargo Ramp Versus Airspeed	5
4	Airplane Longitudinal Dynamic Stability Characteristics	6
5	Summary of Cargo Loads Dropped in Flight Test	7
6	Airplane Flight Restrictions That Would Prohibit Aerial Delivery	8
7	Angles, Forces, and Velocity Components Referred to the Airplane Body Axis System	9
8	Functional Diagram for the Airplane-Pilot Combination	13
9	Comparison of Flight Test Data With Analog Simulation, $i_w/\delta_F = 82.5/0$, 3,000-Pound Gravity Drop	19
10	Peak Responses During Cargo Extraction Simulation, $i_w/\delta_F = 82.5/0$, Gravity Drops	20
11	Peak Responses After Cargo Extraction Simulation, $i_w/\delta_F = 82.5/0$, Gravity Drops	21
12	Analog Simulation Time Histories, $i_w/\delta_F = 82.5/0$, 8,000-Pound Gravity Drop, SAS On, Pilot in Loop	22
13	Analog Simulation Time History, $i_w/\delta_F = 82.5/0$, 8,000-Pound Gravity Drop, SAS On, Pilot out of Loop	23
14	Effect of Short Stroke Actuator on Peak Responses During Cargo Extraction, $i_w/\delta_F = 82.5/0$, Cargo Weight = 8,000 Pounds	24
15	Effect of Conveyor Belt Extraction on Peak Responses During Cargo Delivery, $i_w/\delta_F = 82.5/0$, Cargo Weight = 8,000 Pounds	25

LIST OF ILLUSTRATIONS (Continued)

<u>Figure</u>	<u>Page</u>
16	26
Peak Responses During Cargo Extraction Versus SAS Actuator Stops and Tail Prop Effectiveness, $i_w/\delta_F = 82.5/0$, 8,000-Pound Gravity Drops	
17	27
Peak Responses During Cargo Extraction Versus SAS Pitch Attitude Gain, $i_w/\delta_F = 82.5/0$, 4,000-Pound Gravity Drops	
18	28
Peak Responses During Cargo Extraction Versus SAS Pitch Rate Gain, $i_w/\delta_F = 82.5/0$, 4,000-Pound Gravity Drops	
19	30
Comparison of Flight Test Data with Analog Simulation, $i_w/\delta_F = 30/60$, 3,000-Pound Gravity Drop	
20	31
Peak Responses During Cargo Extraction Simulation, $i_w/\delta_F = 30/60$, Gravity Drops	
21	32
Peak Responses After Cargo Extraction Simulation, $i_w/\delta_F = 30/60$, Gravity Drops	
22	33
Analog Simulation Time Histories, $i_w/\delta_F = 30/60$, 8,000-Pound Gravity Drop, SAS On, Pilot in Loop	
23	35
Effect of Extraction Force on Peak Responses During Cargo Delivery, $i_w/\delta_F = 30/60$, Cargo Weight = 8,000 Pounds	
24	36
Effect of SAS Actuator Stops on Peak Responses During Cargo Extraction, $i_w/\delta_F = 30/60$, 8,000-Pound Gravity Drops	
25	37
Effect of Increase in Tail Prop Effectiveness on Peak Response During Cargo Extraction, $i_w/\delta_F = 30/60$, 8,000-Pound Gravity Drops	
26	38
Effect of SAS Pitch Attitude Gain on Peak Responses During Cargo Extraction, $i_w/\delta_F = 30/60$, Gravity Drops	
27	39
Effect of SAS Pitch Rate Gain on Peak Responses During Cargo Extraction, $i_w/\delta_F = 30/60$, Gravity Drops	

LIST OF ILLUSTRATIONS (Continued)

<u>Figure</u>		<u>Page</u>
28	Effect of SAS Pitch Acceleration Gain on Peak Responses During Cargo Extraction, $i_w/\delta_F = 30/60$, Gravity Drops	40
29	Effect of Feedback of Integral of Pitch Attitude on Peak Responses During Cargo Extraction, $i_w/\delta_F = 30/60$, Gravity Drops	41
30	Peak Responses During Cargo Extraction Simulation, $i_w/\delta_F = 10/60$, Gravity Drops	42
31	Analog Simulation Time Histories, $i_w/\delta_F = 10/60$, 3,000-Pound Gravity Drop, SAS On, Pilot in Loop	43
32	Peak Responses During Cargo Extraction, $i_w/\delta_F = 5/38$, Gravity Drops	44
33	Analog Simulation Time Histories, $i_w/\delta_F = 5/38$, 8,000-Pound Gravity Drop, SAS On, Pilot in Loop	45
34	Peak Responses During Cargo Extraction, $i_w/\delta_F = 5/48$, Parachute Extraction Force = .25 x Cargo Weight	46
35	Peak Responses During Cargo Extraction, $i_w/\delta_F = 5/48$, Parachute Extraction Force = .50 x Cargo Weight	47
36	Analog Simulation Time Histories, $i_w/\delta_F = 5/48$, 8,000-Pound Drop, SAS On, Pilot in Loop, Parachute Extraction Force = .5 x Cargo Weight	50
37	Effect of Parachute Extraction Force on Peak Responses During Cargo Extraction, $i_w/\delta_F = 0/30$, SAS Off, Pilot out of Loop	51
38	Effect of Parachute Extraction Force on Peak Responses After Cargo Extraction, $i_w/\delta_F = 0/30$, SAS Off, Pilot out of Loop	52
39	Peak Responses During Cargo Extraction, $i_w/\delta_F = 0/30$, Parachute Extraction Force = .25 x Cargo Weight	53
40	Peak Responses After Cargo Extraction, $i_w/\delta_F = 0/30$, Parachute Extraction Force = .25 x Cargo Weight	54

LIST OF ILLUSTRATIONS (Continued)

<u>Figure</u>	<u>Page</u>
41	Peak Responses During Cargo Extraction, $i_w/\delta_F = 0/30$, Parachute Extraction Force = .5 x Cargo Weight 55
42	Peak Responses After Cargo Extraction, $i_w/\delta_F = 0/30$, Parachute Extraction Force = .5 x Cargo Weight 56
43	Peak Responses During Cargo Extraction, $i_w/\delta_F = 0/30$, Parachute Extraction Force = .5 x Cargo Weight, $K_q = 2 \times \text{Nominal Value} = -22.78$ 57
44	Peak Responses After Cargo Extraction, $i_w/\delta_F = 0/30$, Parachute Extraction Force = .5 x Cargo Weight, $K_q = 2 \times \text{Nominal Value} = -22.78$ 58
45	Response Matching, Flight Test Data Versus Analog Simulation Data, $i_w/\delta_F = 0/30$, 4,000-Pound Drop, Parachute Extraction Force = .5 x Cargo Weight 59
46	Response Matching, Flight Test Data Versus Analog Simulation Data, $i_w/\delta_F = 0/30$, 4,000-Pound Drop, Parachute Extraction Force = .5 x Cargo Weight 60
47	Response Matching, Flight Test Data Versus Analog Simulation Data, $i_w/\delta_F = 0/30$, 4,000-Pound Drop, Parachute Extraction Force = .5 x Cargo Weight 61
48	Analog Simulation Time Histories, $i_w/\delta_F = 0/30$, 8,000-Pound Drop, SAS Off, Pilot out of Loop, Parachute Extraction Force = .5 x Cargo Weight 62
49	Analog Simulation Time Histories, $i_w/\delta_F = 0/30$, 8,000-Pound Drop, SAS On, Pilot in Loop, Parachute Extraction Force = .5 x Cargo Weight 63
50	Analog Simulation Time Histories, $i_w/\delta_F = 0/30$, 4,000-Pound Drop, SAS Off, Pilot out of Loop, Parachute Extraction Force = .5 x Cargo Weight 64
51	Analog Simulation Time Histories, $i_w/\delta_F = 0/30$, 4,000-Pound Drop, SAS On, Pilot in Loop, Parachute Extraction Force = .5 x Cargo Weight 65
52	Cargo Roll-Out Time After Release Versus Airplane Attitude During Drop - Flight Test Air Delivery Demonstration 67

LIST OF ILLUSTRATIONS (Continued)

<u>Figure</u>		<u>Page</u>
53	Peak Simulation Response Characteristics During an 8,000-Pound Cargo Drop	69
54	Peak Simulation Response Characteristics After an 8,000-Pound Cargo Drop	70
55	XC-142A Response Modes Versus Pilot Gain, $i_w/\delta_F=0/30, \tau_L=1.0, \tau_I=.5, \tau_D=.2$	80
56	XC-142A Response Modes Versus Pilot Gain, $i_w/\delta_F=0/30, \tau_L=1.5, \tau_I=.5, \tau_D=.2$	82
57	XC-142A Response Modes Versus Pilot Gain, $i_w/\delta_F=0/30, \tau_L=.5, \tau_I=.5, \tau_D=.2$	84
58	XC-142A Response Modes Versus Pilot Gain, $i_w/\delta_F=0/30, \tau_L=.5, \tau_I=1.0, \tau_D=.2$	86
59	XC-142A Response Modes Versus SAS Pitch Rate Gain, $i_w/\delta_F=0/30, \text{Pilot Out}$	88
60	XC-142A Pilot Stability Boundary, $i_w/\delta_F=0/30$	91
61	View of Aircraft in Cruise Flight, 0/30 Wing/Flap Configuration	92
62	Left-Hand Side View of Aircraft in Static Condition With the Wing at 90°	93
63	Front View of the Aircraft in Hover Flight With the Wing at Approximately 90°	94
64	Rearward Looking View of the Cargo Compartment Showing the Skate Wheel Conveyors and an A-22 Container	95
65	Forward Looking View of the Cargo Compartment Showing the Skate Wheel Conveyors and a Logistics Platform	96
66	500-Pound Gravity Drop - 0/30 Configuration, 5,000 Feet	97
67	500-Pound Gravity Drop - 15/60 Configuration, 5,000 Feet	98

LIST OF ILLUSTRATIONS (Continued)

<u>Figure</u>		<u>Page</u>
68	1,000-Pound Extraction Drop - 15/60 Configuration, 5,000 Feet	99
69	Five-Percentile Dummy Drop from Cargo Ramp - 0/30 Configuration, 5,000 Feet	100
70	Five-Percentile Dummy Drop from Forward Escape Hatch - 15/60 Configuration, 1,000 Feet	101
71	Ten-Man Free Fall Parachute Jump from Cargo Ramp - 15/60 Configuration, 12,500 Feet	102
72	2,000-Pound Dump Truck Drop - 30/60 Configuration	103
73	Sequential Drop of Four 500-Pound Cargos - 30/60 Configuration	104

LIST OF SYMBOLS

a_c	Cargo acceleration during inflight extraction, ft/sec^2
CG	Airplane center-of-gravity position, % mean geometric chord
F_{CHUTE}	Parachute extraction force, lb
F_n	$n = 1$ to 5 , representative transfer function coefficients
F_x	External force acting along the airplane body x-axis, positive forward
F_z	External force acting along the airplane body z-axis, positive down
g	Gravitational acceleration, $32.2 \text{ ft}/\text{sec}^2$
GW	Airplane gross weight minus cargo weight, lb
h	Altitude, ft
i_w	Wing incidence relative to fuselage water line (WL), deg
I_y	Airplane-plus-cargo pitching moment of inertia, $\text{slug}\cdot\text{ft}^2$
I_{ya}	Airplane-minus-cargo pitching moment of inertia, $\text{slug}\cdot\text{ft}^2$
j	Unit vector for imaginary portion of complex root of characteristic equation
K_L	Longitudinal stick-to-linkage gain, in./in.
K_{p_θ}	Pilot gain, in./rad
K_q	SAS pitch rate gain, in./rad/sec
$K_{\dot{q}}$	SAS pitch acceleration gain, in./rad/sec ²
K_s	Scissors linkage gain, in./in.
$K_{\delta \text{STK}}$	Longitudinal stick position pick-off gain, in./in.
K_θ	SAS pitch attitude gain, in./rad
m_a	Airplane-minus-cargo mass, slugs
m_{cn}	$n = 1, 2, 3$, cargo masses, slugs

M_y	External moment acting about the airplane body y-axis, ft-lb
M_q	$\left(\frac{1}{I_{ya}}\right) \left(\frac{\partial M_y}{\partial q}\right)$, sec ⁻¹
M_u	$\left(\frac{1}{I_{ya}}\right) \left(\frac{\partial M_y}{\partial u}\right)$, (ft-sec) ⁻¹
M_w	$\left(\frac{1}{I_{ya}}\right) \left(\frac{\partial M_y}{\partial w}\right) = \left(\frac{1}{I_{ya} u}\right) \left(\frac{\partial M_y}{\partial \alpha}\right)$, (ft-sec) ⁻¹
$M_{\dot{w}}$	$\left(\frac{1}{I_{ya}}\right) \left(\frac{\partial M_y}{\partial \dot{w}}\right) = \left(\frac{1}{I_{ya} u}\right) \left(\frac{\partial M_y}{\partial \dot{\alpha}}\right)$, ft ⁻¹
$M_{\delta^* \text{UHT}}$	$\left(\frac{1}{I_{ya}}\right) \left(\frac{\partial M_y}{\partial \delta^* \text{UHT}}\right)$, (in.-sec ²) ⁻¹
$M_{\delta^* \text{TP}}$	$\left(\frac{1}{I_{ya}}\right) \left(\frac{\partial M_y}{\partial \delta^* \text{TP}}\right)$, (in.-sec ²) ⁻¹
MEC	Wing mean geometric chord, 8.072 ft
n_z	Airplane normal load factor, g's
q	Airplane pitch rate
\dot{q}	Airplane pitch acceleration, rad/sec ²
SAS	Stability augmentation system
t	Time, sec
TP	Tail propeller
u	Perturbation axial velocity component, ft/sec
\dot{u}	Perturbation axial acceleration component, ft/sec ²
u_0	Trim axial velocity component, ft/sec
U	Trim axial velocity plus perturbation velocity ($u_0 + u$), ft/sec
UHT	Unit horizontal tail
V_c	Calibrated airspeed, knots
w	Perturbation vertical velocity component, ft/sec

\dot{w}	Perturbation vertical acceleration component, ft/sec ²
w_0	Trim vertical velocity component $\sim u_0 \alpha$, ft/sec
w	Trim normal velocity plus perturbation velocity ($w_0 + w$), ft/sec
x, y, z	Orthogonal axes
X_u	$\left(\frac{1}{m_a}\right)\left(\frac{\partial F_x}{\partial u}\right)$, sec ⁻¹
X_w	$\left(\frac{1}{m_a}\right)\left(\frac{\partial F_x}{\partial w}\right) = \left(\frac{1}{m_a u}\right)\left(\frac{\partial F_x}{\partial \alpha}\right)$, sec ⁻¹
$X_{\delta^*_{UHT}}$	$\left(\frac{1}{m_a}\right)\left(\frac{\partial F_x}{\partial \delta^*_{UHT}}\right)$, ft/(sec ² -in.)
$X_{\delta^*_{TP}}$	$\left(\frac{1}{m_a}\right)\left(\frac{\partial F_x}{\partial \delta^*_{TP}}\right)$, ft/(sec ² -in.)
Z_q	$\left(\frac{1}{m_a}\right)\left(\frac{\partial F_z}{\partial q}\right)$, ft/sec
Z_u	$\left(\frac{1}{m_a}\right)\left(\frac{\partial F_z}{\partial u}\right)$, sec ⁻¹
Z_w	$\left(\frac{1}{m_a}\right)\left(\frac{\partial F_z}{\partial w}\right) = \left(\frac{1}{m_a u}\right)\left(\frac{\partial F_z}{\partial \alpha}\right)$, sec ⁻¹
$Z_{\delta^*_{UHT}}$	$\left(\frac{1}{m_a}\right)\left(\frac{\partial F_z}{\partial \delta^*_{UHT}}\right)$, ft/(sec ² -in.)
$Z_{\delta^*_{TP}}$	$\left(\frac{1}{m_a}\right)\left(\frac{\partial F_z}{\partial \delta^*_{TP}}\right)$, ft/(sec ² -in.)
α	Fuselage angle of attack, rad
α^e	Effective wing angle of attack, rad
β_{TP}	Tail propeller blade angle, deg
δ_F	Flap deflection angle, deg
δ^*_{LIM}	SAS actuator stop, in.
δ_{STK}	Longitudinal stick position
δ_{UHT}	Horizontal tail deflection angle, positive TE down, deg
δ^*	Scissors linkage gain output, in.

ζ	Damping ratio
θ	Perturbation pitch attitude angle, deg
θ_0	Trim pitch attitude angle, deg
θ_e	Pilot's pitch attitude reference
μ	Friction coefficient
T_D	Pilot reaction time, sec
T_I	Pilot lag time constant
T_L	Pilot lead time constant
T_N	Pilot neuromuscular time constant
ω_D	Damped frequency, rad/sec
ω_n	Undamped natural frequency, rad/sec

METHOD OF ANALYSIS

BACKGROUND

The XC-142A is a four-engine, turboprop, high-wing transport airplane with interconnected propellers which uses the tilt-wing, deflected-slipstream concept to achieve V/STOL operation. This concept is the principle of obtaining extra lift by deflecting the propeller slipstream downward with highly deflected trailing edge flaps. The flight design gross weight of the aircraft is 37,474 pounds, and its airspeed capabilities range from hovering flight to a speed in excess of 350 knots. Conventional flight is controlled by conventional ailerons, a rudder, and a unit horizontal tail. Wing tilt for V/STOL operation is continuously variable from 0° to 98° wing incidence (i_w) with automatic integration of the conventional and V/STOL flight controls during transition. The V/STOL controls consist of differential main propeller blade angle for roll control, a tail propeller for pitch control, and ailerons for yaw control. The transition flight region is defined as the speed range between hover flight ($i_w = 90^\circ$) and conventional flight ($i_w = 0^\circ$).

Wing trailing edge full-span, double-slotted flaps provide increased airplane lift during landing and takeoff and are normally programmed with wing incidence change for these conditions. In the wing-flap program for takeoff, the flaps are automatically limited to a maximum of 30° of travel (δ_f), whereas the landing program permits a full 60° of travel with change in wing incidence; however, it is possible for the pilot to override the programs and manually control the flaps at any time. Trim airspeed versus airplane wing incidence for the landing flap program is shown in Figure 1.

A dualized stability augmentation system (SAS) is employed in the XC-142A, which provides improved control and flying qualities for the hover and transition flight regimes.

Vertical gyroscopes in the system provide inputs for pitch and roll attitude stabilization, and rate gyro packages provide rate damping signals for pitch, roll, yaw, and altitude rate stabilization. The outputs of the stick and rudder pedal transducers sum with the gyro signals to provide the pilot with increased control sensitivity and attitude and rate command.

The system uses two identical electrical channels in each of the pitch, roll, and yaw control axes with failure monitoring between the channels of each axis. If a malfunction occurs in one channel, the monitor shuts off both channels. The pilot can override the monitor and engage the good channel, resulting in half-gain stability augmentation.

Since stability augmentation is needed only in hover and during the transition between hover and conventional forward flight, the SAS pitch actuators are locked in the cruise mode, and all roll and yaw gains except trim are set to zero.

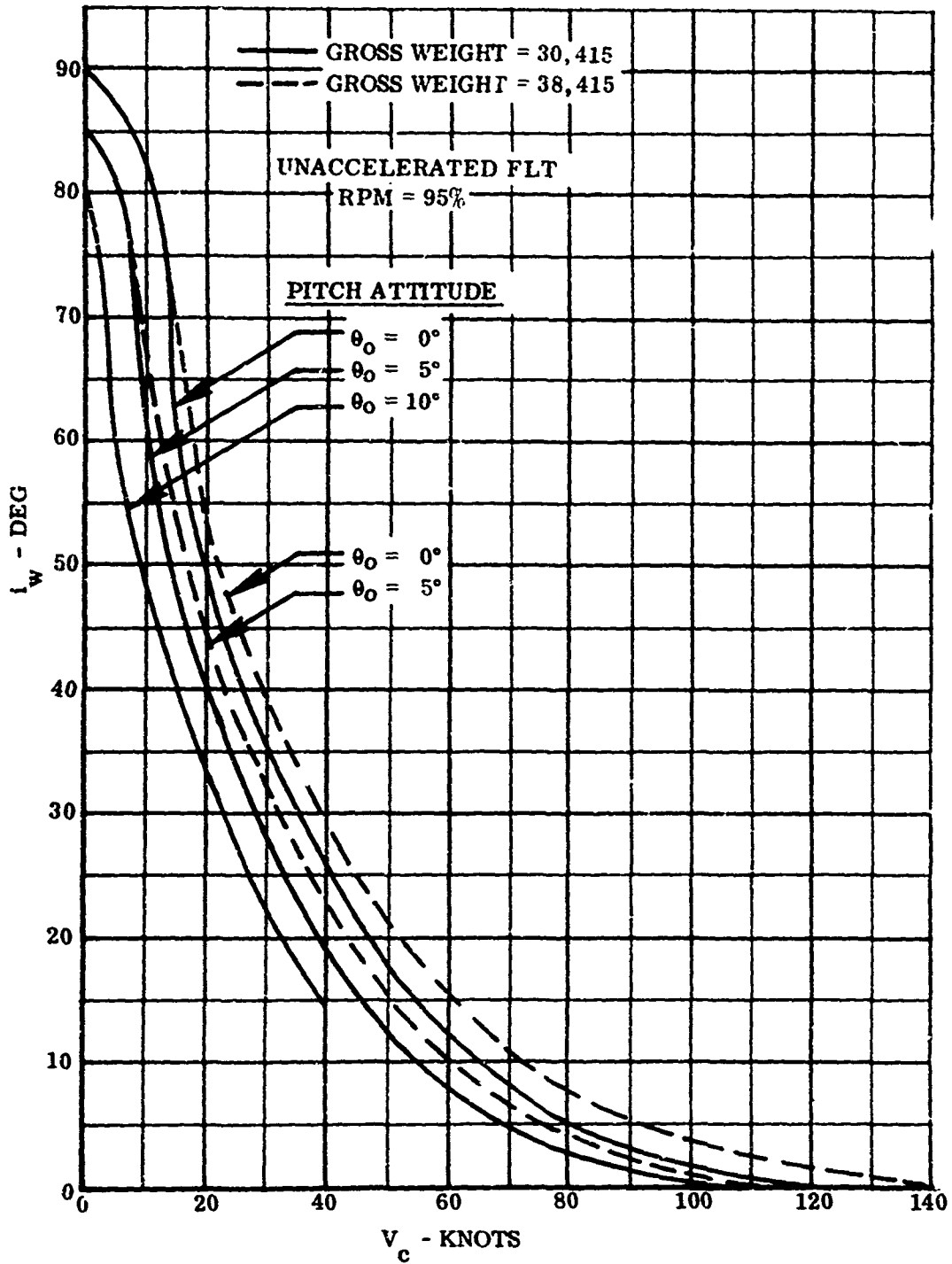


Figure 1. Variation of Airplane Trim Velocity With Wing Incidence - Landing Flap Program

The normal operating center-of-gravity (CG) limit of the XC-142A airplane is 15% to 28% wing mean geometric chord (MGC). Figure 2 presents the tail propeller blade angle required to trim the airplane versus transition velocities for these CG positions plus aft CG positions that could occur with cargo lodged on the rear of the cargo ramp. Figure 3 presents the maximum cargo weight that can be balanced on the airplane's cargo ramp or tail gate with the available longitudinal control power. Figure 4 presents the airplane's longitudinal dynamic stability characteristics (SAS on) for aft CG positions. These data indicate that, while it is feasible to fly and control the airplane (SAS on) with a large cargo weight on the ramp, it would be an emergency condition resulting from cargo's being lodged during extraction.

Figure 5 presents an envelope of the cargo weights that have been dropped during flight tests and the manner in which the cargo was extracted. Photographs of selected cargo drops are given in Appendix III.

Figure 6 presents the airplane's flight restrictions due to induced lateral-directional disturbances in the proximity of the ground. This disturbance is thought to be caused by the propeller slipstream deflecting off the ground and recirculating ahead of the aircraft. This restriction prohibits air drops from 35° to 30° wing incidence configurations below an altitude of 26 feet.

STATEMENT OF PROBLEM

The potential ability of V/STOL aircraft to perform Army drop missions at various altitudes while flying at speeds from hover to conventional flight could provide a basis for precision in-flight delivery and could overcome major operational restrictions associated with many of the conventional air-drop techniques.

Low-speed drop capability of a V/STOL transport aircraft could make possible precision air drop of loads at gross weights substantially greater than those associated with VTOL landing capability at the target.

The purpose of this program is to study the dynamics of in-flight delivery from the XC-142A V/STOL transport aircraft in the zero to conventional flight speed range and to identify the relationships between aircraft characteristics and the air-drop sequence. If low-speed delivery of equipment, cargo and personnel was found to be incompatible with current Army air-drop methods, guidelines were to be formed by which air-drop techniques and/or aircraft stability, control and performance characteristics may be changed and/or modified so that the slow-speed (hover to conventional flight speeds) air-drop mission may be accomplished.

APPROACH TO PROBLEM

The 3-degree-of-freedom airframe equations for the XC-142A air-drop system were developed using a body axis system (Figure 7) with the origin at the airplane CG and the x-axis forward in the waterline plane of the CG.

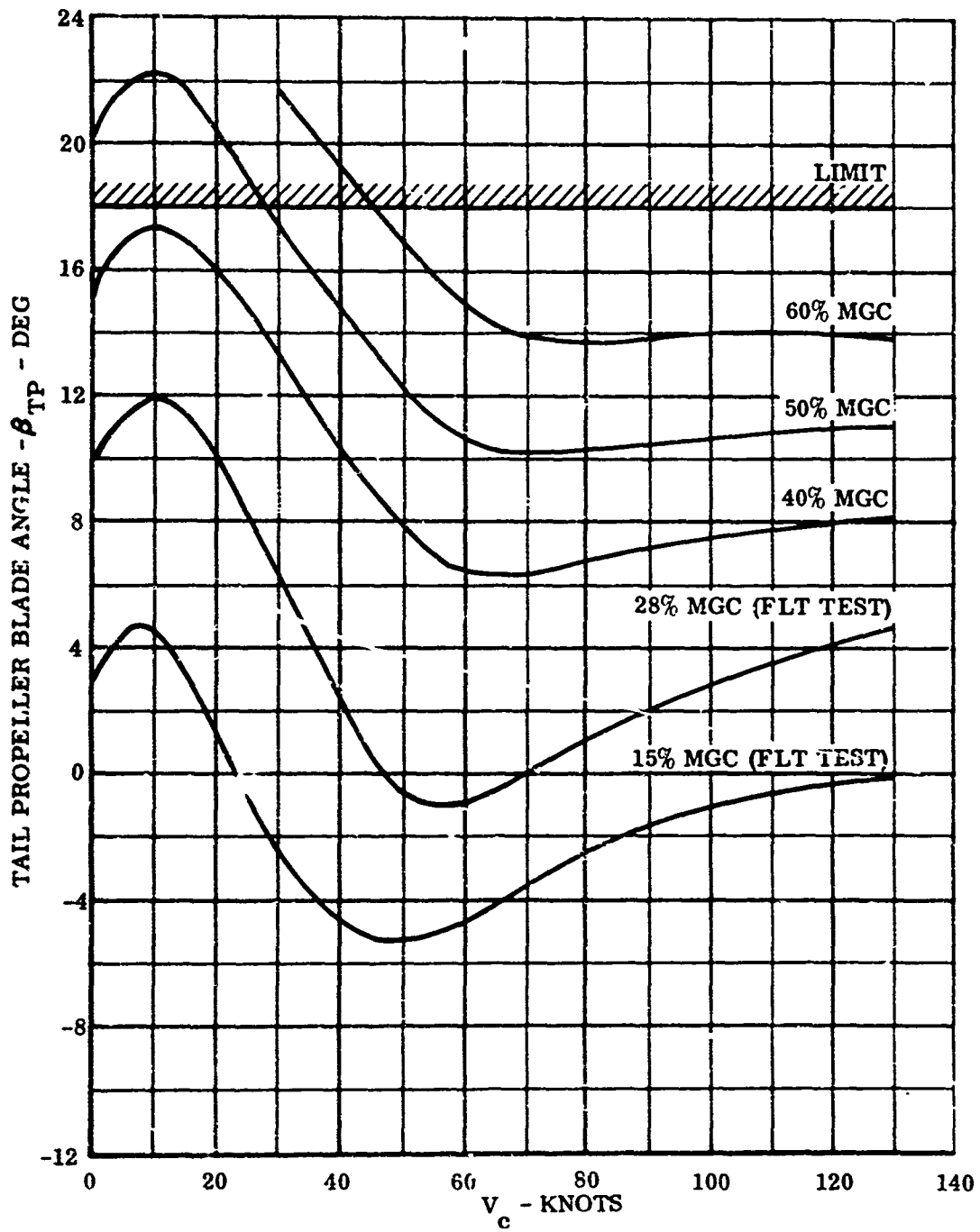


Figure 2. Variation of Tail Propeller Required to Trim Versus Velocity and CG Position

CARGO WEIGHT BASED ON MAXIMUM AVAILABLE β_{TP}
 AIRPLANE GROSS WEIGHT LESS CARGO = 30,415 POUNDS, $\theta_0 = 0^\circ$

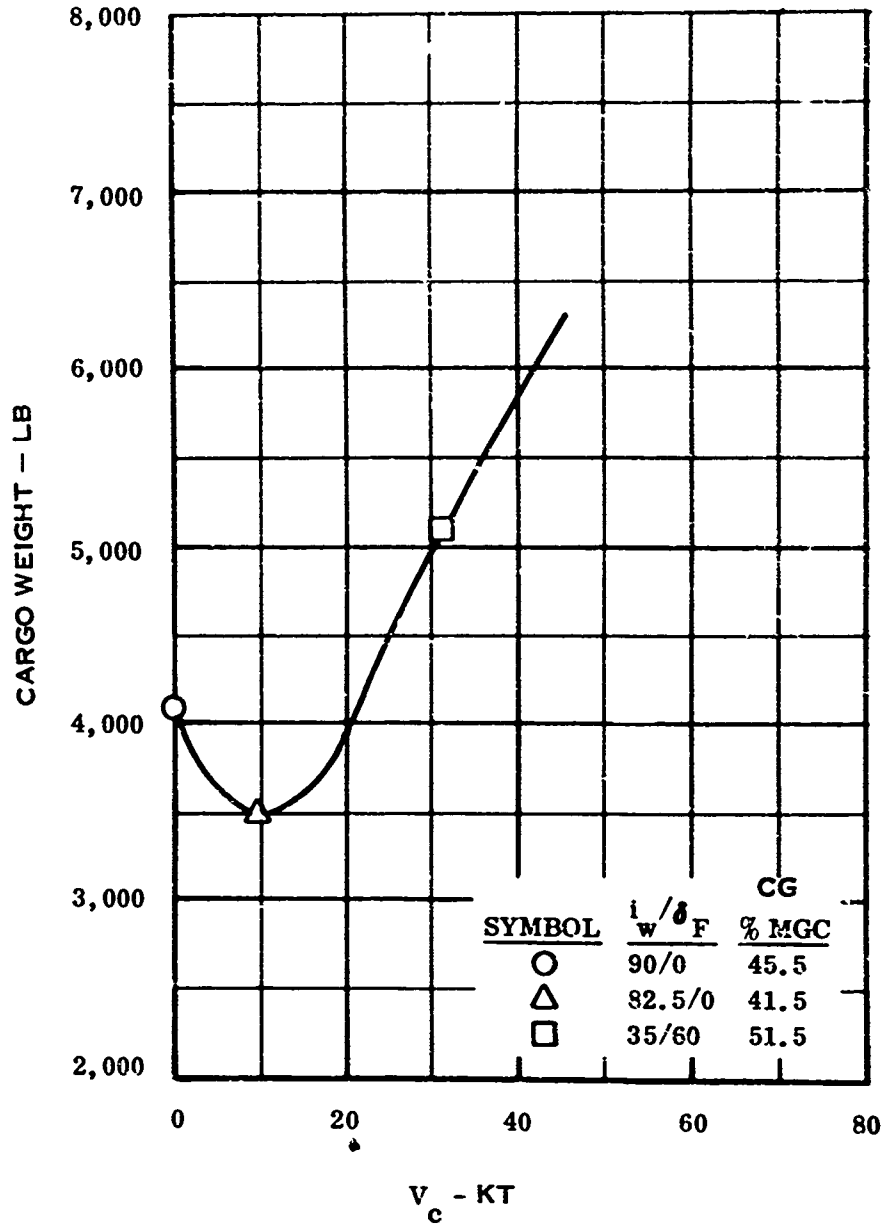


Figure 3. Maximum Cargo Weight That Can Be Carried on the Airplane Cargo Ramp Versus Airspeed

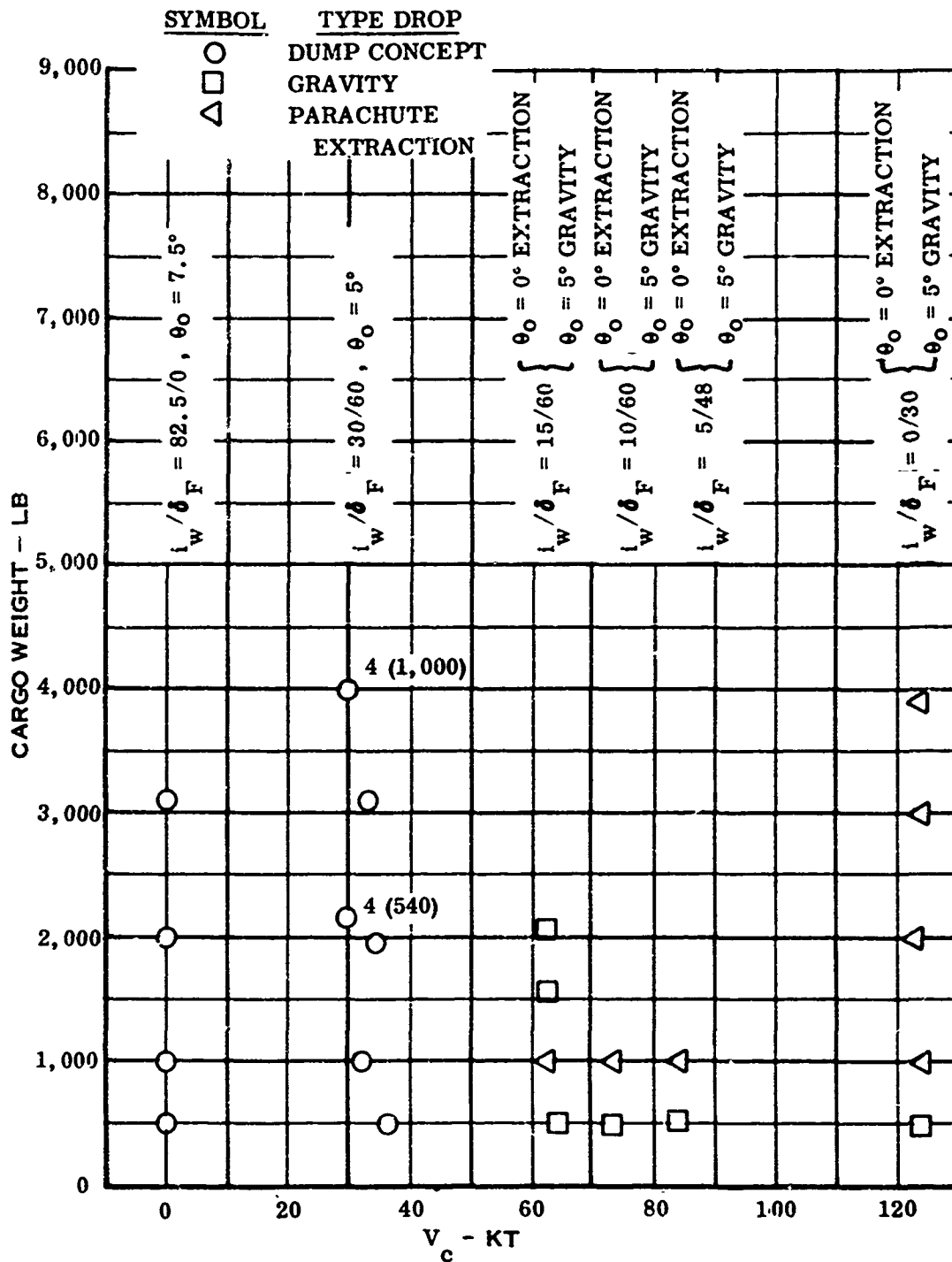


Figure 5. Summary of Cargo Loads Dropped in Flight Test

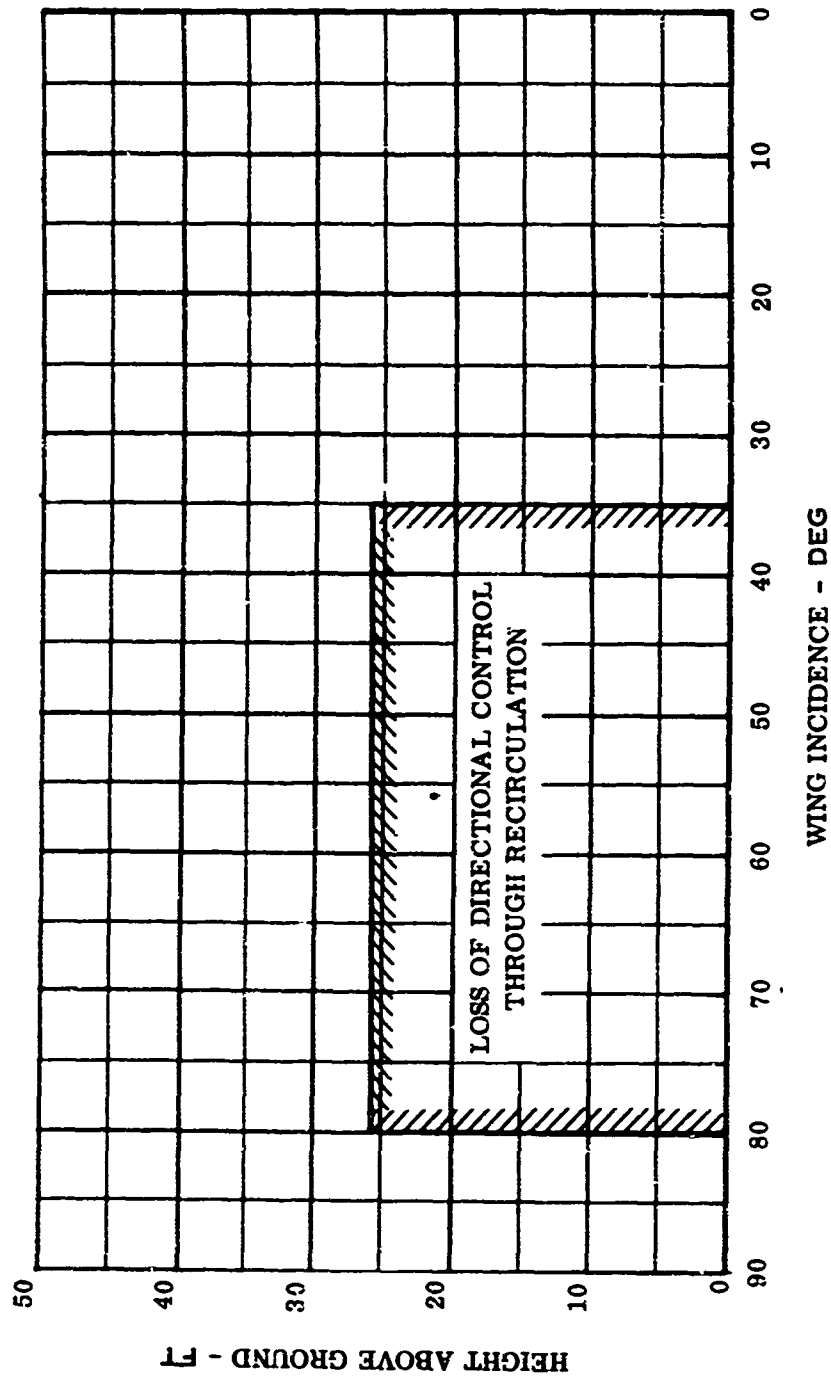
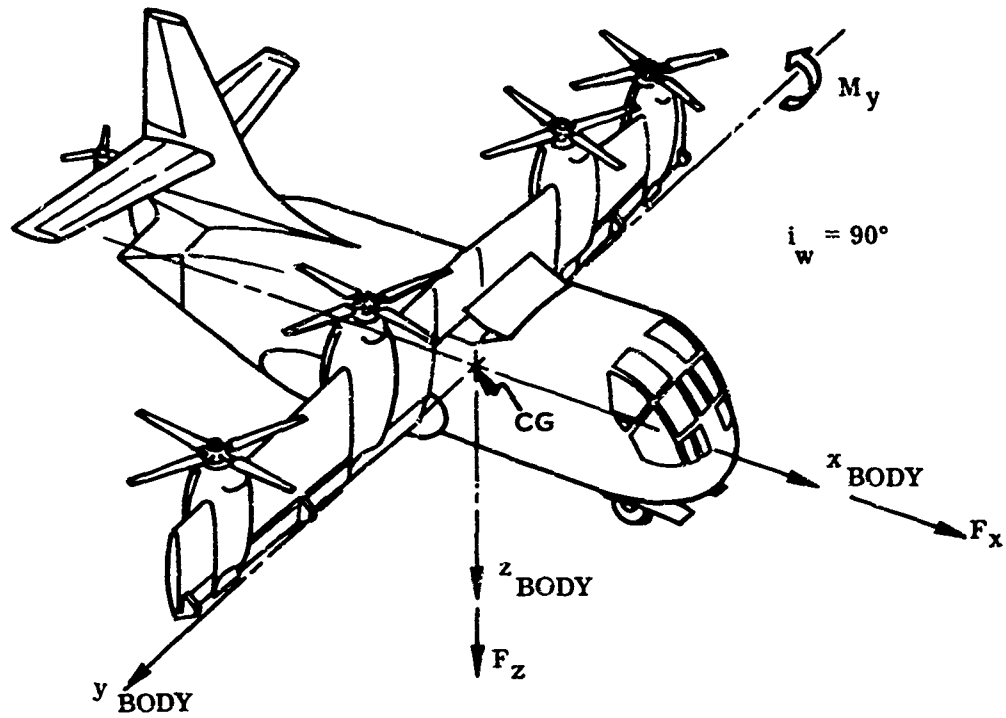
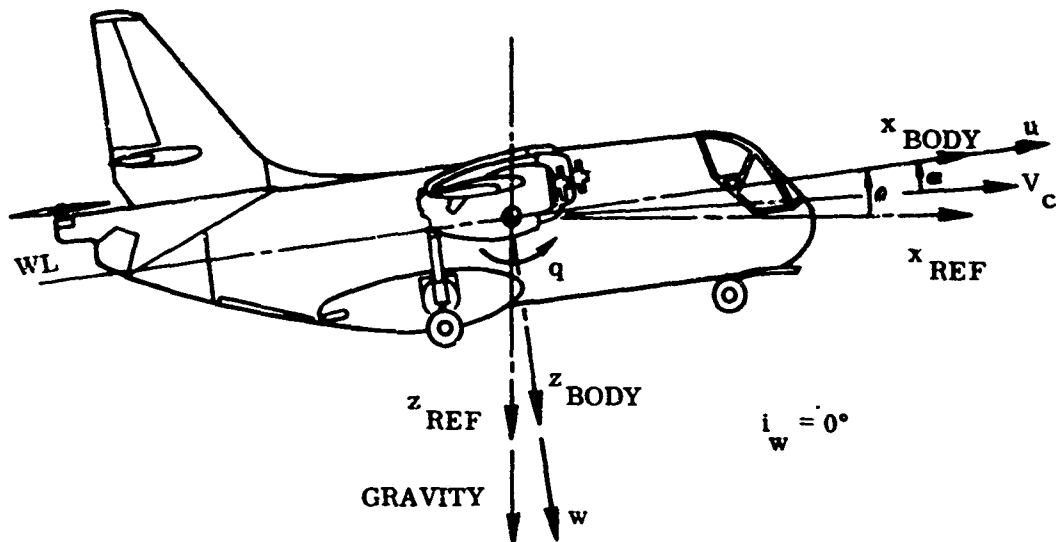


Figure 6. Airplane Flight Restrictions That Would Prohibit Aerial Delivery



BODY AXES, LONGITUDINAL EXTERNAL FORCES AND MOMENT ORIENTATION



COMPONENT VELOCITY ORIENTATIONS

Figure 7. Angles, Forces, and Velocity Components Referred to the Airplane Body Axis System

Using the Euler equations of motion for the airframe,

$$\Sigma F_x = m[\dot{u} + Wq + g\theta]$$

$$\Sigma F_z = m[\dot{w} - Uq]$$

$$\Sigma M_y = I_y[\dot{q}]$$

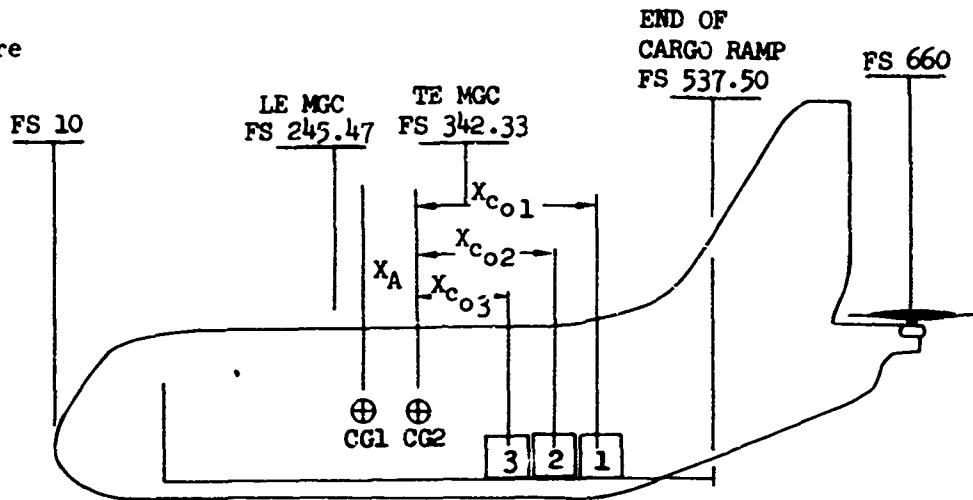
Adding airplane aerodynamic derivatives and effects of cargo masses,

$$\dot{u} + (w_0 + w)q + g\theta = \frac{m_a}{m_{c1} + m_{c2} + m_{c3} + m_a} [X_u u + X_w w + X_{\delta^*_{UHT}} \delta^*_{UHT}]$$

$$\dot{w} - (u_0 + u)q = \frac{m_a}{m_{c1} + m_{c2} + m_{c3} + m_a} [Z_u u + Z_w w + Z_q q + (Z_{\delta^*_{TP}} + Z_{\delta^*_{UHT}}) \delta^*_{UHT}]$$

$$\dot{q} = \frac{I_{ya}}{m_{c1}(X_{c1} + X_A)^2 + m_{c2}(X_{c2} + X_A)^2 + m_{c3}(X_{c3} + X_A)^2 + I_{ya}} \left[M_u u + M_w w + M_q q + (M_{\delta^*_{r}} + M_{\delta^*_{UHT}}) \delta^* - \frac{g}{I_{ya}} (m_{c1} X_{c1} + m_{c2} X_{c2} + m_{c3} X_{c3} + m_a X_A) \right]$$

Where



X_A = Airplane CG change due to installation of all cargo

$X_{c_{o1}}$ = Distance from cargo 1 to CG 2

$X_{c_{o2}}$ = Distance from cargo 2 to CG 2

$X_{c_{o3}}$ = Distance from cargo 3 to CG 2

$$X_{c1} = X_{c_{o1}} - X_1 \quad X_1, X_2, X_3 = \int_0^t \int_0^t a_c dt dt$$

$$X_{c2} = X_{c_{o2}} - X_2 \quad a_{c1, 2, 3} = \frac{F_{CHUTE}}{m_{c1,2,3}} + g[(\theta_0 + \theta) - \mu]$$

$$X_{c3} = X_{c_{o3}} - X_3$$

Other auxiliary equations are as follows:

$$\alpha'' = \alpha''_{TRIM} + \frac{w}{u_0 + u}$$

$$\Delta h = \int_0^t [(u_0 + u) \sin \theta - w \cos \theta] dt$$

$$\Delta n_{ZCG} = - \left[\frac{\dot{w} - (u_0 + u)q}{32.2} \right]$$

$$\Delta n_{ZPILOT SEAT} = \Delta n_{ZCG} + .508 \dot{q}$$

The aerodynamic data used in this study were obtained from Reference 2. The airplane's gross weight and inertia value were calculated for the No. 4 XC-142A airplane used in air-drop flight testing at El Centro, California (Reference 3).

As noted, the control derivatives in the airframe perturbation equations are a function of δ^* or longitudinal control linkage travel on the SAS actuator scissors output level. Values of UHT and β_{TP} were generated from the relationship between δ^* and the control actuator outputs. In order to use perturbation equations to simulate this problem, all values of δ^* and longitudinal stick position, δ_{STK} , are perturbations from zero. For the simulation of flight conditions with large trim values of UHT and β_{TP} as in the nose-high gravity drops, stops were set on δ^* corresponding to the limited travel between β_{TP} trim and their maximum available travel.

The equations for the stabilization and control system may be obtained from the block diagram, Figure 8. The XC-142A longitudinal stabilization system consists of two channels of pitch attitude and pitch rate stabilization in the hover and transition flight regimes. In the event of an electrical power failure in the airplane, only the channel with the power failure will become inoperative; for this analog study, only the two channels ON or OFF have been evaluated.

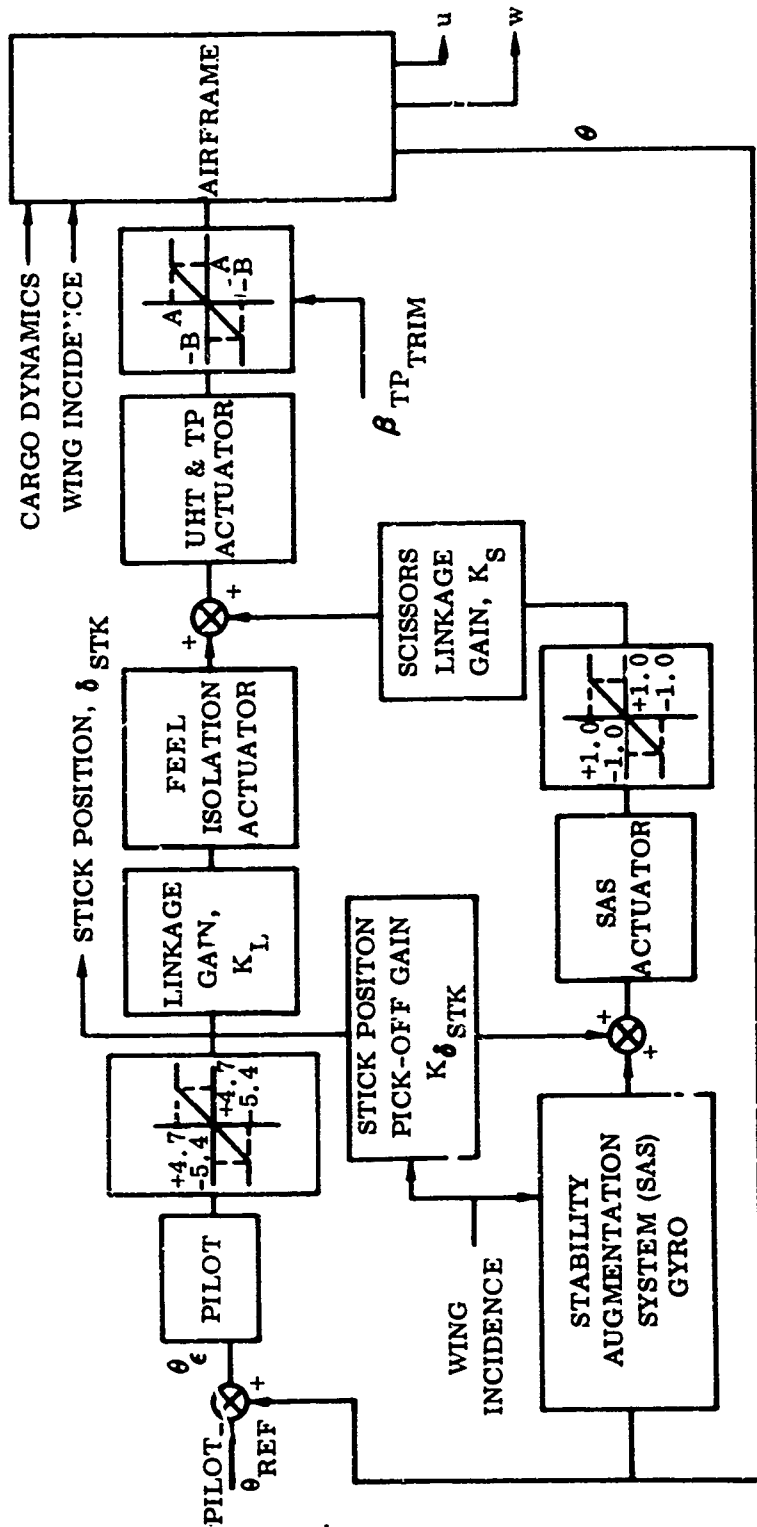
The block diagram describes the mathematical model of the XC-142A longitudinal control system, including the pilot. Since the pilot's response to an air drop is very important to the dynamic response of the total system, this analysis has included a root locus study of pilot gains (Appendix II). A general discussion of the pilot transfer function follows.

The pilot transfer function used in this work was obtained from Reference 1. As given in the above reference, the pilot is a linear mechanism, consisting of a gain, a transport lag, two poles, and one zero.

$$\frac{\delta_{STK}}{\theta_e} = \frac{Kp_e e^{-\tau D^S} (\tau_L S + 1)}{(\tau_N S + 1)(\tau_I S + 1)}$$

In the above, longitudinal stick position, δ_{STK} , is the pilot's output and θ_e is his input, where θ_e is defined in Figure 8.

The parameters in the above equation are understood to be variable from pilot to pilot and may even vary between maneuvers. Given particular pilot along with a particular test condition, the neuromuscular time constant, τ_N , and the pilot's reaction time, τ_D , will be relatively constant. The typical pilot has a $\tau_N = 0.1$ second and a $\tau_D = 0.2$ second as determined from tests discussed in Reference 1. The pilot's gain, Kp_e , and his lead time constant, τ_L , are capable of being varied by the pilot from one maneuver to another in an effort to create a desirable system



NOTES

1. THE OUTPUT OF THE STAB ACTUATOR IS ALSO RATE LIMITED AT ± 4.0 IN/SEC.
2. STAB SYSTEM GYRO DYNAMICS HAVE BEEN NEGLECTED.
3. THE STOPS ON THE UHT ACTUATOR ARE SET SO AS TO REPRESENT THE STOPS ON TAIL PROP POSITION. THEREFORE, A AND B ARE A FUNCTION OF TAIL TRIM POSITION.
4. SEE PAGE 14 FOR THE CONTENTS OF EACH BOX IN THE ABOVE DIAGRAM.

Figure 8. Functional Diagram for the Airplane-Pilot Combination

COMPONENT	TRANSFER FUNCTION
PILOT	$\frac{K_{P\theta} e^{-\tau_D S} (\tau_L S + 1)}{(\tau_I S + 1)}$
STICK POSITION PICK-OFF GAIN	$K_{\theta \text{ STK}}$
SAS GYROS	$K_q S + K_\theta$
LINKAGE GAIN	$K_L = .324$
FEEL ISOLATION ACTUATOR	$\frac{15}{(S+15)}$
SAS ACTUATOR	$\frac{21.5}{(S + 21.5)}$
SCISSORS LINKAGE GAIN	$K_S = .470$
UHT AND TP ACTUATOR	$\frac{20}{(S+20)}$
PILOT TRANSPORT LAG, $e^{-\tau_D S}$	$e^{-\tau_D S} \approx \frac{1}{(1 + .6 \tau_D S)(1 + .4 \tau_D S + .16 \tau_D^2 S^2)}$

Figure 8. Functional Diagram for the Airplane-Pilot Combination (Concluded)

response. In this work, T_N is neglected, $T_D = 0.2$ second, and the other parameters are varied to make the theoretical pilot response match the flight test pilot response.

For a more detailed discussion of the pilot transfer function and some remarks on its derivation, consult Reference 1.

One objection to this representation of the pilot arises from the assumption that he holds his five time constants and gains constant during a given maneuver. Flight test records obtained in this study suggest that the pilot tends to lower his gain after the cargo leaves the airplane. This is illustrated in the section which includes drops from the 0/30 configuration.

The functional diagram for the system (Figure 8) shows that there is an additional unknown involved in pilot synthesis: the pilot θ reference, or in words, the pitch attitude that appears desirable to the pilot. Schematically, the pilot looks at the airplane pitch attitude, subtracts θ reference to get θ_e , and then tries to drive θ_e to zero by moving the stick. But θ reference is an unknown figment of the pilot's mind which, therefore, inserts a degree of uncertainty into the problem. Throughout this analysis, pilot θ reference has been held constant versus time at a value of zero degrees.

SIMULATION TEST PROGRAM

The analog simulation test program was first conducted to select pilot gains that result in a match of the airplane's response from the heaviest cargo weights dropped in flight test. Using these pilot gains, an airplane response simulation from cargo drops up to the maximum payload of 8,000 pounds for the lower speeds and 12,000 pounds for the highest speed condition was conducted.

The airplane flight conditions used in this study were the same as those in the air-drop flight demonstration. They are as follows:

Wing Incidence/ Flap Deflection ($i_w/\delta_F \sim \text{deg/deg}$)	Pitch Attitude ($\theta_0 \sim \text{deg}$)	Velocity ($\bar{v}_c \sim \text{kts}$)
82.5/0	7.5	0
30/60	5.0	30
10/60	5.0	54.68
5/38	5.0	77.93
5/48	0	79.75
0/30 TP ON	0	127.62
0/30 TP OFF	0	127.62

The air-drop parameters and methods of extraction considered in this study are as follows:

HUMAN PILOT EQUATION

Pilot Gain Delay and Lead-Lag Time Constant

The values of the parameters used were selected from analog duplication of the airplane's response from the cargo weights dropped in flight tests and from the tests discussed in Reference 1.

LONGITUDINAL SAS AND CONTROL POWER

SAS Actuator Authority

The longitudinal SAS has 1.0 inch of control linkage authority upstream of a .47 linkage gain compared to 1.6 inches from the pilot. Changes in the amount of SAS linkage travel are considered.

SAS Rate and Attitude Gains

The longitudinal SAS includes rate and attitude stabilization. The stabilization gains are optimized for general airplane flying qualities. This study considers the effect of their variation.

Addition of SAS Gains K_q^* and $\int \theta$

Additional SAS gains K_q^* (pitch acceleration) and $\int \theta$ (integral of pitch attitude) were added individually to determine their effect.

Longitudinal Control Effectiveness

The longitudinal control power effectiveness M_δ^* is provided by the tail propeller in hover and transition up to speeds where the UHT becomes effective. Percentage increases in tail propeller effectiveness were simulated to represent changes in tail propeller size or degrees of blade change per inch of linkage travel.

SAS Rate Limit

The longitudinal SAS has a rate capability of 1.7 inches of control linkage travel per second. The effect of changes in this limit was studied.

CARGO WEIGHT

Cargo Weights

Individual cargo weights up to 8,000 pounds in the lower speed region and 12,000 pounds in the 0/30 configuration or higher speed region of transition were considered. Sequential drops of three 2,666-pound packages were simulated.

Initial Loading

The effect of roll-out distance and initial CG position as determined by the location of the stowed cargo before it starts out of the airplane was simulated.

Initial Pitch Attitude and Coefficient of Friction

The initial pitch attitude (θ_0) of the airplane at the start of a gravity drop and the coefficient of friction between the cargo and cargo delivery rails were considered.

METHODS OF EXTRACTION

Gravity

The gravity extraction method consists of flying the airplane in a positive pitch attitude such that the cargo will slide out when released. This method has been demonstrated throughout transition speeds. Near the ground, the cargo was allowed to fall free; but at higher altitudes, a cargo parachute was used. The low-level method was simulated in this study.

Parachute Extraction

The parachute extraction method consists of allowing the force of a towed parachute to pull the cargo from the airplane. This method has been demonstrated by the XC-142A at airspeeds as low as 63 knots. This method was simulated in this study.

Short Stroke Actuator

A feasible air-drop technique is to give the cargo an initial boost with a short stroke actuator rather than to depend entirely on gravity for its extraction. This study considered the effects of variations in this type force acting through the first 5 feet of cargo travel.

Ground Extraction Forces

This study considered cargo extractions with a force applied to the cargo throughout its extraction from the airplane. The force is representative of a ground extraction system used to pull the cargo from the airplane at forward transition speeds.

Conveyor Belt

This study considered the simulation of an endless conveyor belt within the cargo compartment to extract the cargo at zero pitch attitude rather than to rely on gravity.

The following sections present summary data from the simulation programs.

$L_w/\delta F = 82.5/0$ CONFIGURATION, $\theta_0 = 7.5^\circ$, GRAVITY DROPS

Figure 9 presents a comparison of a simulated 3,000-pound gravity drop with test data from the aerial delivery flight test program at El Centro, California. Figures 10 and 11 present the airplane's peak responses during and after extraction of the cargo versus cargo weight. Figures 12 and 13 present analog records of an 8,000-pound cargo drop with and without pilot inputs. With the pilot, the airplane pitched up 20° and had only moderate damping; without the pilot, the airplane pitched up to a much higher attitude but had a lower frequency and better damping after the drop. The pitch attitude can be reduced to less than 20° with a higher gain pilot, but the pilot must reduce his gain after the drop in order to improve the system response. A detailed analysis of pilot gains is included in Appendix II.

The following data in this section are concerned with the improvement of the hover aerial delivery capability. These data are shown in Figures 14 through 18.

Figure 14 shows the effect of variations in extraction force acting through 5 feet on the maximum pitch response during an 8,000-pound delivery.

AIRPLANE GROSS WEIGHT = 31,300 POUNDS. $\theta_0 = 7.5^\circ$

— FLIGHT TEST - - - SIMULATION

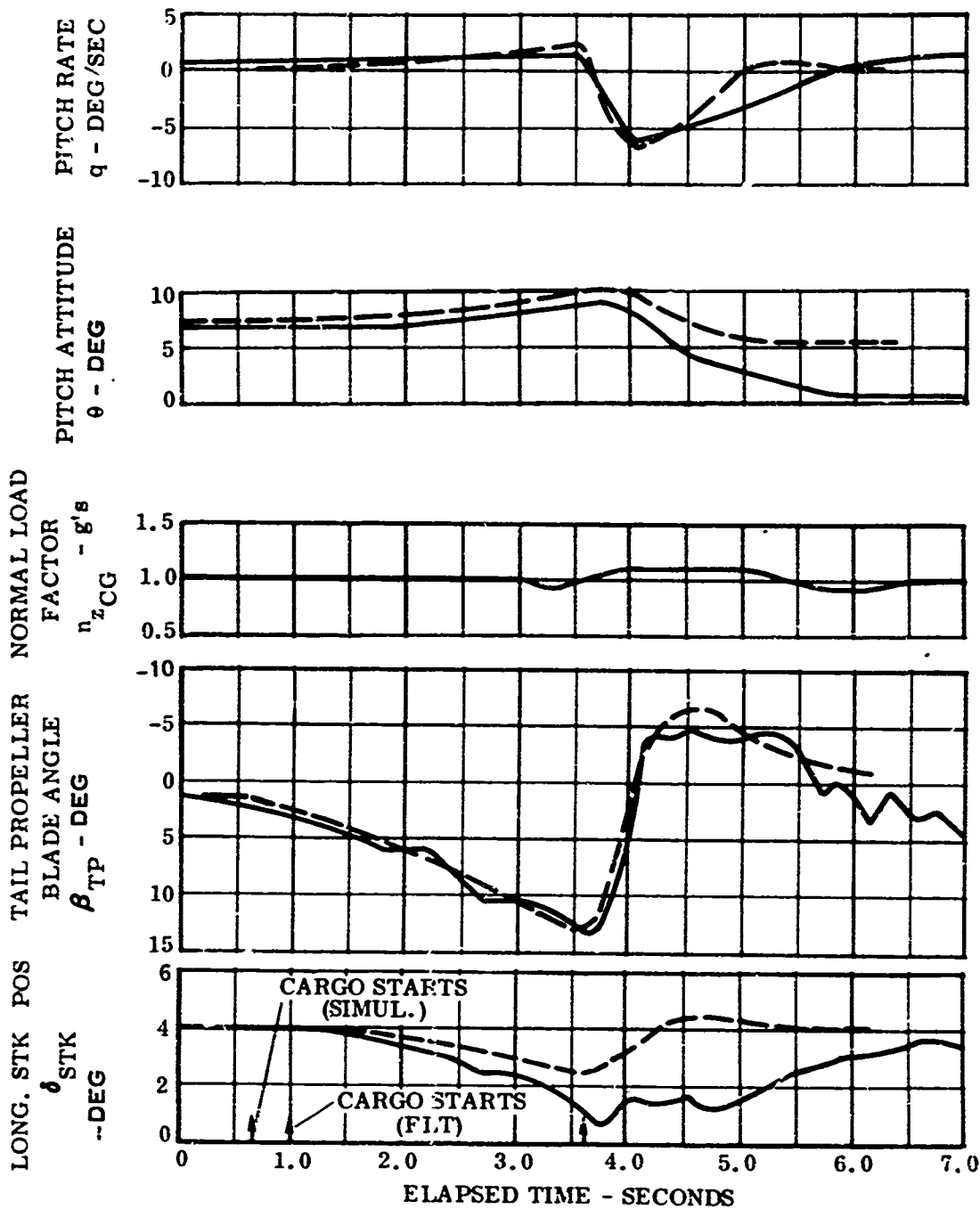


Figure 9. Comparison of Flight Test Data With Analog Simulation, $i_v/\delta_F = 82.5/0$, 3,000-Pound Gravity Drop

AIRPLANE GROSS WEIGHT = 31,300 POUNDS
 NOMINAL SAS, CG = 21.6% MGC

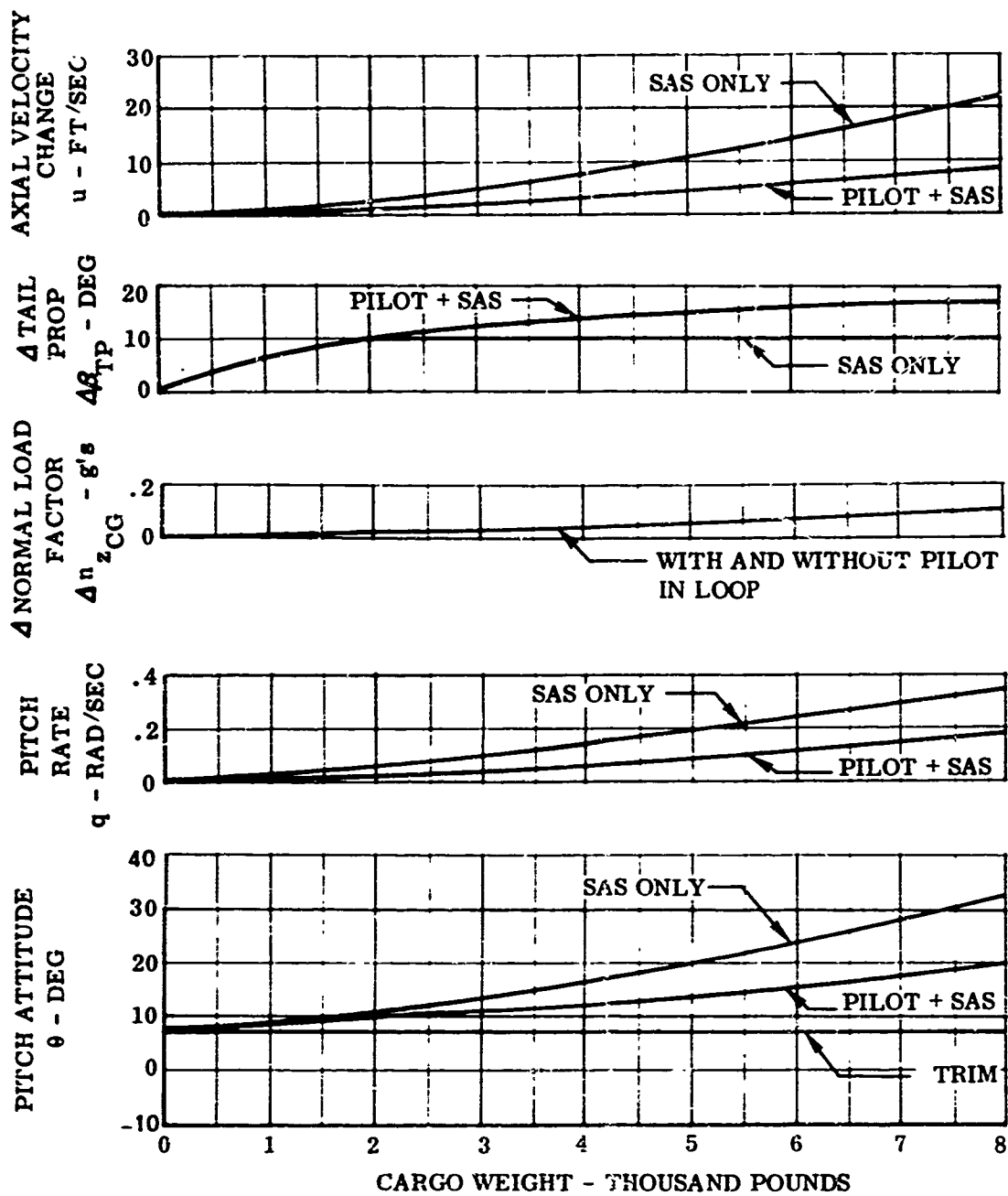


Figure 10. Peak Responses During Cargo Extraction Simulation, $i_w/\delta_F = 82.5/0$, Gravity Drops

AIRPLANE GROSS WEIGHT = 31,300 POUNDS
 NOMINAL SAS
 CG = 21.6 % MGC

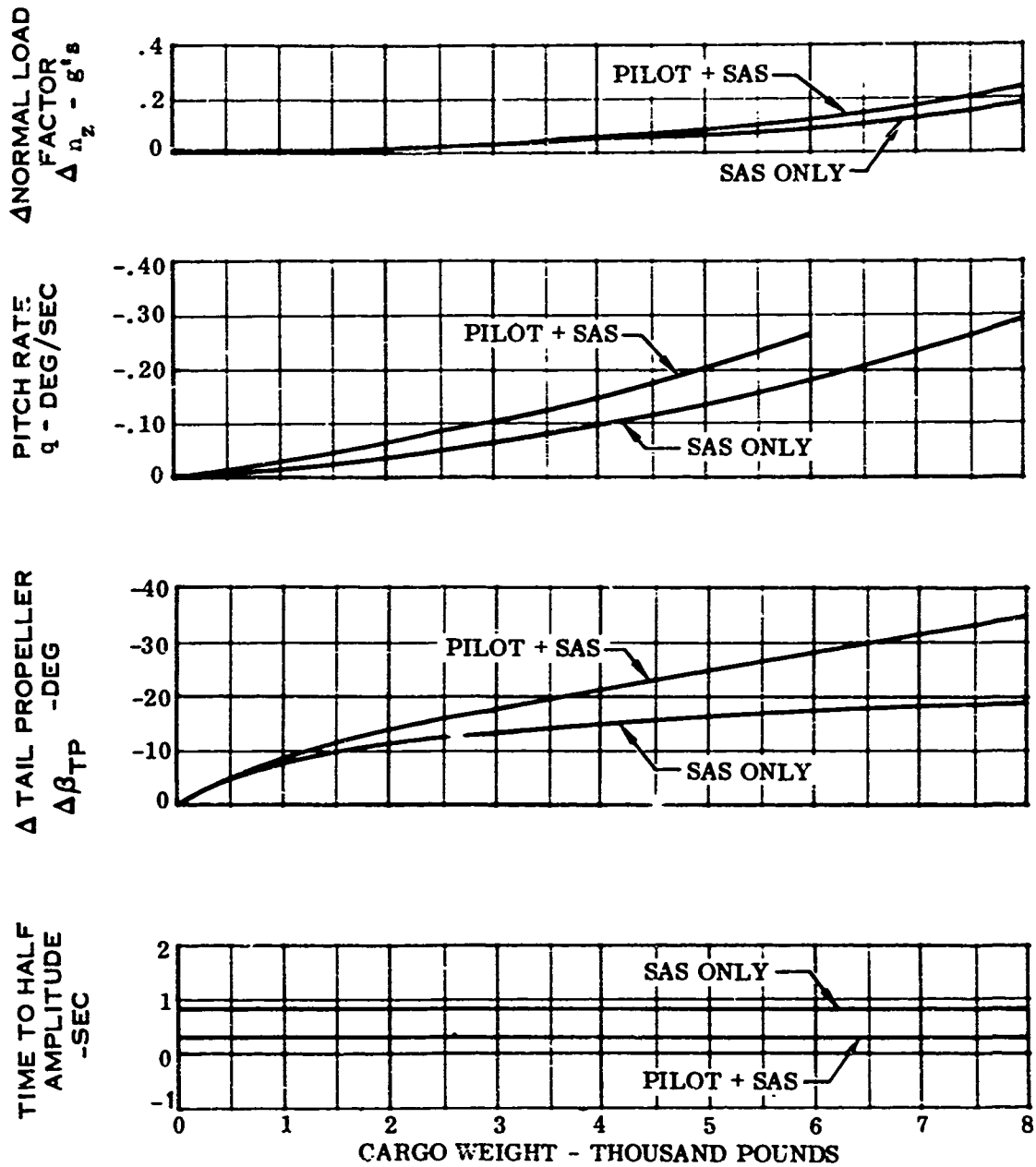


Figure 11. Peak Responses After Cargo Extraction Simulation,
 $i_w/\delta_p = 82.5/0$, Gravity Drops

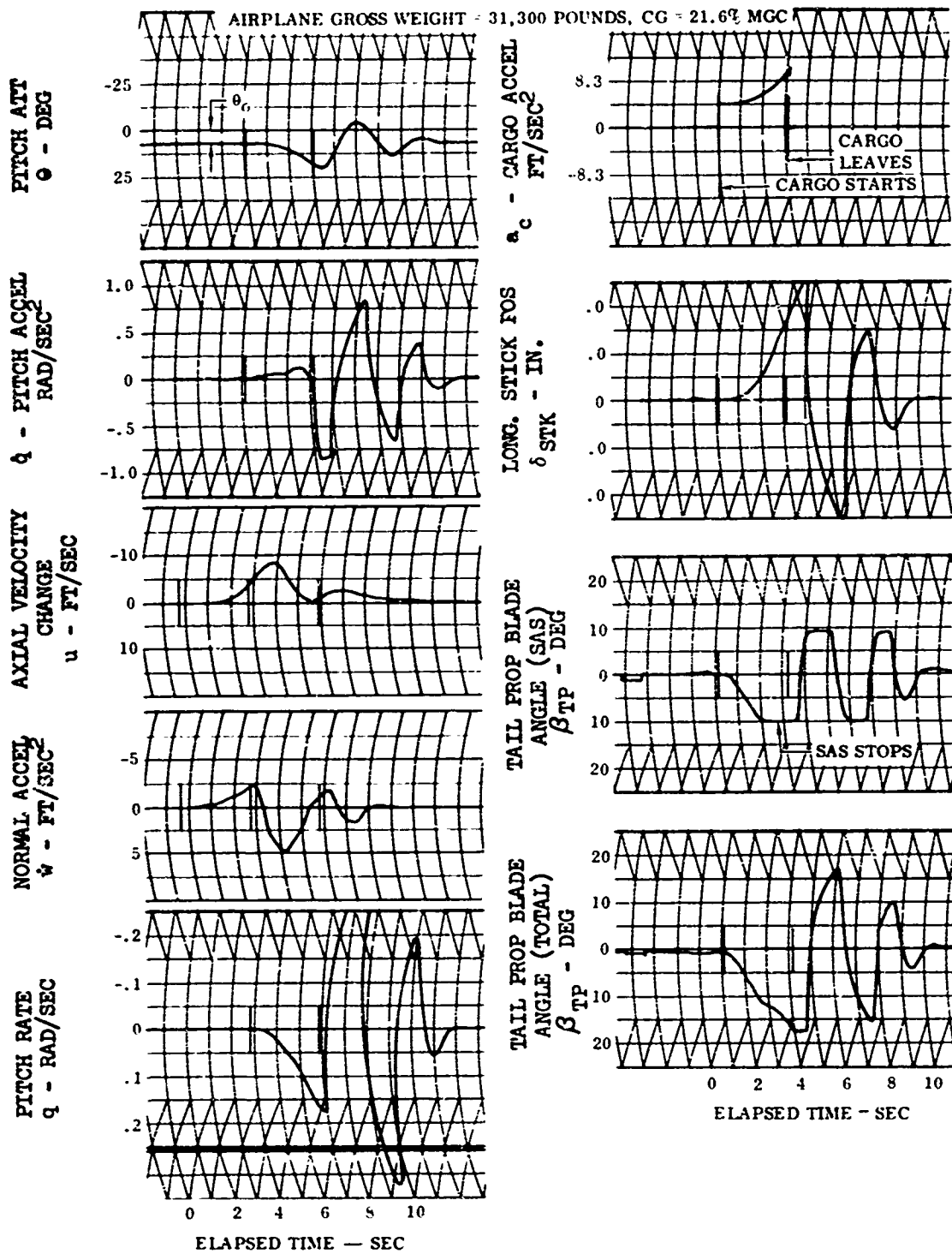


Figure 12. Analog Simulation Time Histories, $I_w/\delta_F = 82.5/0$,
 8,000-Pound Gravity Drop, SAS On, Pilot in Loop

AIRPLANE GROSS WEIGHT = 31,300 POUNDS, CG = 21.6% MGC

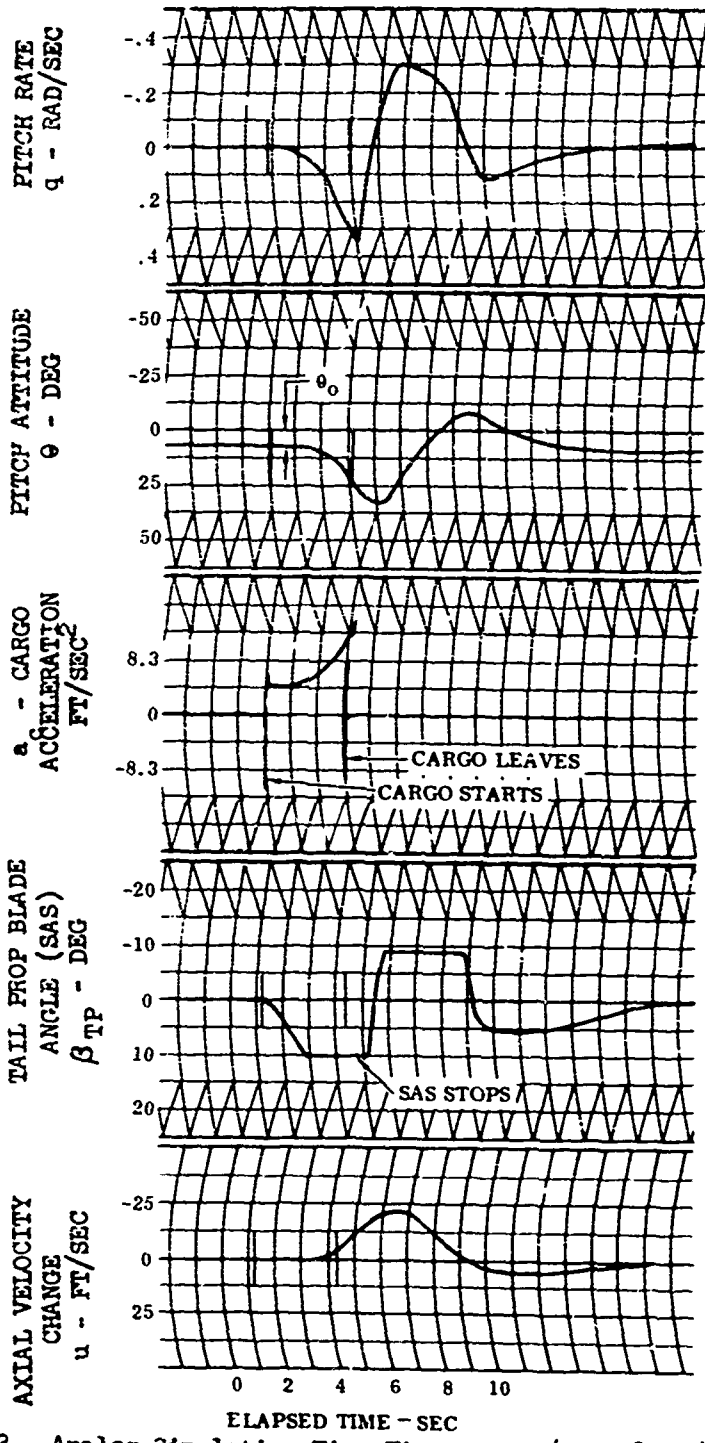
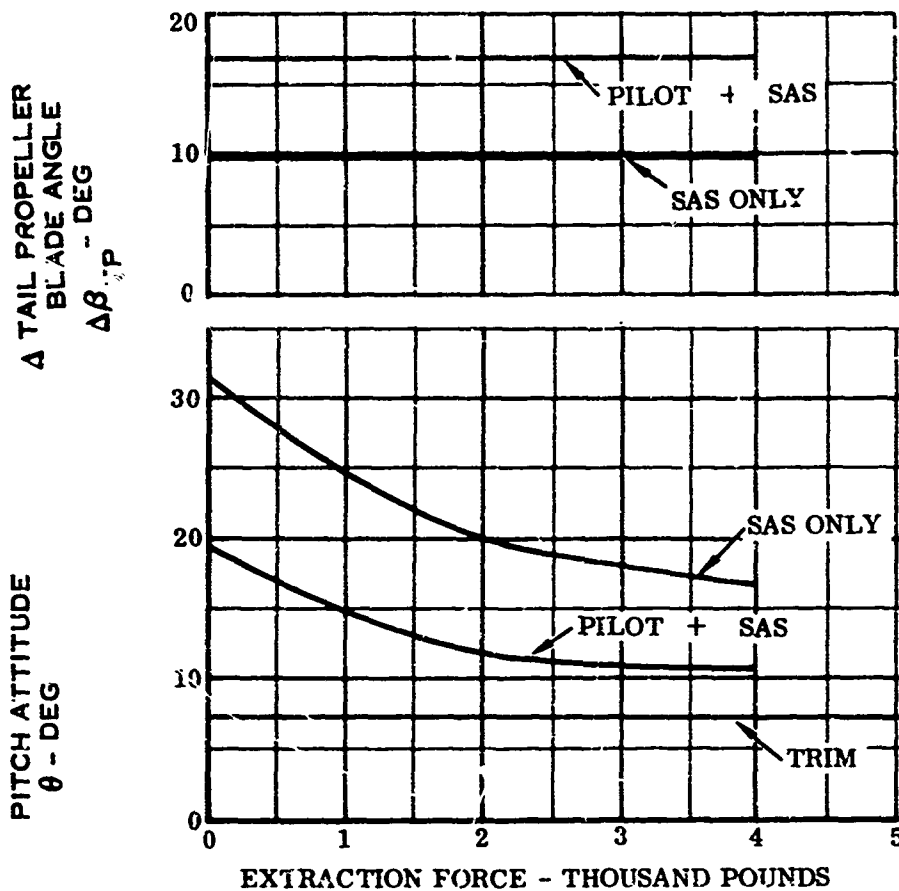


Figure 13. Analog Simulation Time History, $1_v/5 F = 82.5/0$, 8,000-Pound Gravity Drop, SAS On, Pilot out of Loop



NOTE:

ACTUATOR FORCE IS FOR THE FIRST FIVE FEET
OF CARGO TRAVEL

AIRPLANE GROSS WEIGHT = 31,300 POUNDS

$\theta_0 = 7.5^\circ$

Figure 14. Effect of Short Stroke Actuator on Peak Responses
During Cargo Extraction, $l_w/\delta_F = 82.5/0$, Cargo
Weight = 8,000 Pounds

AIRPLANE GROSS WEIGHT = 31,300 POUNDS, $\theta_0 = 0^\circ$

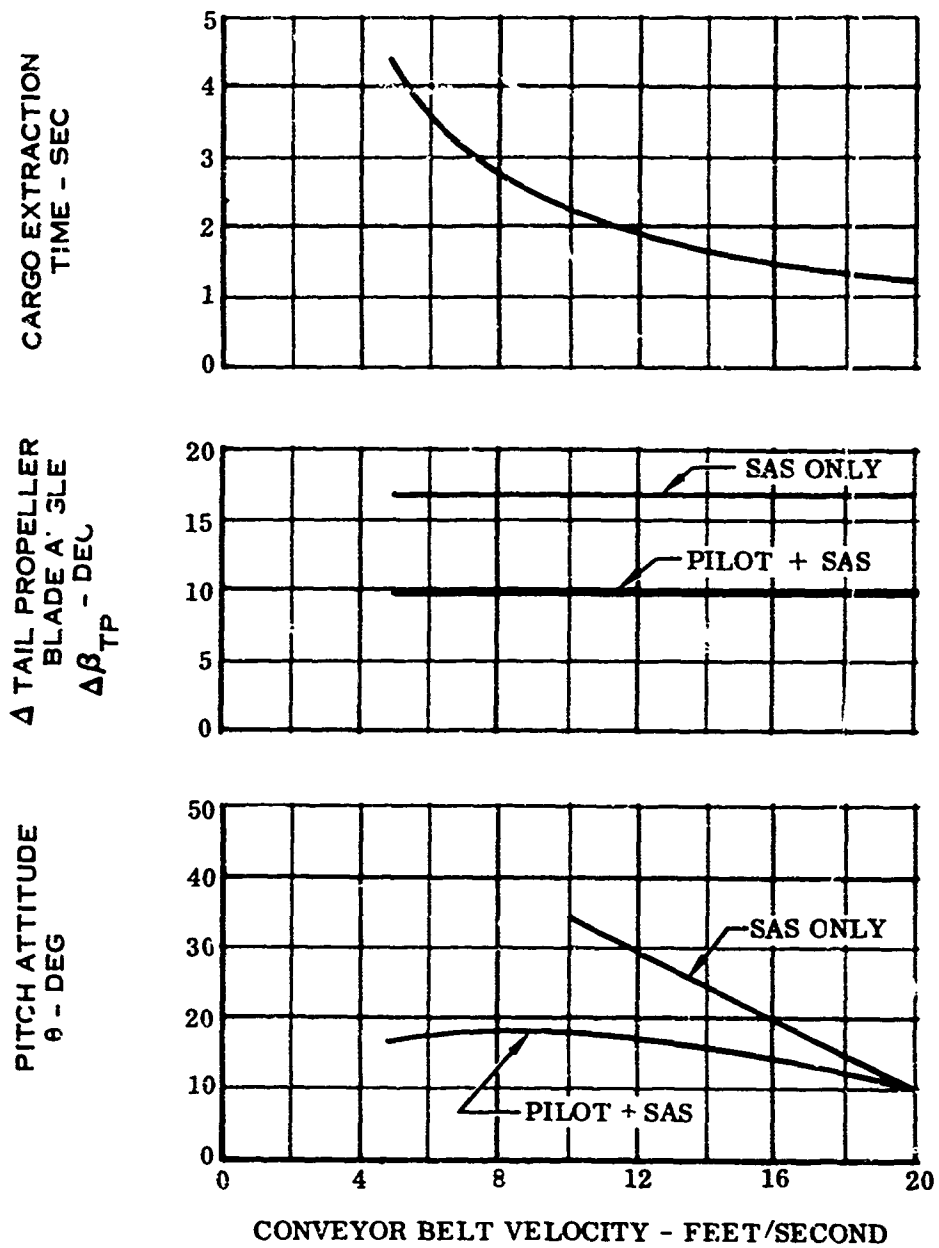


Figure 15. Effect of Conveyor Belt Extraction on Peak Responses During Cargo Delivery, $i_w/\delta_F = 82.5/0$, Cargo Weight = 8,000 Pounds

AIRPLANE GROSS WEIGHT = 31,300 POUNDS

CG = 21.6% MGC

$\theta_0 = 7.5^\circ$

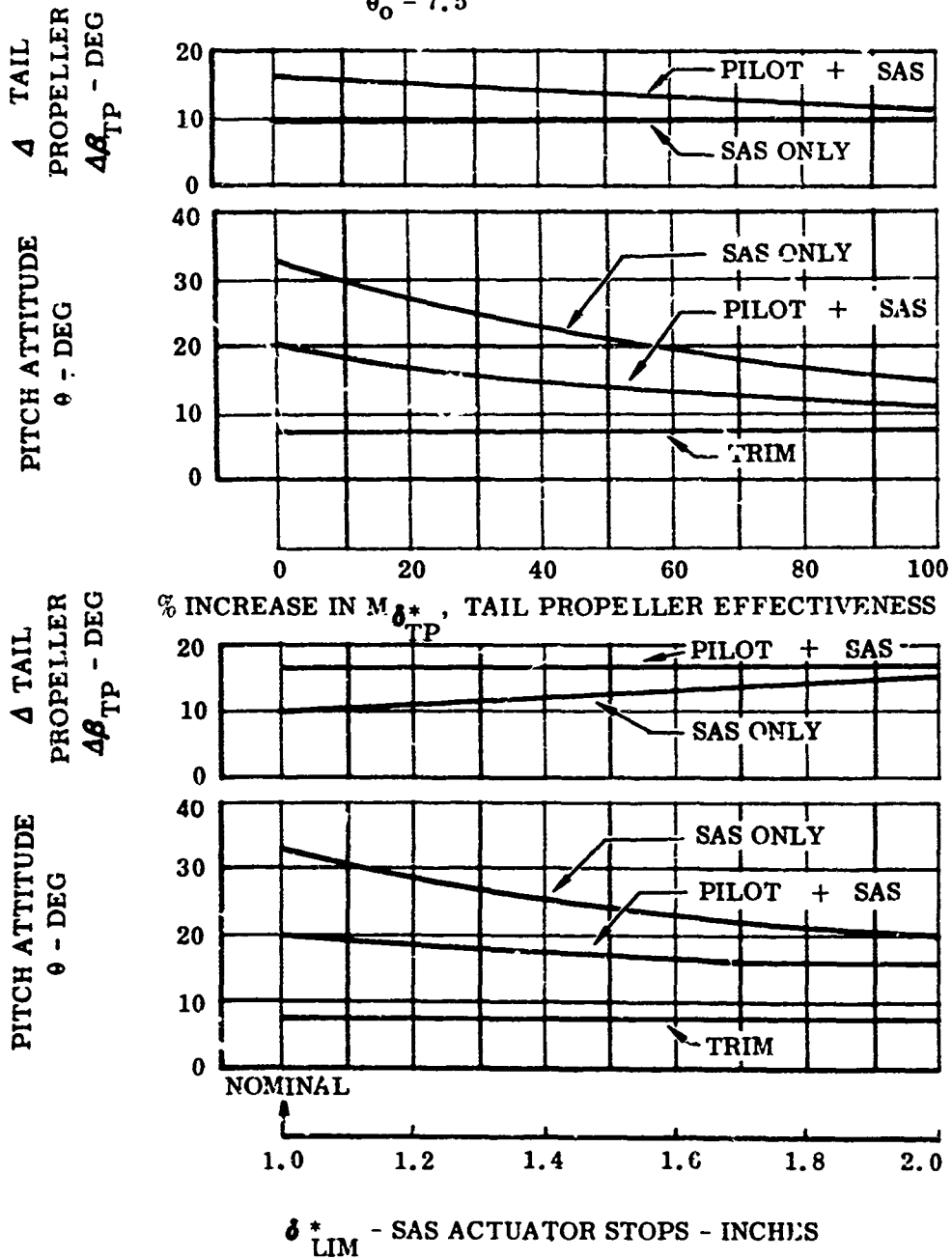


Figure 16. Peak Responses During Cargo Extraction Versus SAS Actuator Stops and Tail Prop Effectiveness, $i_w/\delta_F = 82.5/0$, 8,000-Pound Gravity Drops

AIRPLANE GROSS WEIGHT = 31,300 POUNDS

CG = 21.6 % MGC

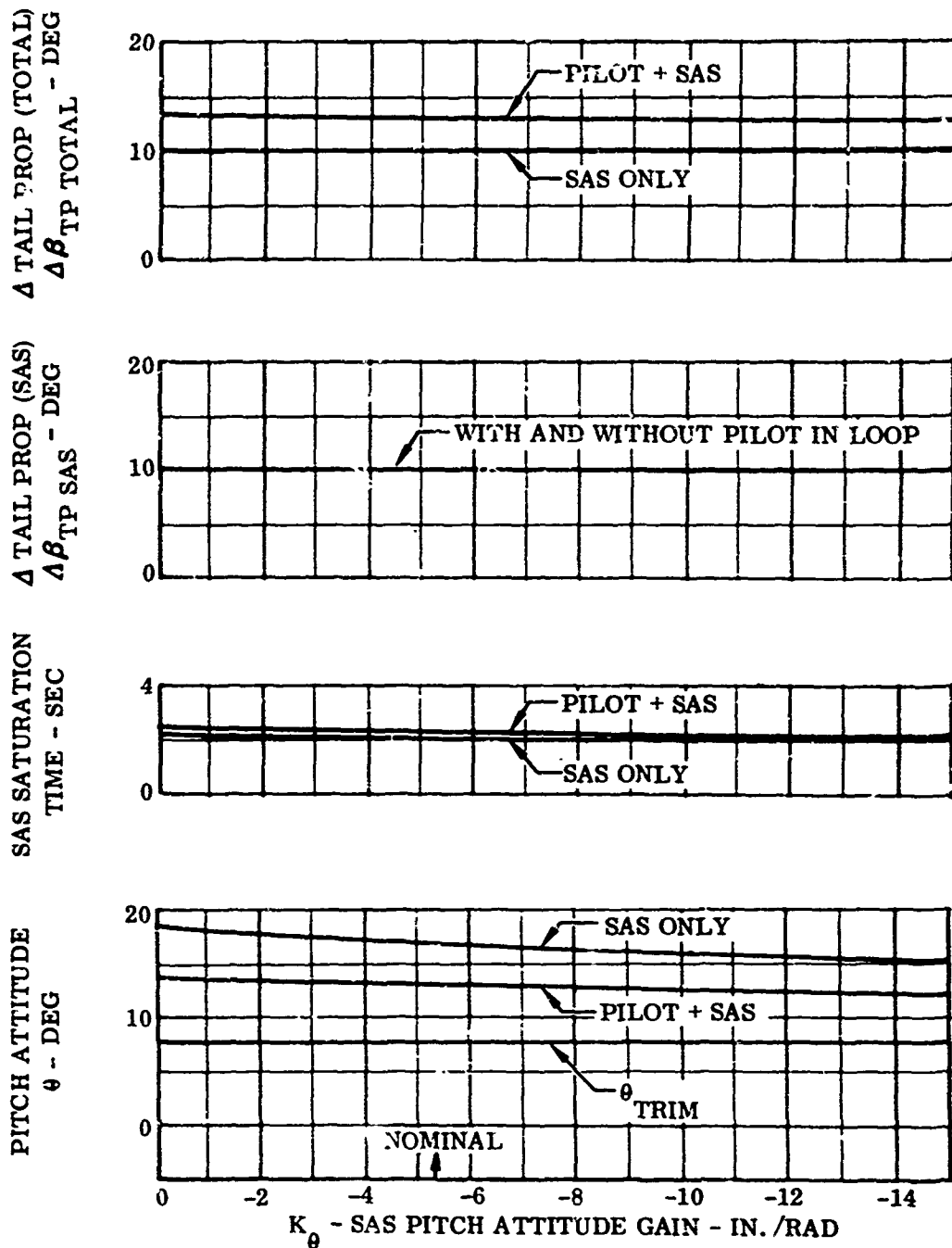


Figure 17. Peak Responses During Cargo Extraction Versus SAS Pitch Attitude Gain, $i_w/\delta_P = 82.5/0$, 4,000-Pound Gravity Drops

AIRPLANE GROSS WEIGHT = 31,300 POUND
 CG = 21.6 % MGC

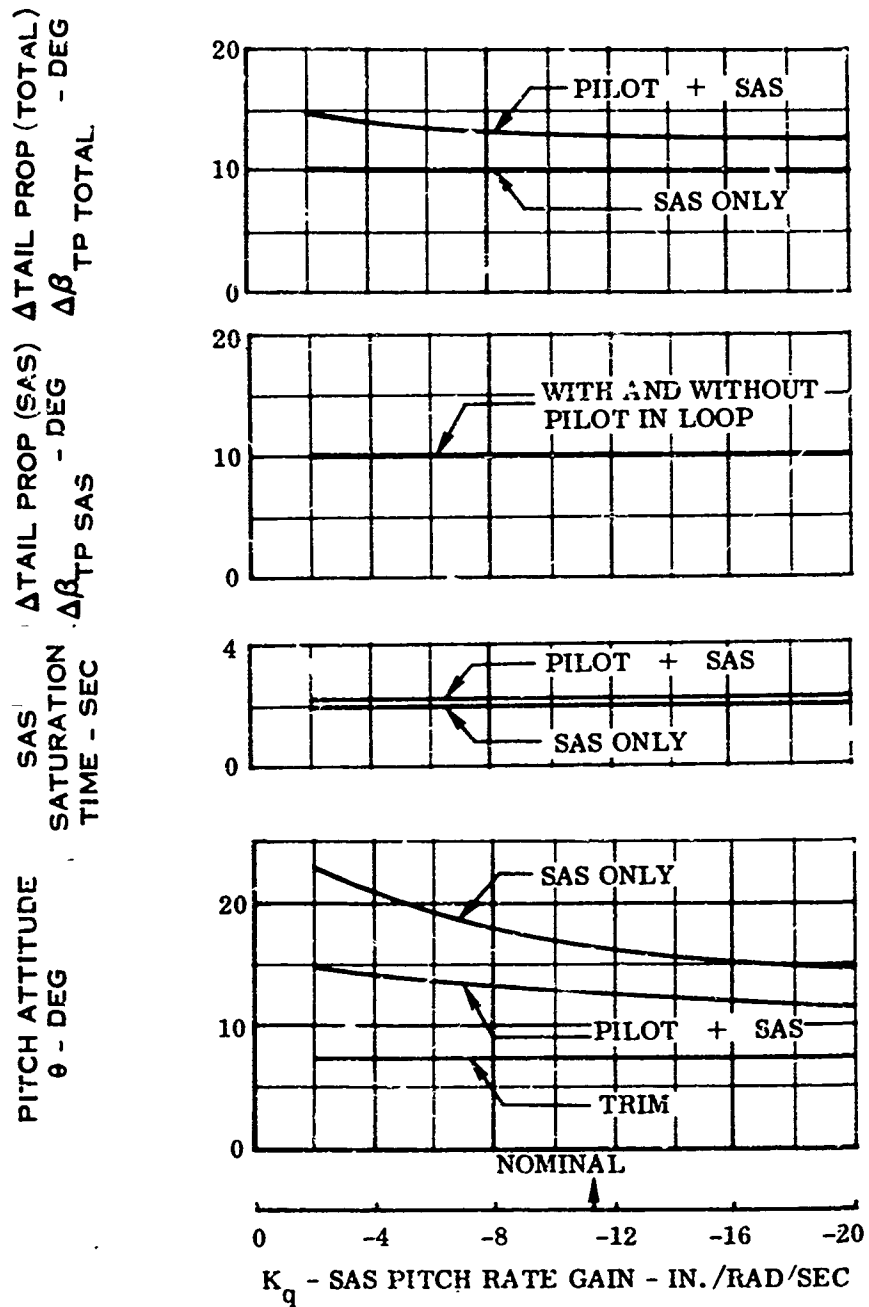


Figure 18. Peak Responses During Cargo Extraction Versus SAS Pitch Rate Gain, $\frac{z_w}{\delta P} = 82.5/0$, 4,000-Pound Gravity Drops

Figure 15 shows the effect of using a moving conveyor belt to extract the cargo. Increasing the conveyor belt speed reduces the cargo extraction time and reduces the airplane maximum pitch attitude reached during the air-drop maneuver.

Figure 16 shows the effect of increasing the tail propeller effectiveness, $M\delta_{TP}$. An increase in tail propeller effectiveness of 50% reduces the maximum pitch attitude from 20 degrees to 14 degrees. A 100% increase in effectiveness only reduces the pitch attitude to 11 degrees. The present XC-142A tail propeller is effective enough to maintain reasonable pitch attitudes during air-drop maneuver.

Figures 17 and 18 show the effect of changing the SAS pitch attitude and pitch rate gains. Increasing SAS pitch attitude or rate gain does not result in a large change in the airplane pitch attitude reached in the air-drop maneuver. The present SAS attitude and rate gains are adequate.

These data indicate that an 8,000-pound cargo load can be delivered in hover with the existing XC-142A longitudinal control system, providing the load leaves the airplane within an extraction time of not more than 3 seconds. If the cargo hangs up or leaves the airplane slowly, sufficient longitudinal control power is not available to balance the aft CG shift. The present XC-142A longitudinal control with 18° of blade angle can balance approximately 4,000 pounds on the airplane tail gate (Reference 3). Approximately 20% more tail prop thrust is available by going to blade angles greater than 18° , but this is impractical because the power required is almost doubled. The airplane SAS and pilot equation used in this study just barely command the stops on the tail propeller during an 8,000-pound, 3-second gravity extraction, as shown in Figure 12.

$i_w/\delta F = 30/60$ CONFIGURATION, $\theta_0 = 5^\circ$, GRAVITY DROPS

Figure 19 presents a comparison of a simulated 3,000-pound gravity drop with test data from the aerial delivery flight tests at El Centro, California. Figure 20 presents the peak airplane response during aerial cargo delivery versus cargo weight. Figure 21 presents the peak airplane response after the cargo has left the aircraft. Figure 22 presents analog record of an 8,000-pound drop with pilot inputs. This analysis indicates that the airplane will change pitch attitude from 5° to 17° with an effective angle-of-attack change from 10.7° to 20° . As in the hover case, the pilot could increase his gain and reduce this pitch attitude, then reduce his gain after the drop. No provision in this study was made for changing thrust. In flight tests, the pilot could increase thrust during this type of drop, eliminating the high effective angle of attack and buffet encountered during pitch-up.

The following data in this section are concerned with various ways of improving the airplane's aerial delivery capability for this configuration.

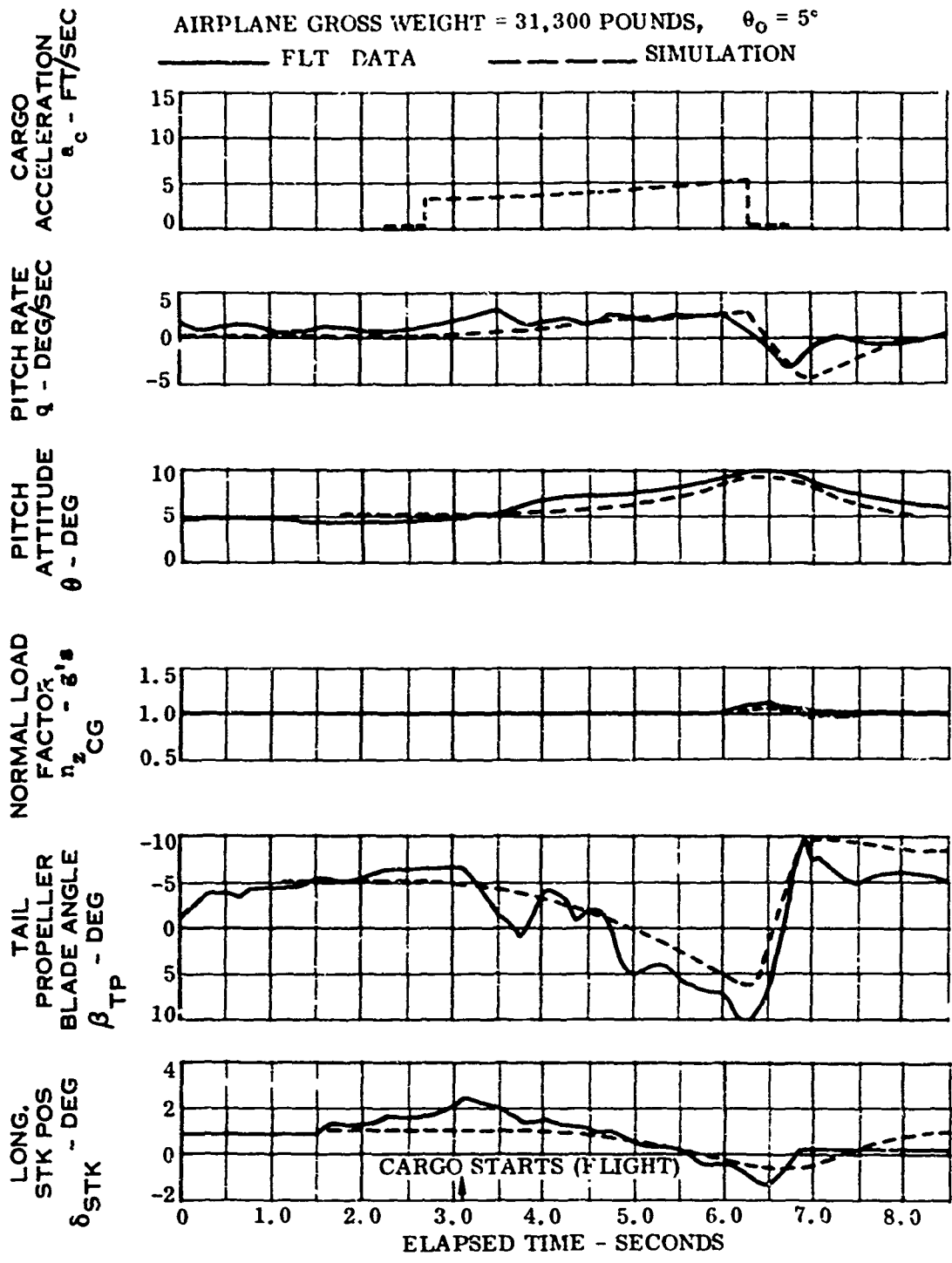


Figure 19. Comparison of Flight Test Data with Analog Simulation, $i_w/\delta_F = 30/60$, 3,000-Pound Gravity Drop

AIRPLANE GROSS WEIGHT = 31,300 POUNDS
 INITIAL CG POSITION = 21.6 % MGC
 TWO-CHANNEL PITCH SAS OPERATION

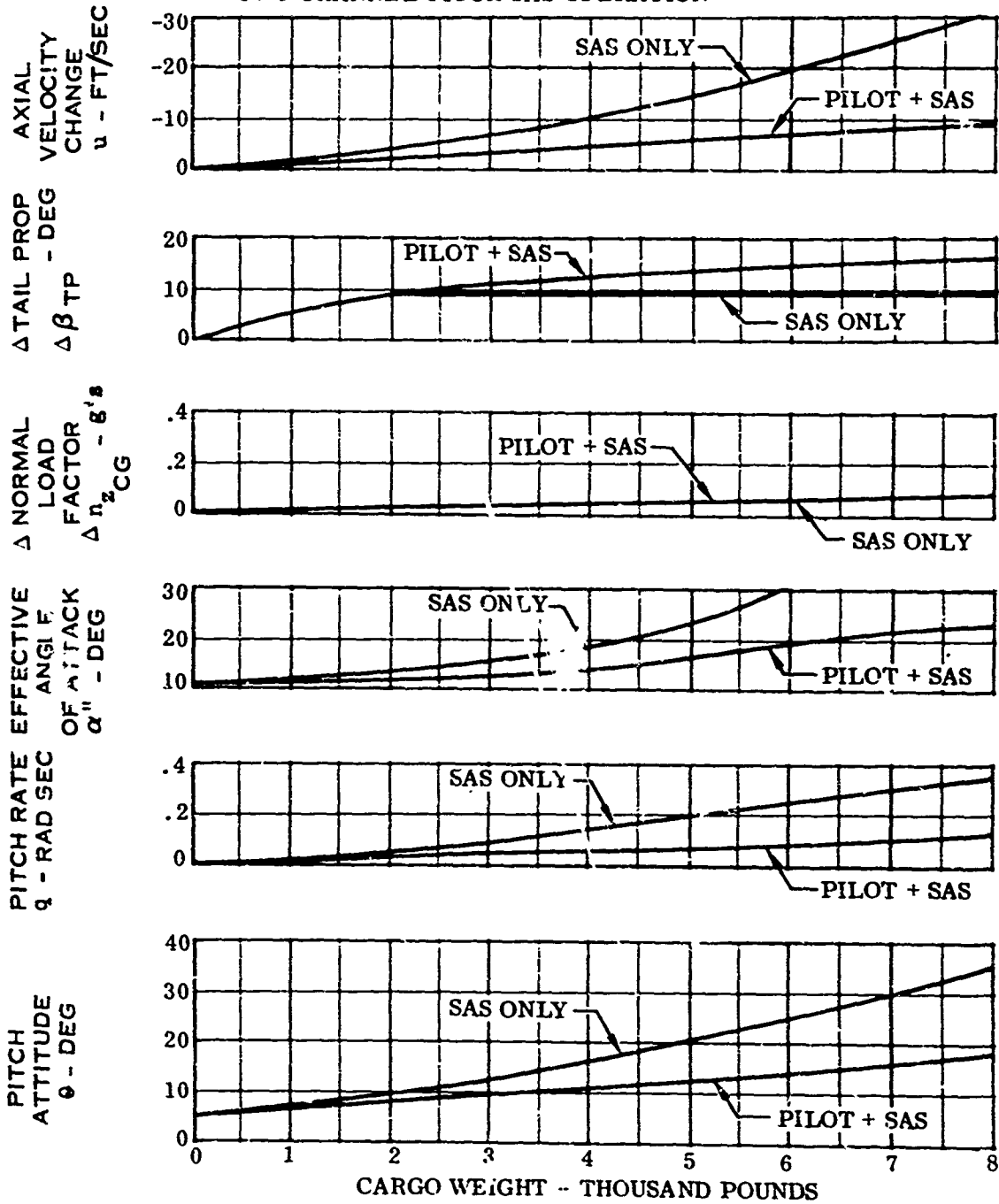


Figure 20. Peak Responses During Cargo Extraction Simulation, $I_w/\delta P = 30,60$, Gravity g

AIRPLANE GROSS WEIGHT = 31,300 POUNDS
 INITIAL CG POSITION = 21.6 % MGC
 TWO-CHANNEL PITCH SAS OPERATION

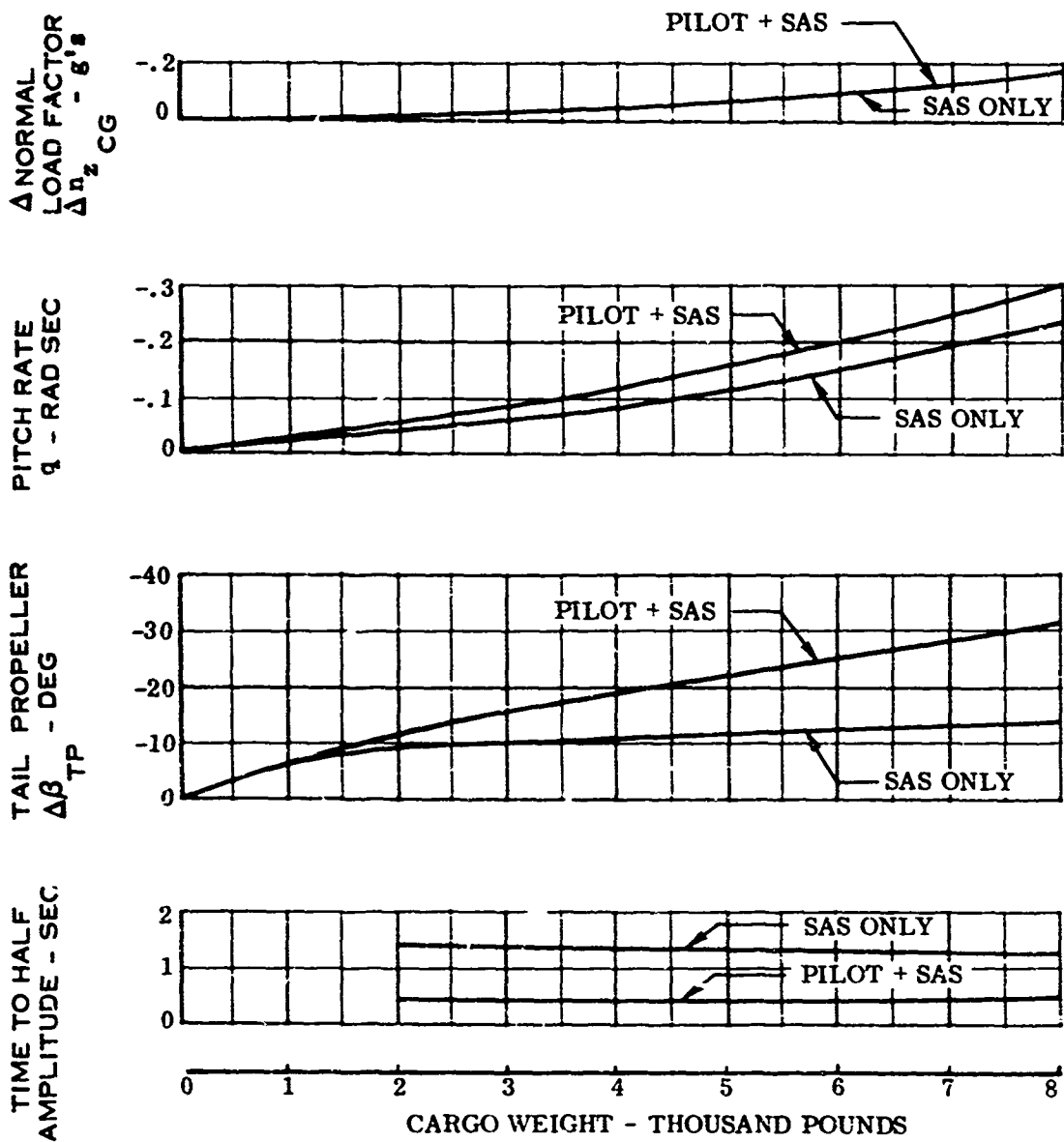


Figure 21. Peak Responses After Cargo Extraction Simulation,
 $i_w/\delta_F = 30/60$, Gravity Drops

AIRPLANE GROSS WEIGHT = 31,300 POUNDS, CG = 21.6% MGC

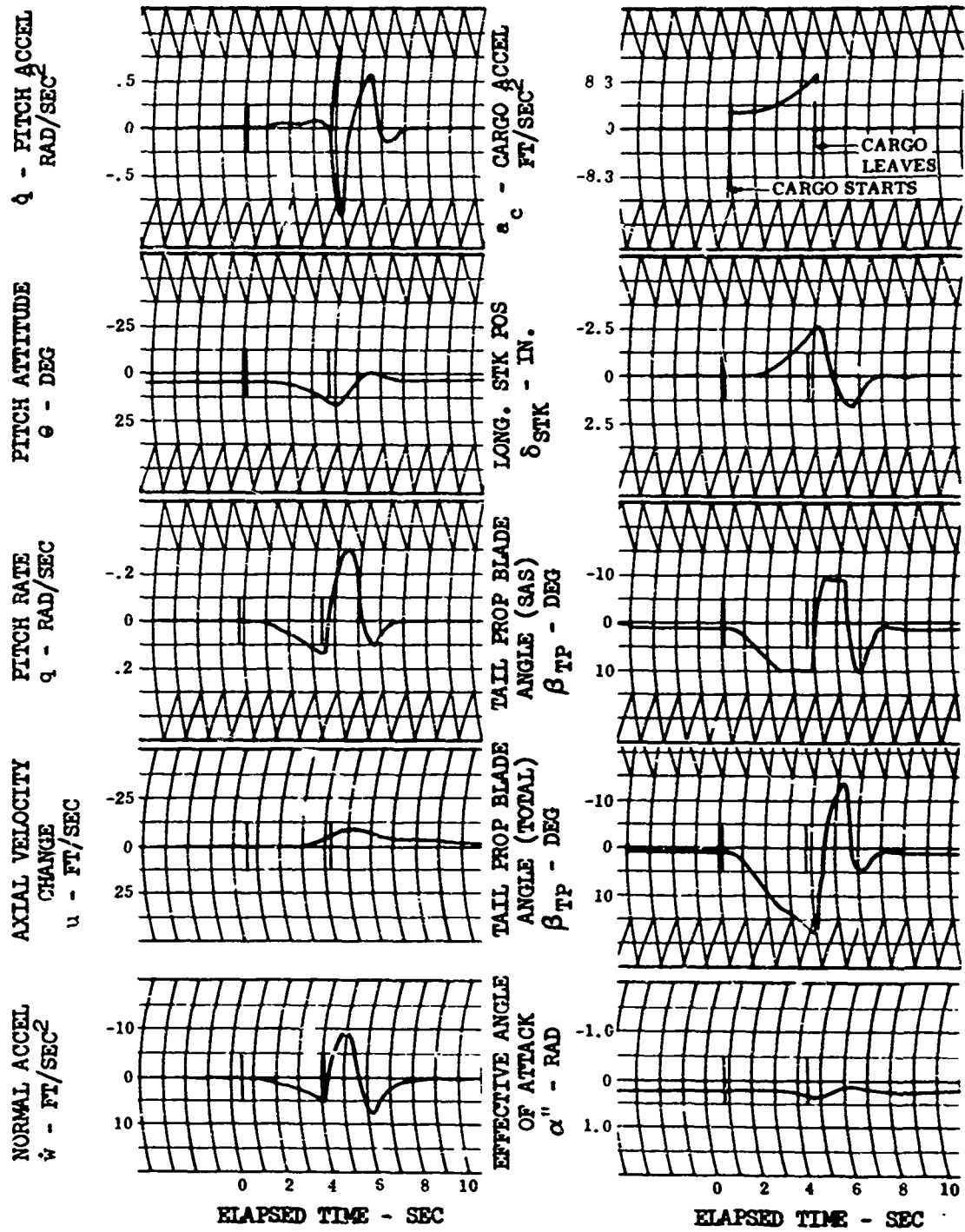


Figure 22. Analog Simulation Time Histories, $I_w/\delta_F = 30/60$, 8,000-Pound Gravity Drop, SAS On, Pilot in Loop

Figure 23 presents data showing the airplane plus SAS peak response to an 8,000-pound drop versus cargo extraction force as might be applied from a ground extraction system. Data are also shown for a short stroke actuator producing 1,000 pounds of push for the first 1/2 feet of cargo travel. In each case, the extraction time is reduced and the peak response is less.

Figure 24 is concerned with increasing the SAS actuator authority from its nominal value of ± 1.0 inch of travel. Essentially, this is a system with more authority. Some improvement is noted with the pilot in the loop with much improvement with SAS only.

Figure 25 shows the effect of increasing the tail propeller effectiveness for an 8,000-pound gravity drop. With increased tail propeller effectiveness, the effective angle of attack is reduced below 20 degrees with pilot and SAS in the loop. The present XC-142A airplane would encounter light buffet at 20 degrees effective angle of attack.

Figures 26 and 27 show the effect on peak response from changing the SAS pitch attitude gain, K_θ , and the SAS pitch rate gain, $K_{\dot{\theta}}$. Figures 28 and 29 show the same effect from the addition of a pitch acceleration gain, $K_{\ddot{\theta}}$, and the integral of the pitch attitude gain, $\int \theta$. Some improvement is noted; however, the rapid saturation (hitting authority limits) of the SAS actuators during an 8,000-pound drop partially eliminates the benefit of higher and different SAS gains.

During an air drop with this type of aircraft, both the pilot and SAS are opposing the airplane pitching movement as the cargo slides out. The stick pick-off gain which assists in keeping the SAS actuators from saturating during normal pilot maneuvers actually helps to saturate the SAS since the pilot and SAS are both moving the longitudinal control in the same direction.

As in the hover case, it is possible to drop the maximum XC-142A payload from a 30/60 configuration with the existing longitudinal control system with proper pilot technique and short cargo extraction times.

$i_w/\delta F = 10/60$ CONFIGURATION, $\theta_0 = 5^\circ$, GRAVITY DROPS

Figure 30 presents peak values of airplane response during cargo delivery versus cargo weight, with and without pilot inputs. Figure 31 presents analog records of an 8,000-pound drop with pilot inputs. These data indicate that, with pilot inputs, no limiting flight condition will be encountered during the aerial delivery of the maximum payload from this configuration.

$i_w/\delta F = 5/38$ CONFIGURATION, $\theta_0 = 5^\circ$, GRAVITY DROPS

Figure 32 presents peak values of airplane response during air cargo delivery versus cargo weight, with and without pilot inputs. Figure 33

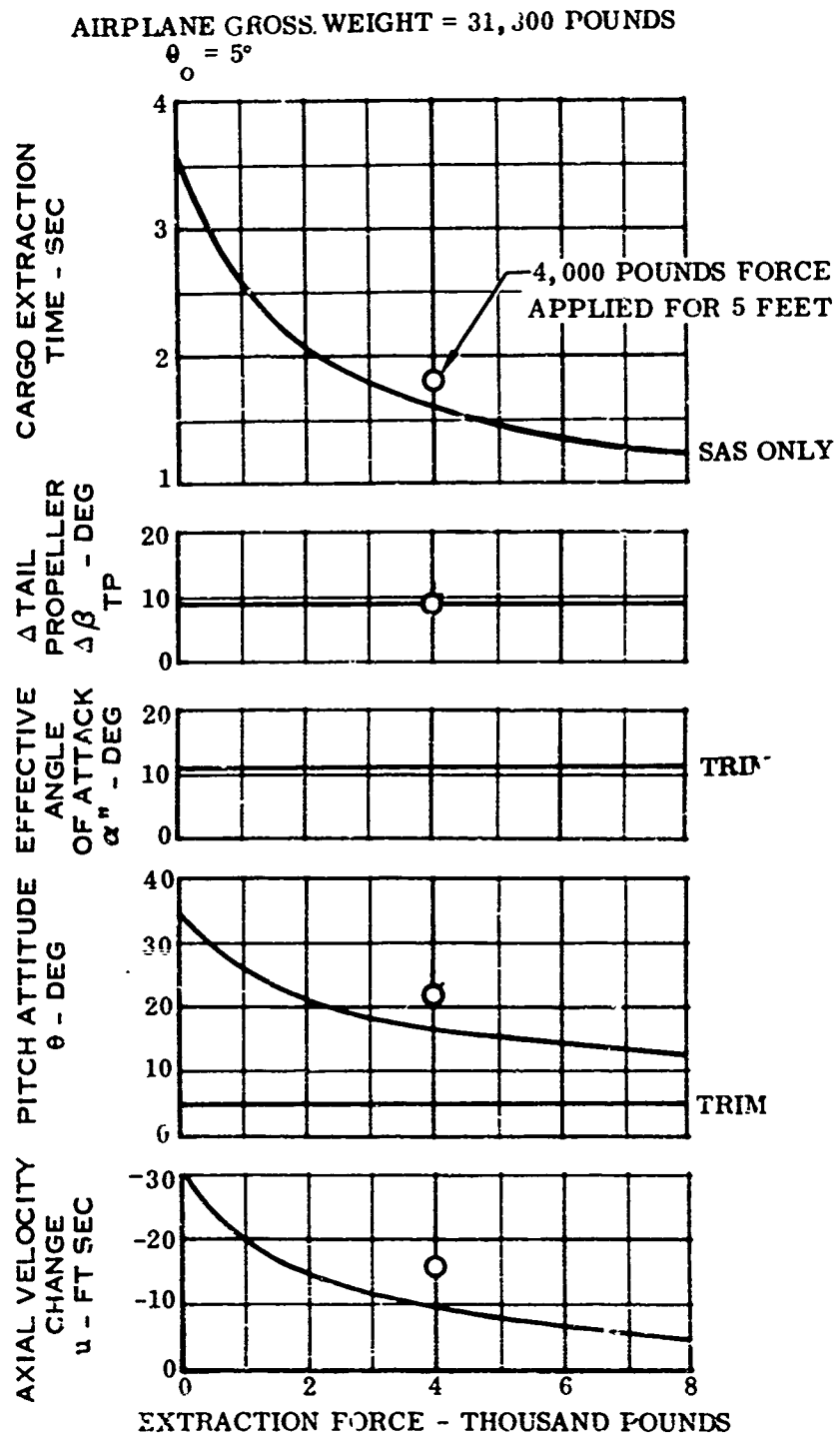


Figure 23. Effect of Extraction Force on Peak Responses During Cargo Delivery, $i_w/\delta p = 30/60$, Cargo Weight = 8,000 Pounds

AIRPLANE GROSS WEIGHT = 31,300 POUNDS, $\theta_0 = 5^\circ$

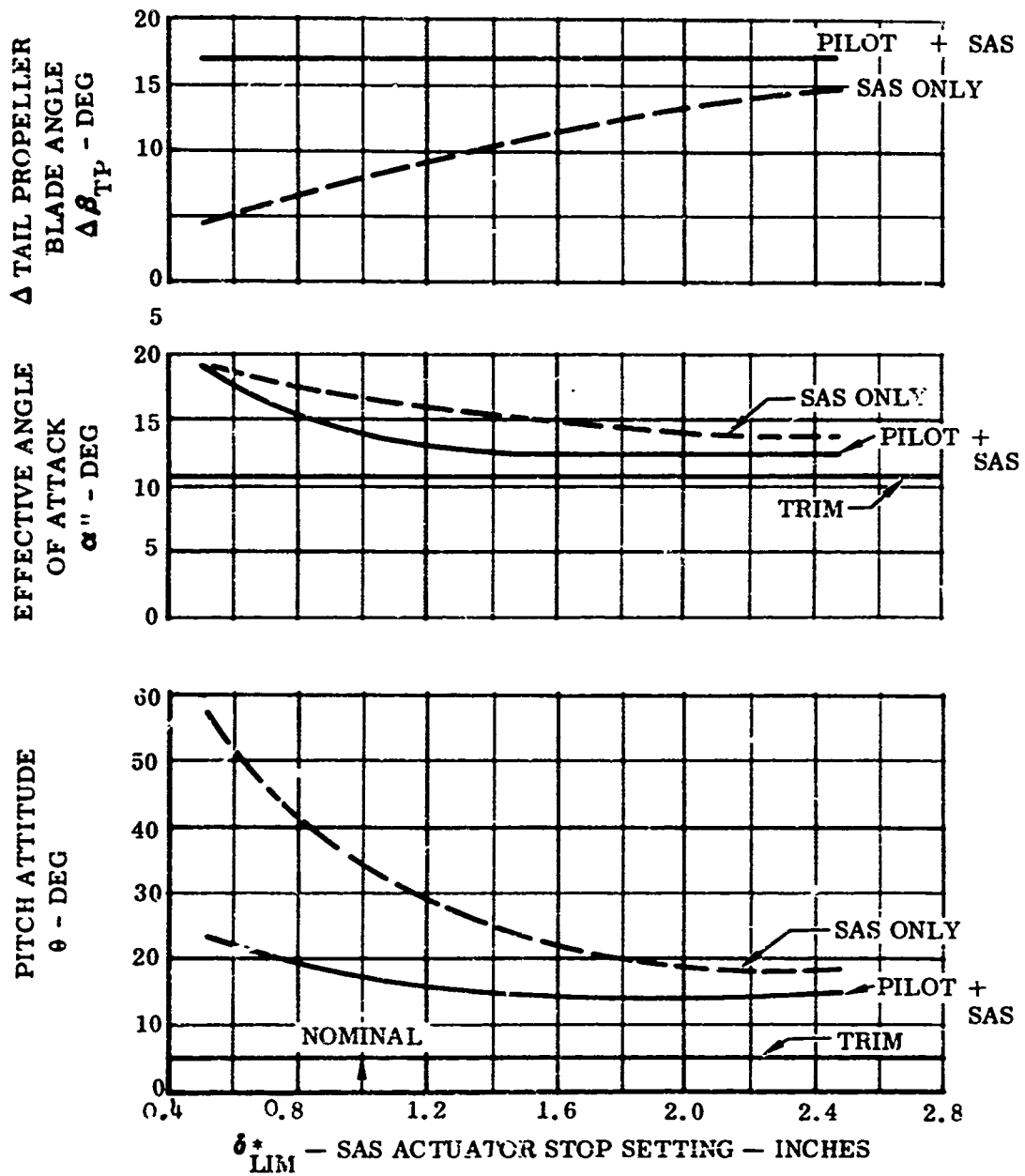


Figure 24. Effect of SAS Actuator Stops on Peak Responses During Cargo Extraction, $i_w/\delta_P = 30/60$, 8,000-Pound Gravity Drops

AIRPLANE GROSS WEIGHT = 31,300 POUNDS, $\theta_0 = 5^\circ$

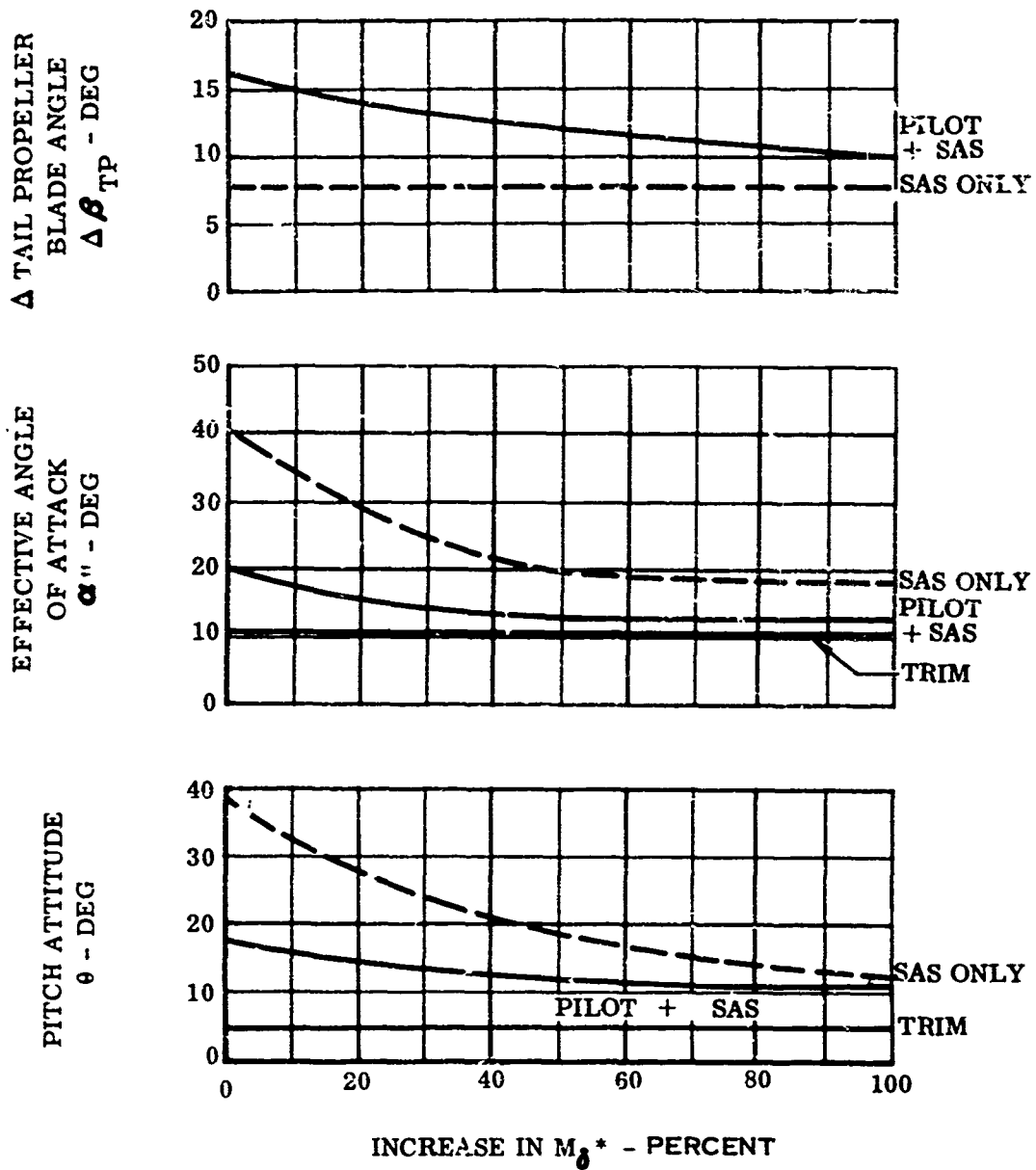
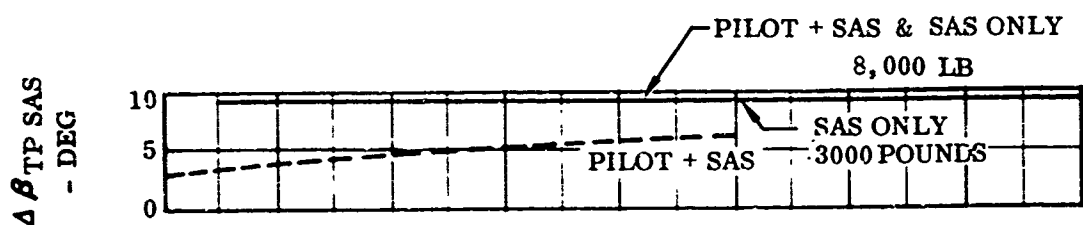
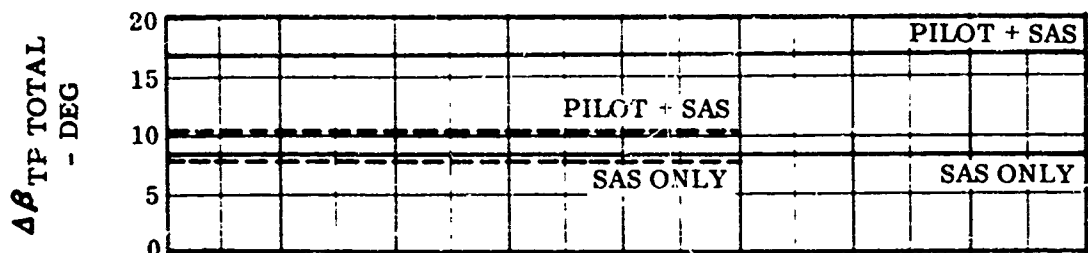


Figure 25. Effect of Increase in Tail Prop Effectiveness on Peak Response During Cargo Extraction, $l_w/\delta_F = 30/60$, 8,000-Pound Gravity Drops

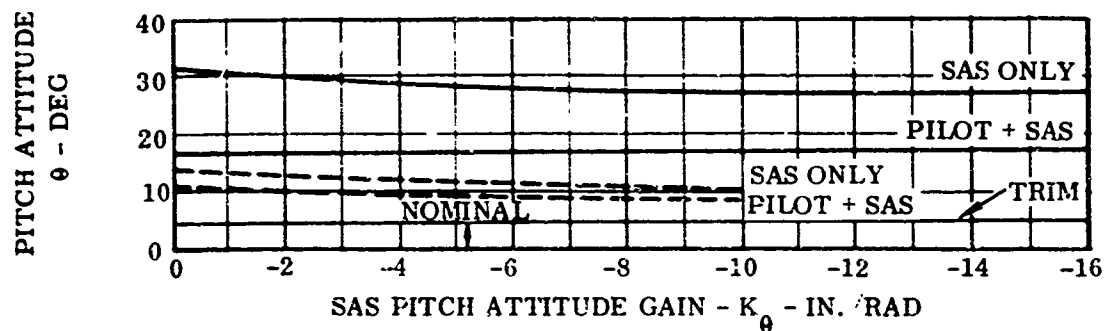
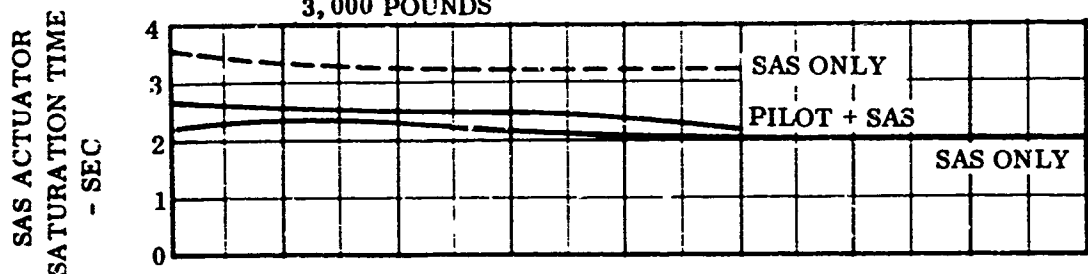
AIRPLANE GROSS WEIGHT = 31,300 POUNDS

$$\theta_0 = 5^\circ$$

— CARGO WEIGHT = 8,000 POUNDS - - - CARGO WEIGHT = 3,000 POUNDS



NOTE: STOPS NOT ENCOUNTERED WITH PILOT IN LOOP, 3,000 POUNDS



Figur 26. Effect of SAS Pitch Attitude Gain on Peak Responses During Cargo Extraction, $1_w/\delta_F = 3C/60$, Gravity Drops

AIRPLANE GROSS WEIGHT = 31,300 POUNDS, $\theta_0 = 5^\circ$

— 8,000 POUND CARGO WEIGHT - - - 3,000 POUND CARGO WEIGHT

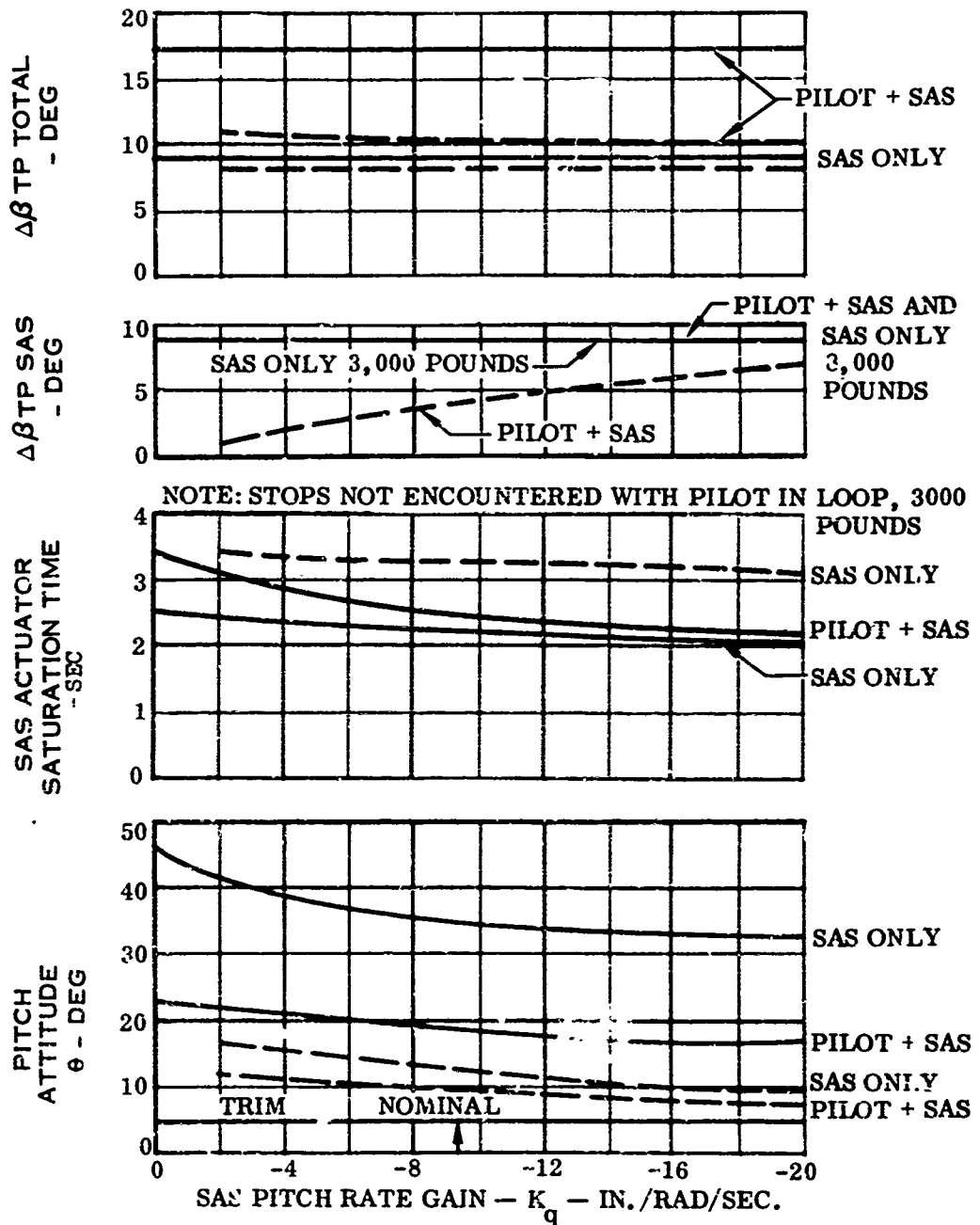


Figure 27. Effect of SAS Pitch Rate Gain on Peak Responses During Cargo Extraction, $i_w/\delta p = 30/60$, Gravity Drops

PILOT OUT OF LOOP

AIRPLANE GROSS WEIGHT = 31,300 POUNDS, $\theta_0 = 5^\circ$

———— = CARGO WEIGHT = 8,000 POUNDS
 - - - - = CARGO WEIGHT = 2,000 POUNDS

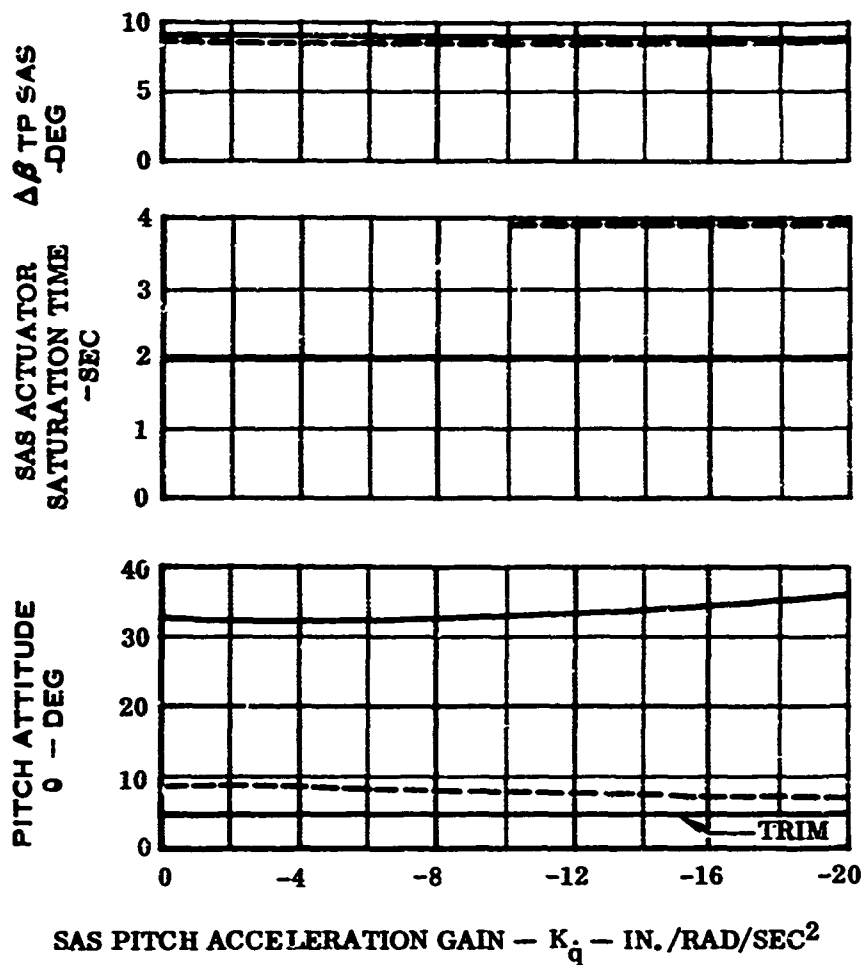


Figure 28. Effect of SAS Pitch Acceleration Gain on Peak Responses During Cargo Extraction, $i_v/\delta_F = 30/60$, Gravity Drops

PILOT OUT OF LOOP
 AIRPLANE GROSS WEIGHT = 31,300 POUNDS, $\theta_0 = 5^\circ$
 — 8,000 POUND CARGO - - - 2,000 POUND CARGO

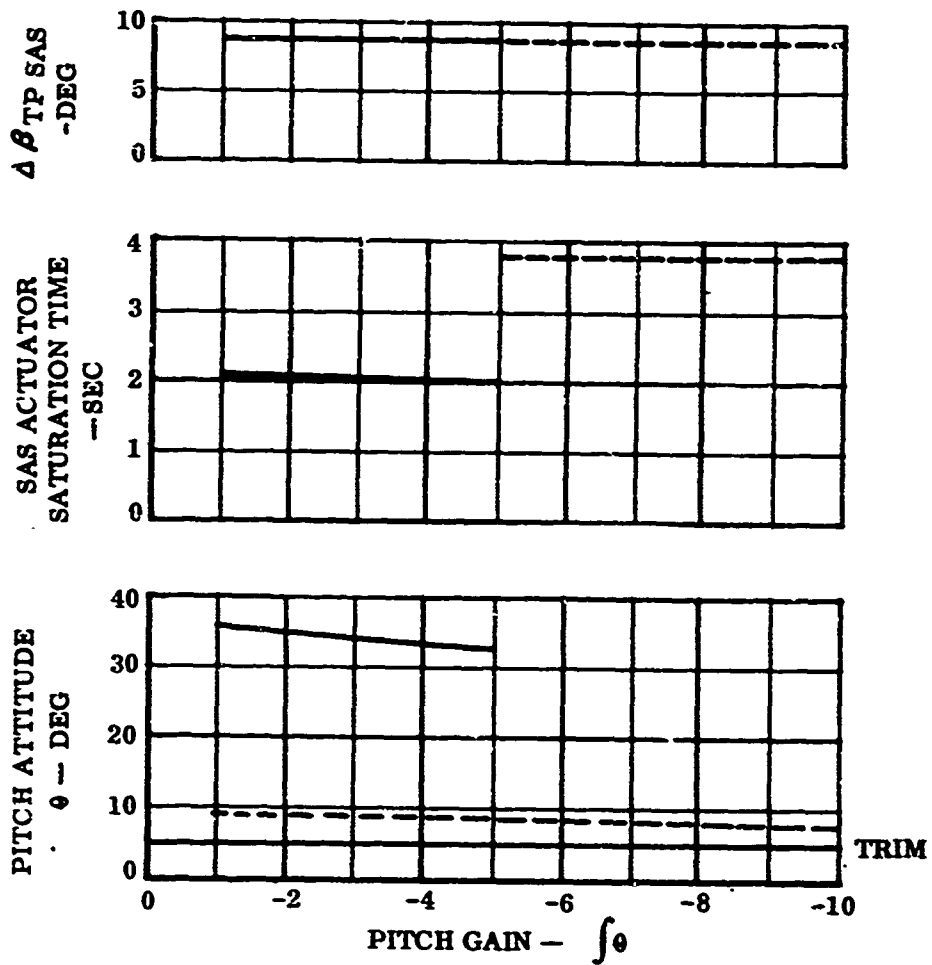


Figure 29. Effect of Feedback of Integral of Pitch Attitude on Peak Responses During Cargo Extraction, $i_w/\delta_F = 30/60$, Gravity Drops

AIRPLANE GROSS WEIGHT = 31,300 POUNDS, $\theta_0 = 5^\circ$, INITIAL CG POS. = 21.6% MGC
 TWO-CHANNEL PITCH SAS OPERATION

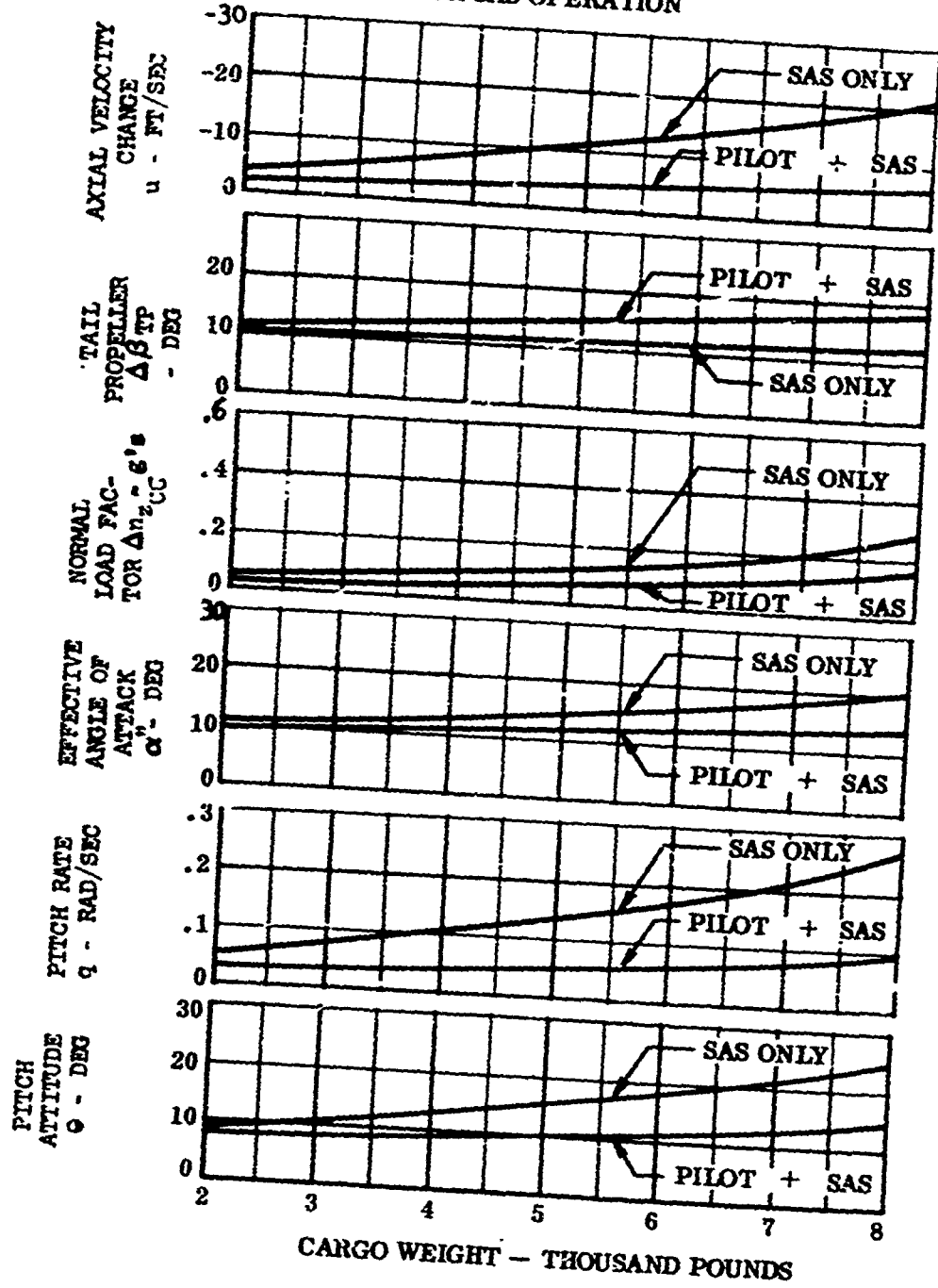


Figure 30. Peak Responses During Cargo Extraction Simulation, $1_v/8_F = 10/60$, Gravity Drops

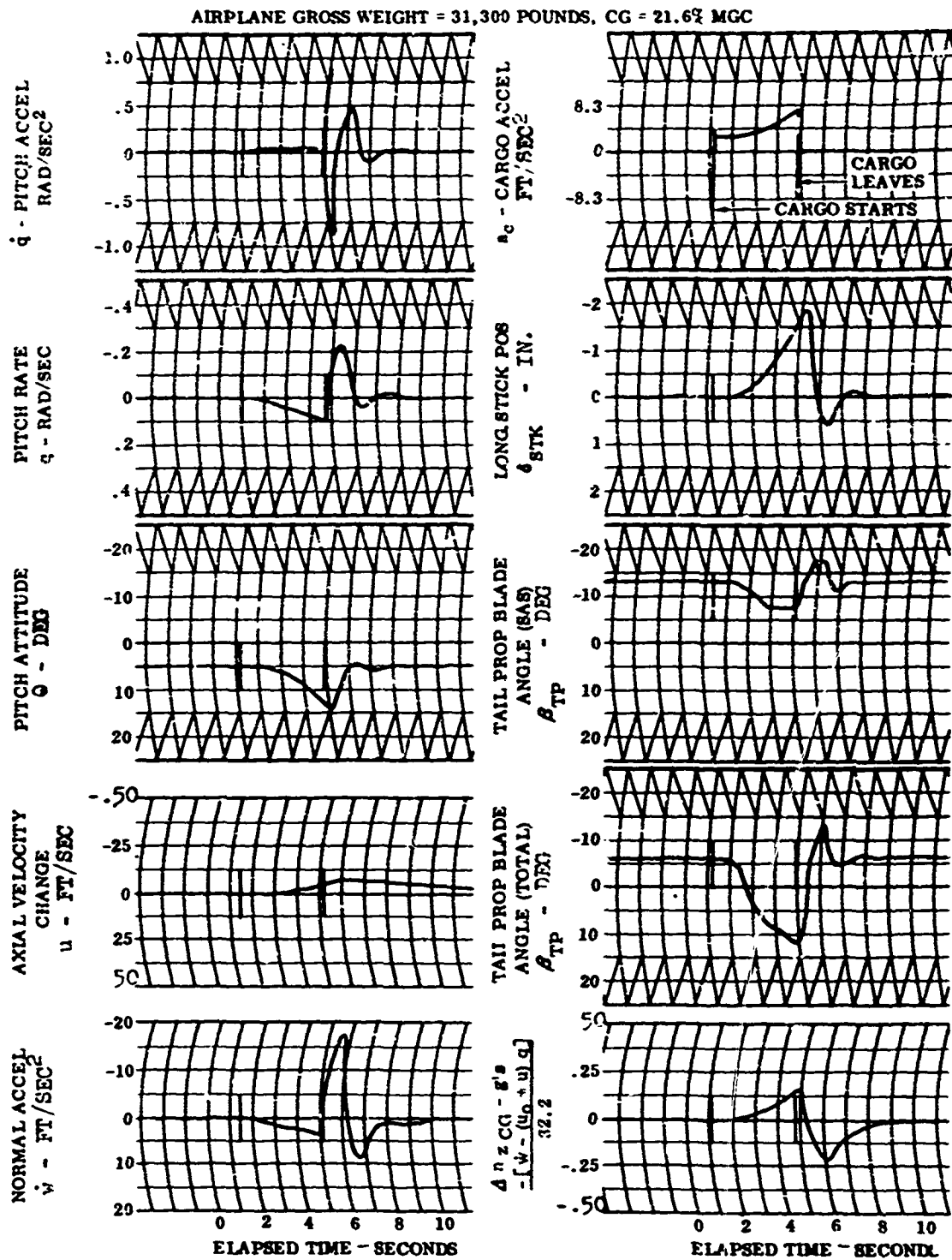


Figure 31. Analog Simulation Time Histories, $i_w/\delta p = 10/60$, 8,000-Pound Gravity Drop, SAS On, Pilot in Loop

AIRPLANE GROSS WEIGHT = 31,300 POUNDS, $\theta_0 = 5^\circ$

INITIAL CG POSITION = 21.6 % MGC

TWO-CHANNEL PITCH SAS OPERATION

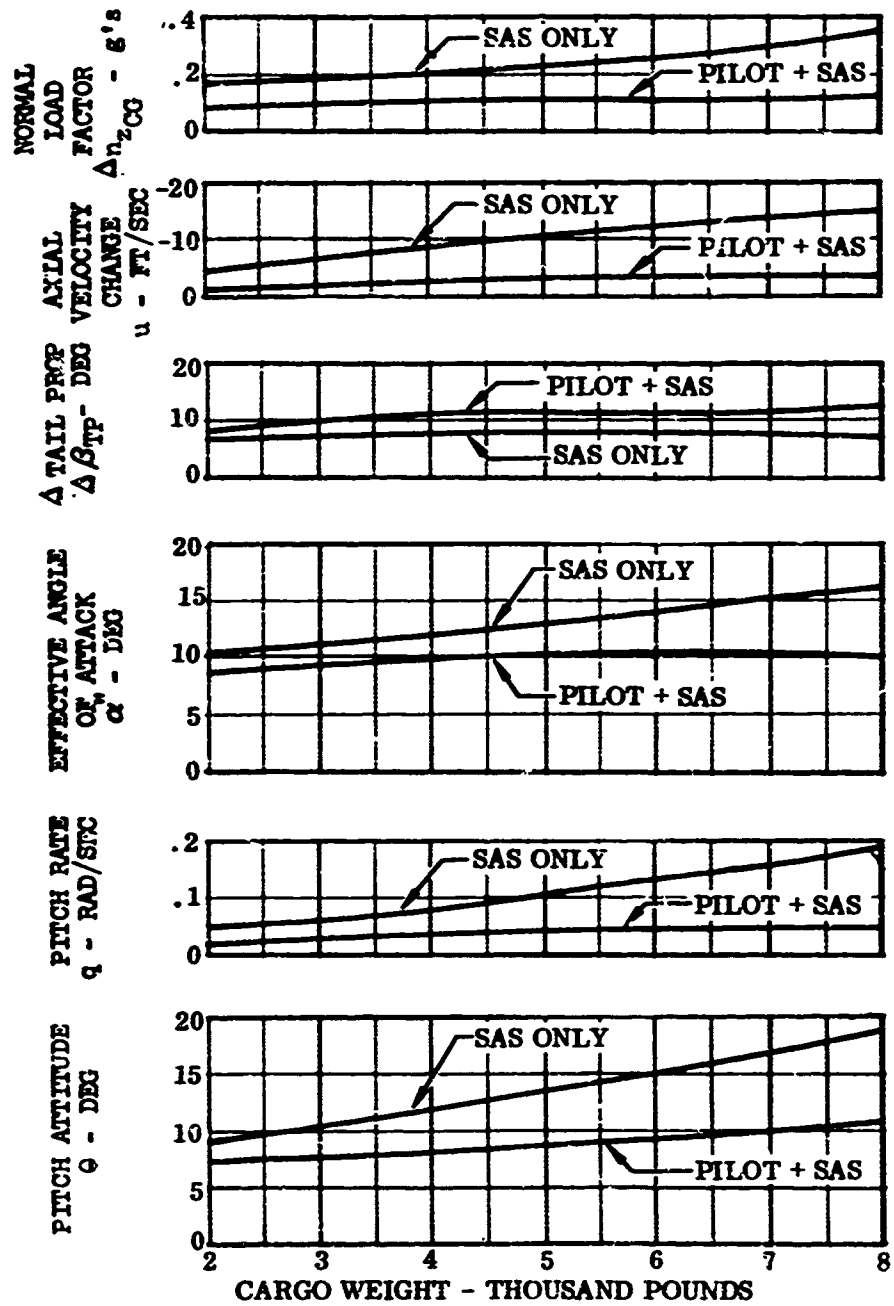


Figure 32. Peak Responses During Cargo Extraction,
 $\dot{w}/\delta F = 5/38$, Gravity Drops

AIRPLANE GROSS WEIGHT = 31,500 POUNDS, CG = 21.6% MGC

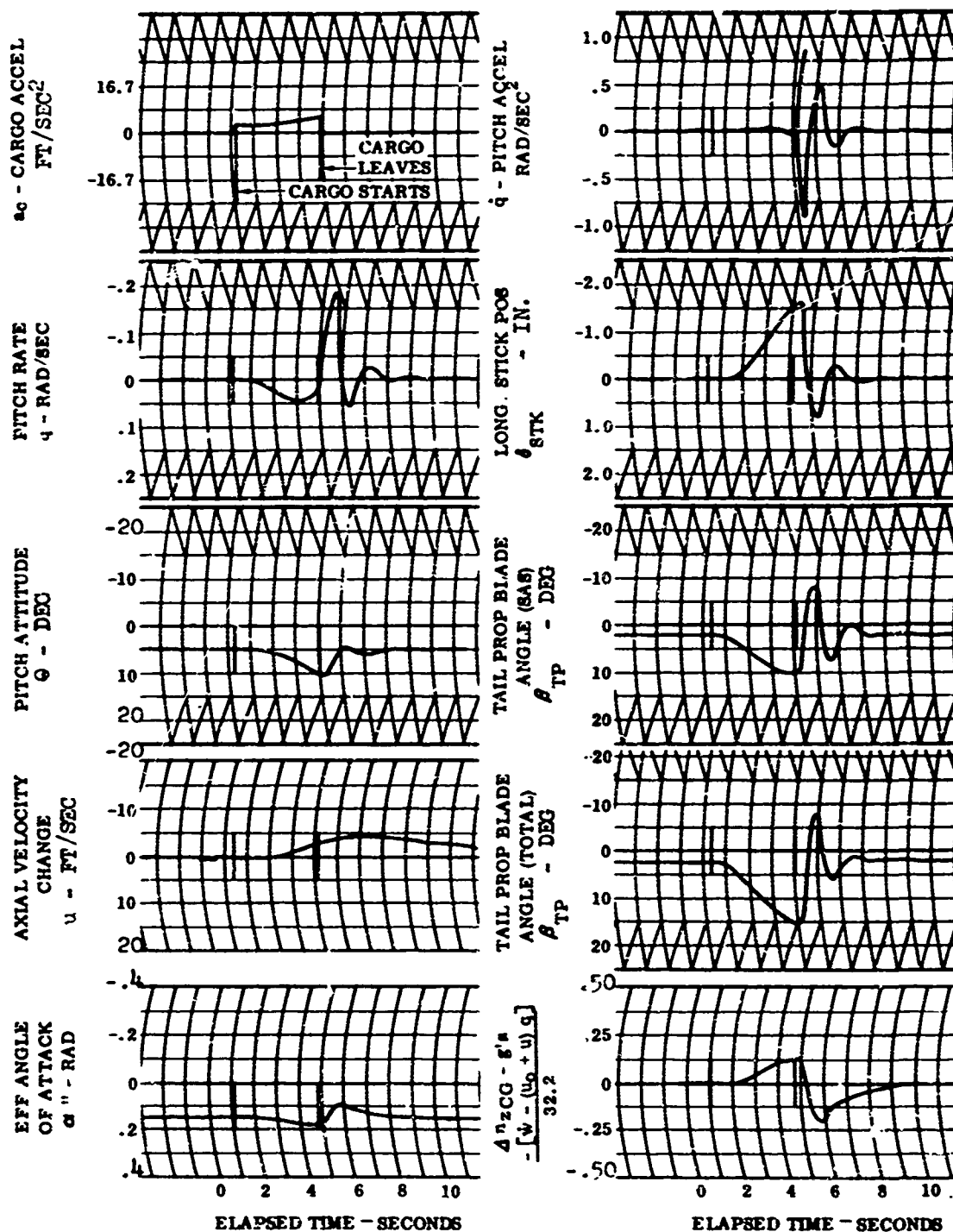


Figure 33. Analog Simulation Time Histories, $I_w/\delta_F = 5/38$, 8,000-Pound Gravity Drop, SAS On, Pilot in Loop

TWO-CHANNEL PITCH SAS OPERATION
 INITIAL CG POSITION = 21.8% MGC, $\theta_0 = 0^\circ$

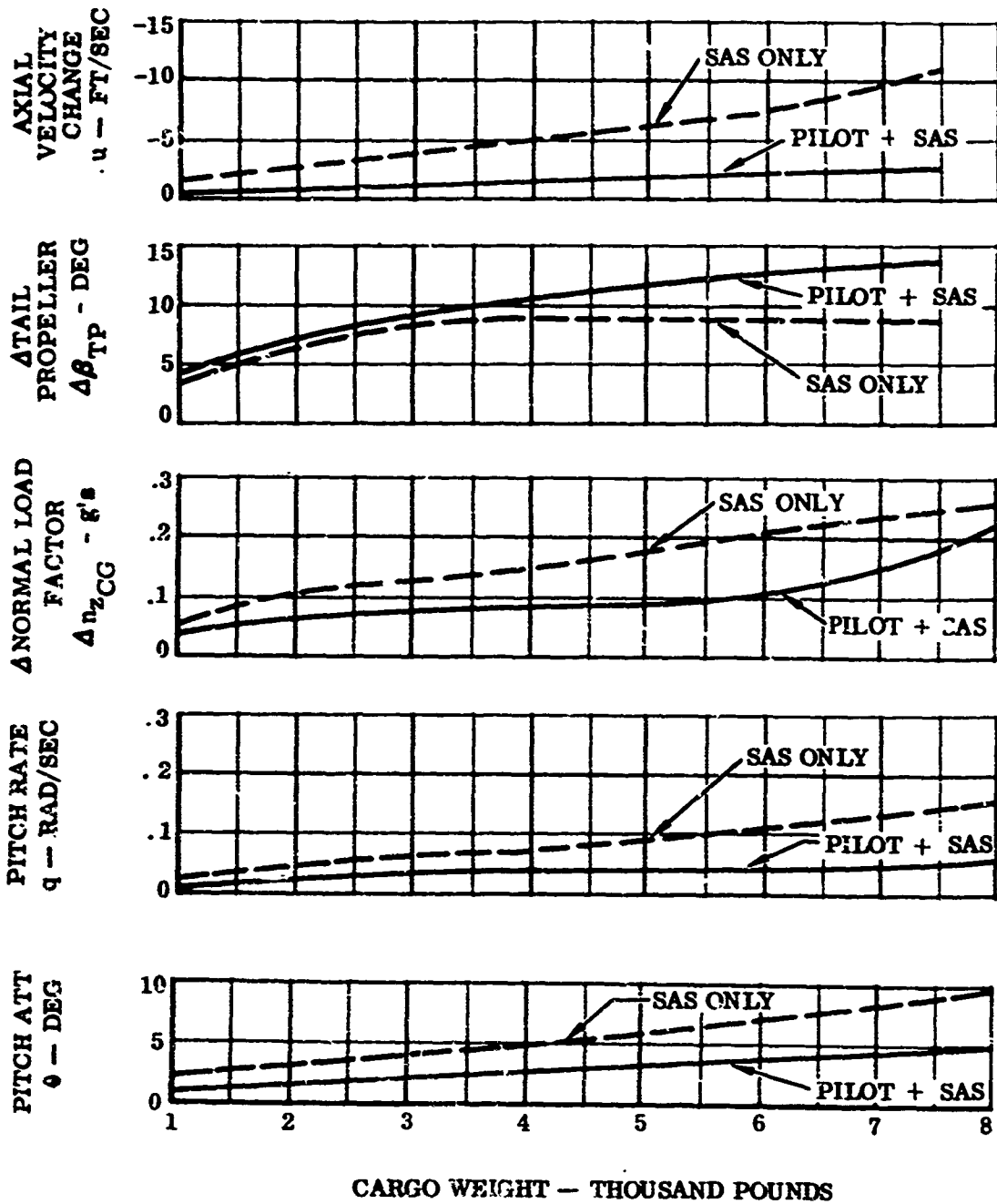


Figure 34. Peak Responses During Cargo Extraction, $l_w/\delta_p = 5/48$,
 Parachute Extraction Force = .25 x Cargo Weight

TWO-CHANNEL PITCH SAS OPERATION
 INITIAL CG POSITION = 21.6% MGC, $\theta_0 = 0^\circ$

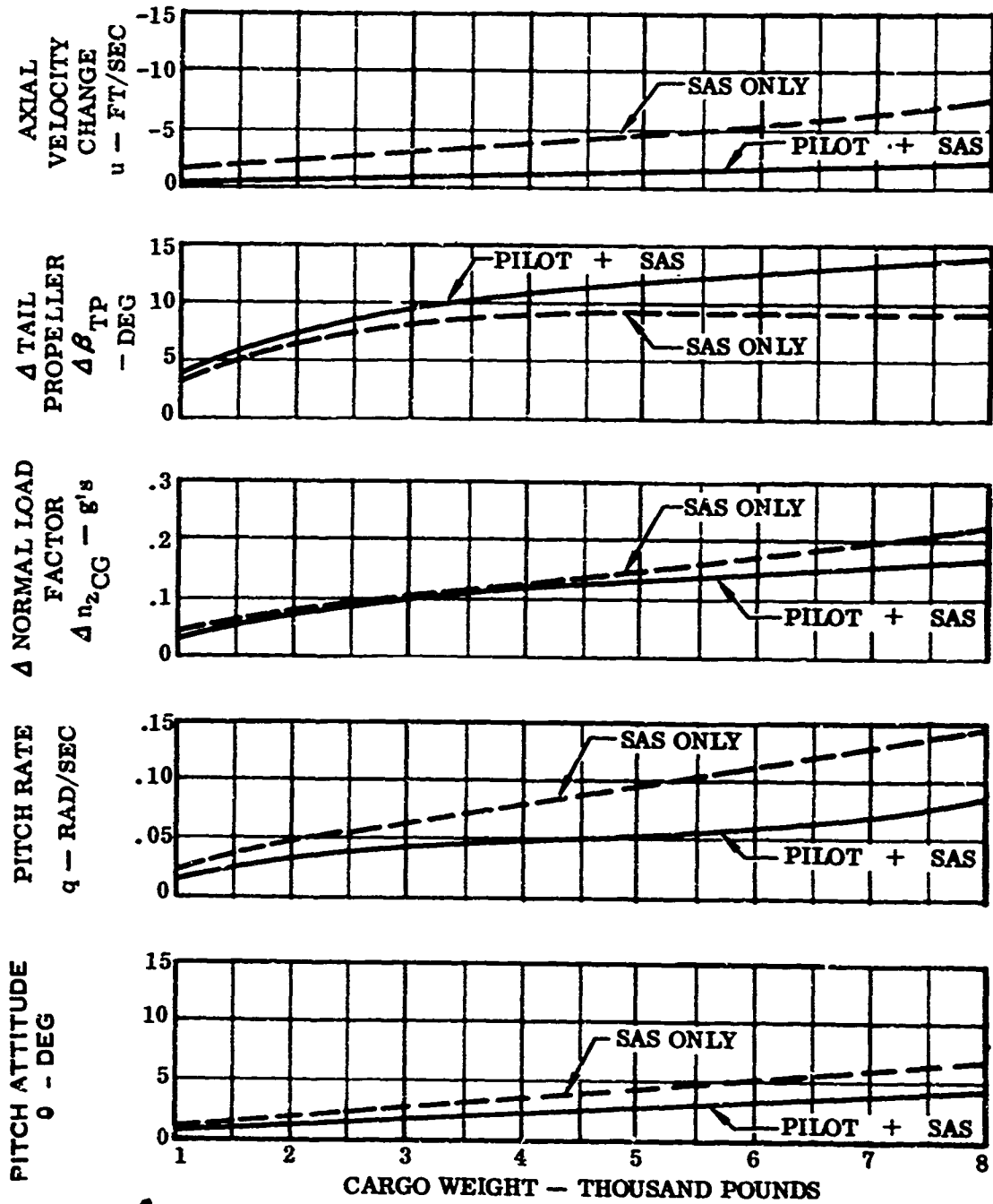


Figure 35. Peak Responses During Cargo Extraction, $i_w/\delta_F = 5/48$, Parachute Extraction Force = .50 x Cargo Weight

presents analog records of an 8,000-pound drop with pilot inputs. These data indicate that, with pilot inputs, no limiting flight condition will be encountered during the aerial delivery of the maximum payload from this configuration.

$i_w/\delta F = 5/48$ CONFIGURATION, $\theta_0 = 0^\circ$, PARACHUTE EXTRACTIONS

Figures 34 and 35 present peak values of airplane response during air cargo delivery with parachute extraction forces equal to 0.25 and 0.50 times the cargo weight, with and without pilot inputs. Figure 36 presents analog records of an 8,000-pound drop with pilot inputs. These data indicate that, with pilot inputs, no limiting flight condition will be encountered during the aerial delivery of the maximum payload from this configuration: however, as in the case of the 0/30 configuration, parachute extractions, no structural dynamics were included.

$i_w/\delta F = 0/30$ (TP ON AND OFF) CONFIGURATIONS, $\theta_0 = 0^\circ$, PARACHUTE EXTRACTIONS

Air cargo delivery at 130 knots was simulated on the analog computer with the airplane configured at 0° wing incidence and 30° flap setting. Parachute extraction was used as the method for getting the cargo out of the airplane. Drops were simulated with the SAS on and off, both with and without the pilot. The SAS-off conditions also represent tail propeller off. In conjunction with the analog study, a root locus analysis on the 0/30 configuration is presented in Appendix II.

Peak responses obtained in the analog study versus cargo weight are summarized in Figures 37 through 44. Figures 37 and 38 show the effect of the parachute extraction force on peak response and peak overshoot. Figures 39 and 40 show the effect of the addition of the pilot model to the system with a parachute extraction force = $0.25 \times$ cargo weight. Figures 41 and 42 are the same as Figures 39 and 40, except the parachute extraction force = $0.5 \times$ cargo weight. In Figures 43 and 44, the SAS pitch rate gain is two times nominal value and the parachute extraction force is $0.5 \times$ cargo weight.

Attempts to match flight test data for a 4,000-pound drop are presented in Figures 45 through 47. In Figures 46 and 47, K_{p_0} , the pilot gain, was programmed to go to zero after the cargo extraction. This was done in an effort to get the pilot model to move the stick realistically. The best of the three matches presented is Figure 47, which has double the nominal SAS pitch rate gain along with the programmed pilot.

Some typical time histories from the analog simulation of parachute extractions from the 0/30 configuration are presented in Figures 48 through 51. Figure 48 is an 8,000-pound drop with no pilot and the SAS turned off. Figure 49 is an 8,000-pound drop with the SAS on and K_{p_0} the pilot gain, programmed to zero after the cargo extraction. Figures 50 and 51 are similar time histories for 4,000-pound drops.

Figures 48 and 49 show that, theoretically, 8,000 pounds can be dropped satisfactorily from the 0/30 configuration. Pitch-up indicated (with the pilot and stability augmentation removed from the system) is only 14° ; with the pilot and SAS in the system, pitch-up is less than 5° . The airplane response in both cases appears to damp out quickly.

However, the above remarks must be qualified because of the discrepancies between flight test data and attempts to match same. Figure 47, as stated above, represents the closest match, but it represents an unrealistic configuration since the SAS pitch rate gain is twice the nominal value on the analog run. Before a more definite conclusion can be made, flight test data from the 4,000-pound drop, 0/30 configuration, must be matched.

One possible cause of the moderately damped oscillation encountered during a flight test drop of 4,000 pounds from the 0/30 configuration (see Figure 47) could be the coupling of the body bending modes with the airplane response modes through the SAS gyros. The analysis at this time does not include these effects. The root locus plot in Figure 50 suggests another change to the mathematical model which would produce better simulation of flight test data for this configuration. Increasing the SAS lags in Figure 50 would have an appreciable destabilizing effect on the theoretical short-period mode, thereby bringing it into agreement with flight test data.

AIRPLANE GROSS WEIGHT = 31,300 POUNDS, CG = 21.6% MGC

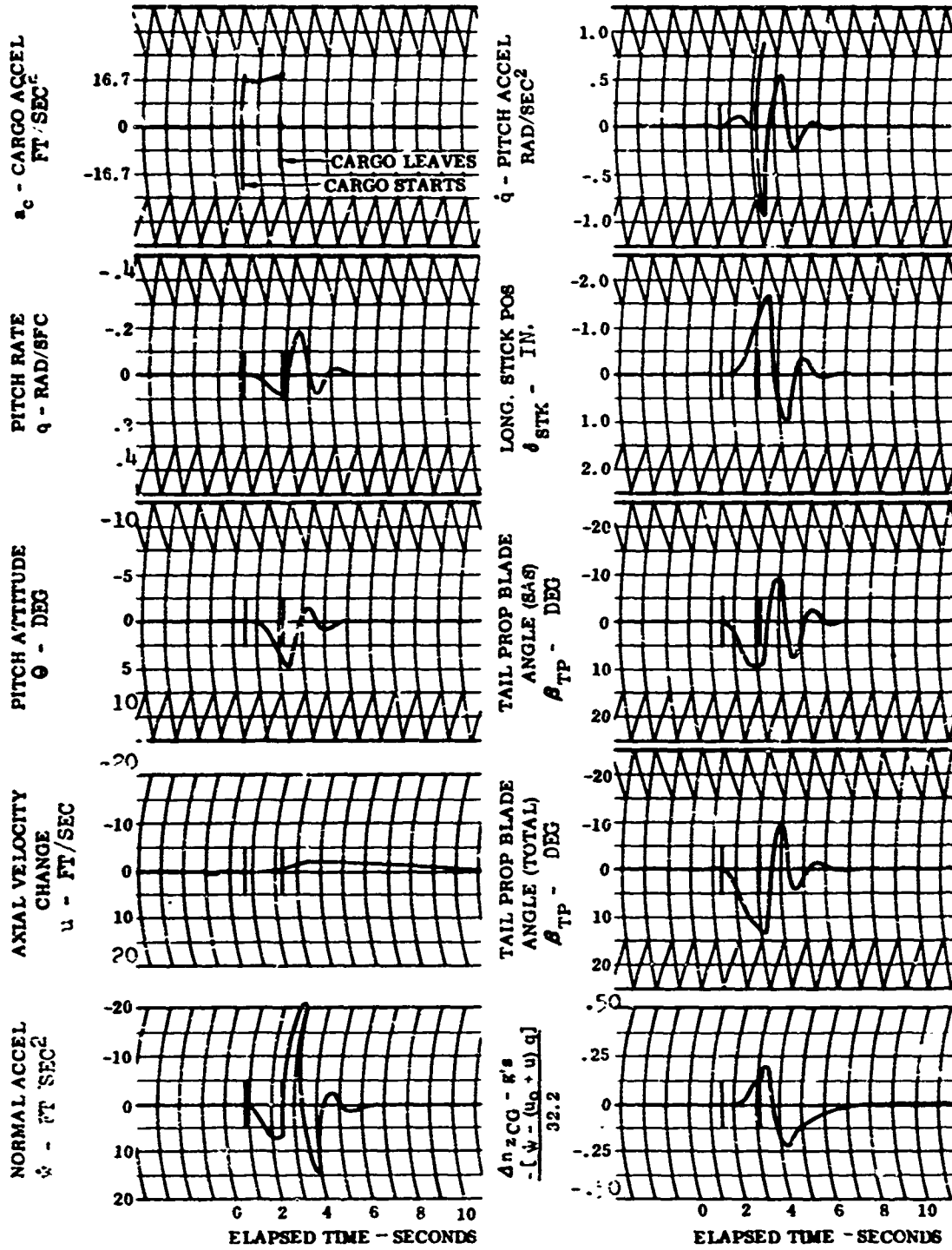


Figure 36. Analog Simulation Time Histories, $z_w/\delta_P = 5/48$, 8,000-Pound Drop, SAS On, Pilot in Loop, Parachute Extraction Force = .5 x Cargo Weight

AIRPLANE GROSS WEIGHT = 31,300 POUNDS
CG = 21.6% MGC

———— PARACHUTE EXTRACTION FORCE = .25 TIMES CARGO WEIGHT
- - - - - PARACHUTE EXTRACTION FORCE = .5 TIMES CARGO WEIGHT

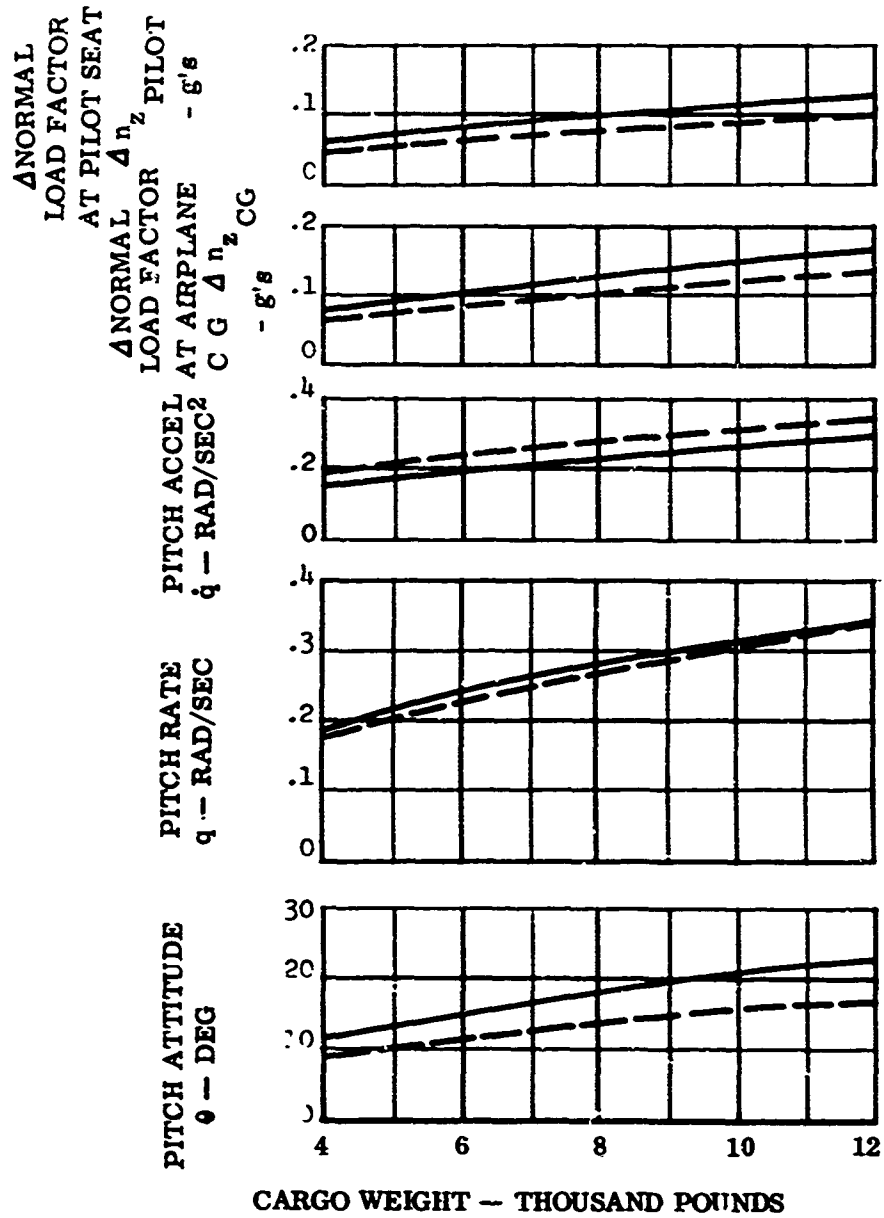


Figure 37. Effect of Parachute Extraction Force on Peak Responses During Cargo Extraction, $i_w/\delta_F = 0/3C$, SAS Off, Pilot out of Loop

AIRPLANE GROSS WEIGHT = 31,300 POUNDS
 CG = 21.6% MGC

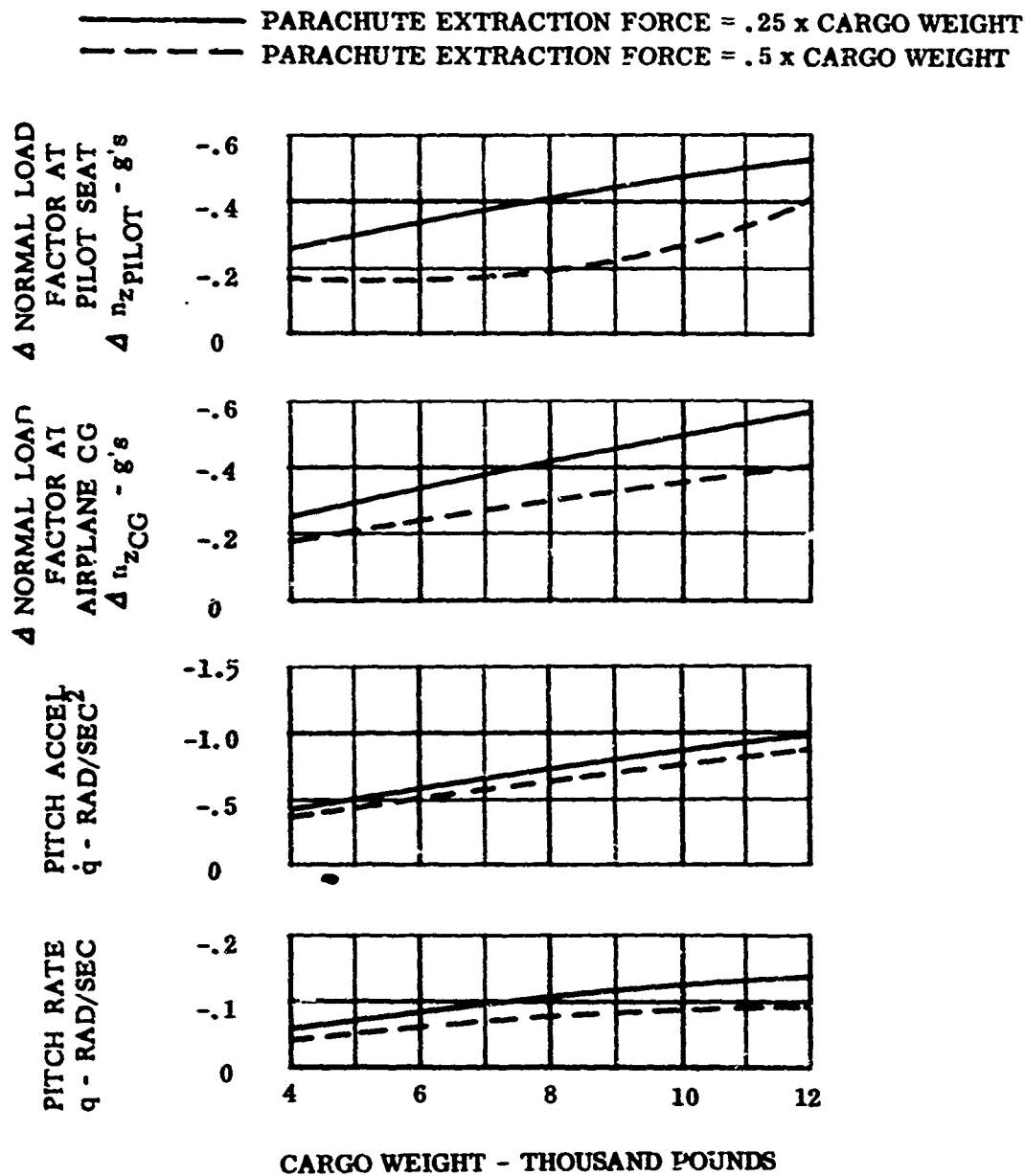


Figure 38. Effect of Parachute Extraction Force on Peak Responses After Cargo Extraction, $1/\delta_P = 6/30$, SAS Off, Pilot out of Loop

AIRPLANE GROSS WEIGHT = 31,300 POUNDS
 INITIAL CG POSITION = 21.6 % MGC
 TWO-CHANNEL SAS OPERATION

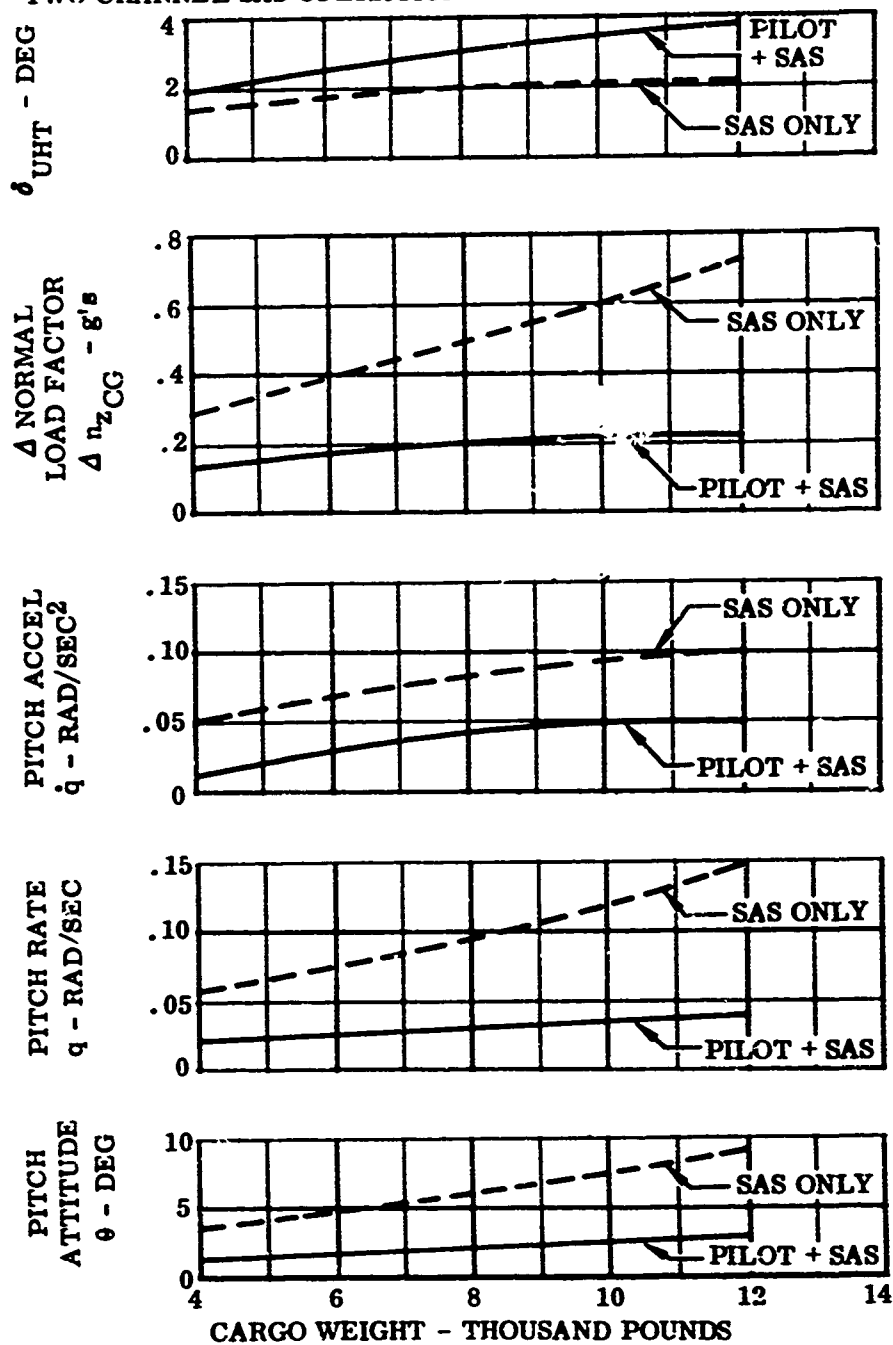


Figure 39. Peak Responses During Cargo Extraction, $i_w/\delta_F = 0/30$, Parachute Extraction Force = .25 x Cargo Weight

AIRPLANE GROSS WEIGHT = 31,300 POUNDS
 INITIAL CG POSITION = 21.6% MGC
 TWO-CHANNEL SAS OPERATION

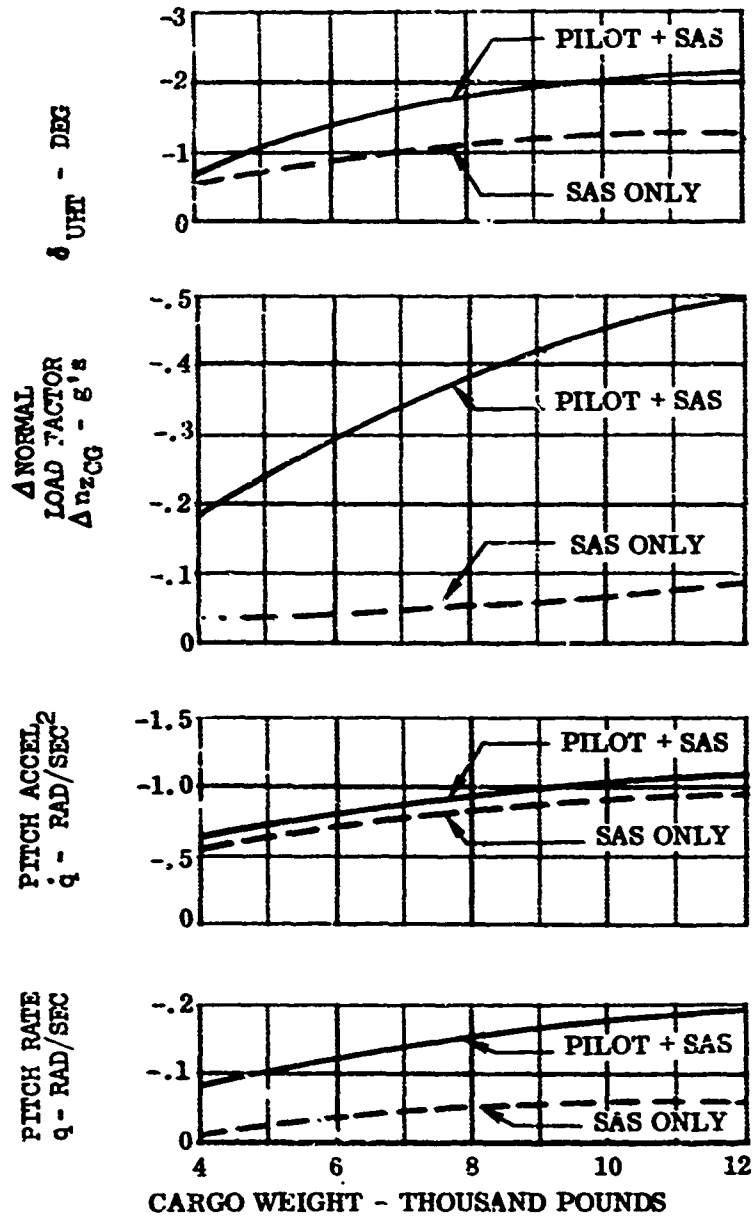


Figure 40. Peak Responses After Cargo Extraction, $i_v/\delta p = 0/30$, Parachute Extraction Force = $.25 \times$ Cargo Weight

AIRPLANE GROSS WEIGHT = 31,300 POUNDS
 INITIAL CG POSITION = 21.6% MGC
 TWO-CHANNEL SAS OPERATION

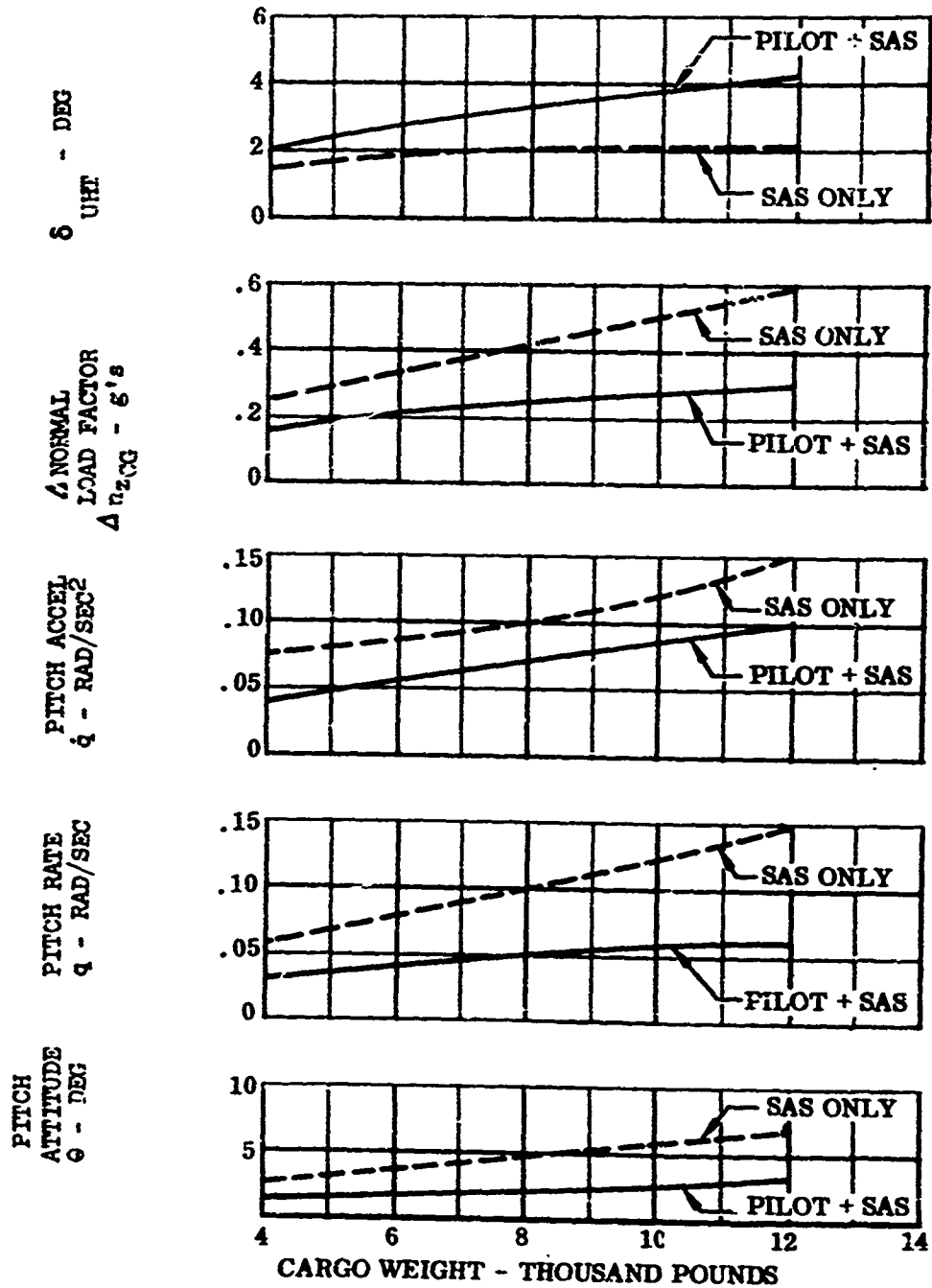


Figure 41. Peak Responses During Cargo Extraction, $i_w/\delta F = 0/30$, Parachute Extraction Force = .5 x Cargo Weight

AIRPLANE GROSS WEIGHT = 31,300 POUNDS
 INITIAL CG POSITION = 21.6 % MGC
 TWO-CHANNEL SAS OPERATION

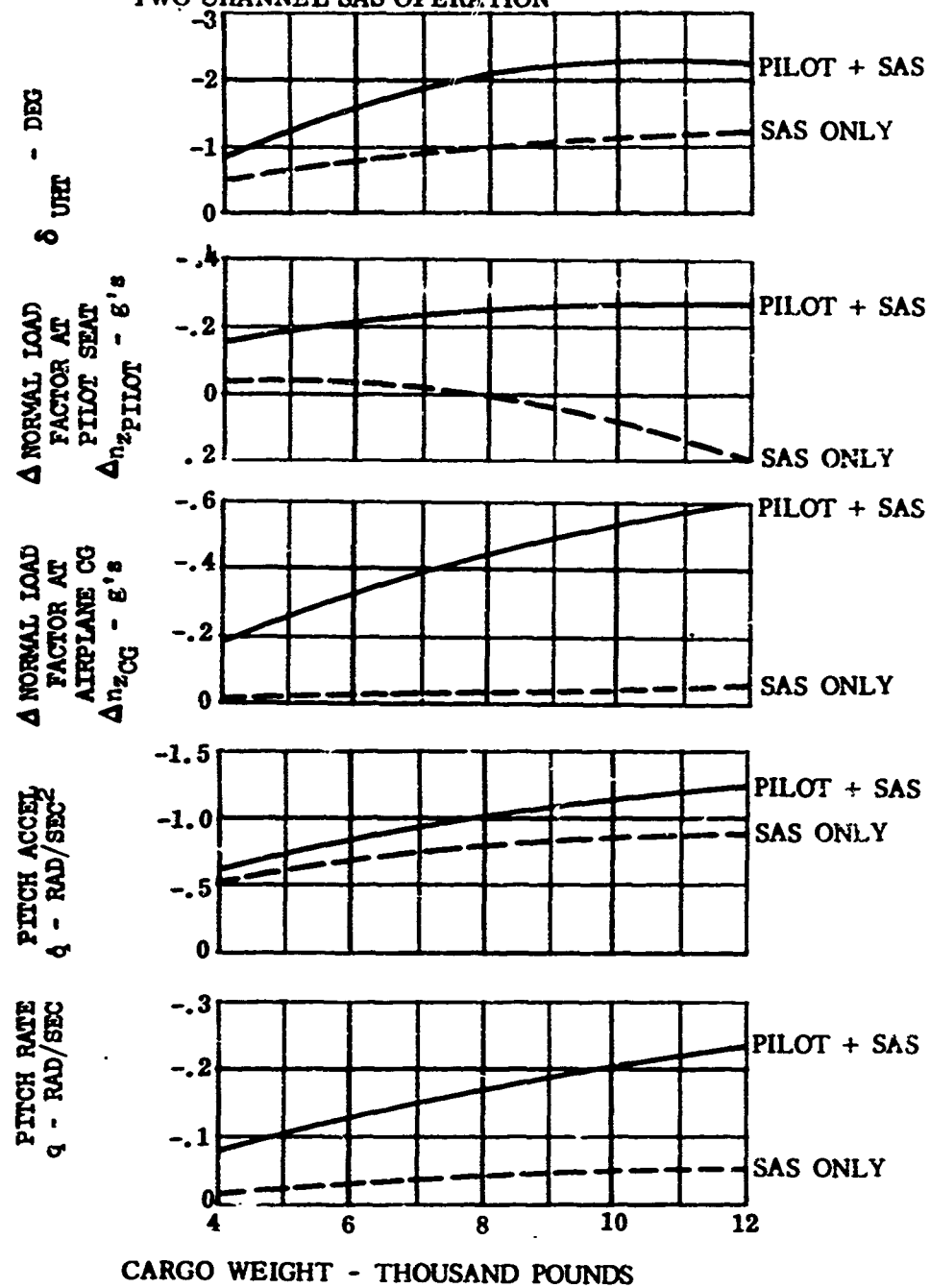


Figure 42. Peak Responses After Cargo Extraction, $i_w/\delta_F = 0/30$, Parachute Extraction Force = .5 x Cargo Weight

AIRPLANE GROSS WEIGHT = 31,300 POUNDS
 INITIAL CG POSITION = 21.6% MGC
 TWO-CHANNEL SAS OPERATION

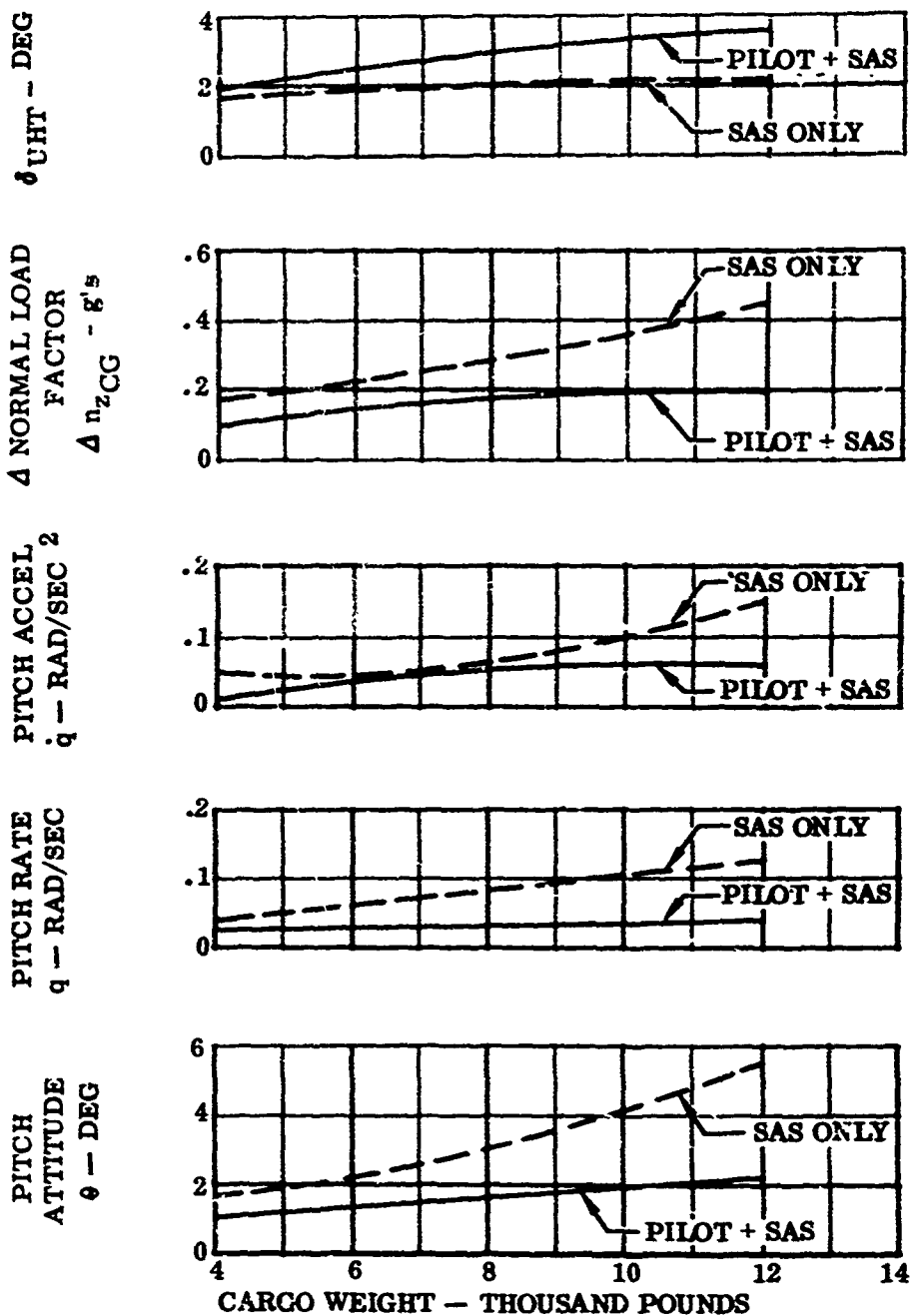


Figure 43. Peak Responses During Cargo Extraction, $i_w/\delta P = 0/30$,
 Parachute Extraction Force = .5 x Cargo Weight,
 $K_Q = 2 \times \text{Nominal Value} = -22.78$

AIRPLANE GROSS WEIGHT = 31,300 POUNDS
 INITIAL CG POSITION = 21.6% MGC
 TWO-CHANNEL SAS OPERATION

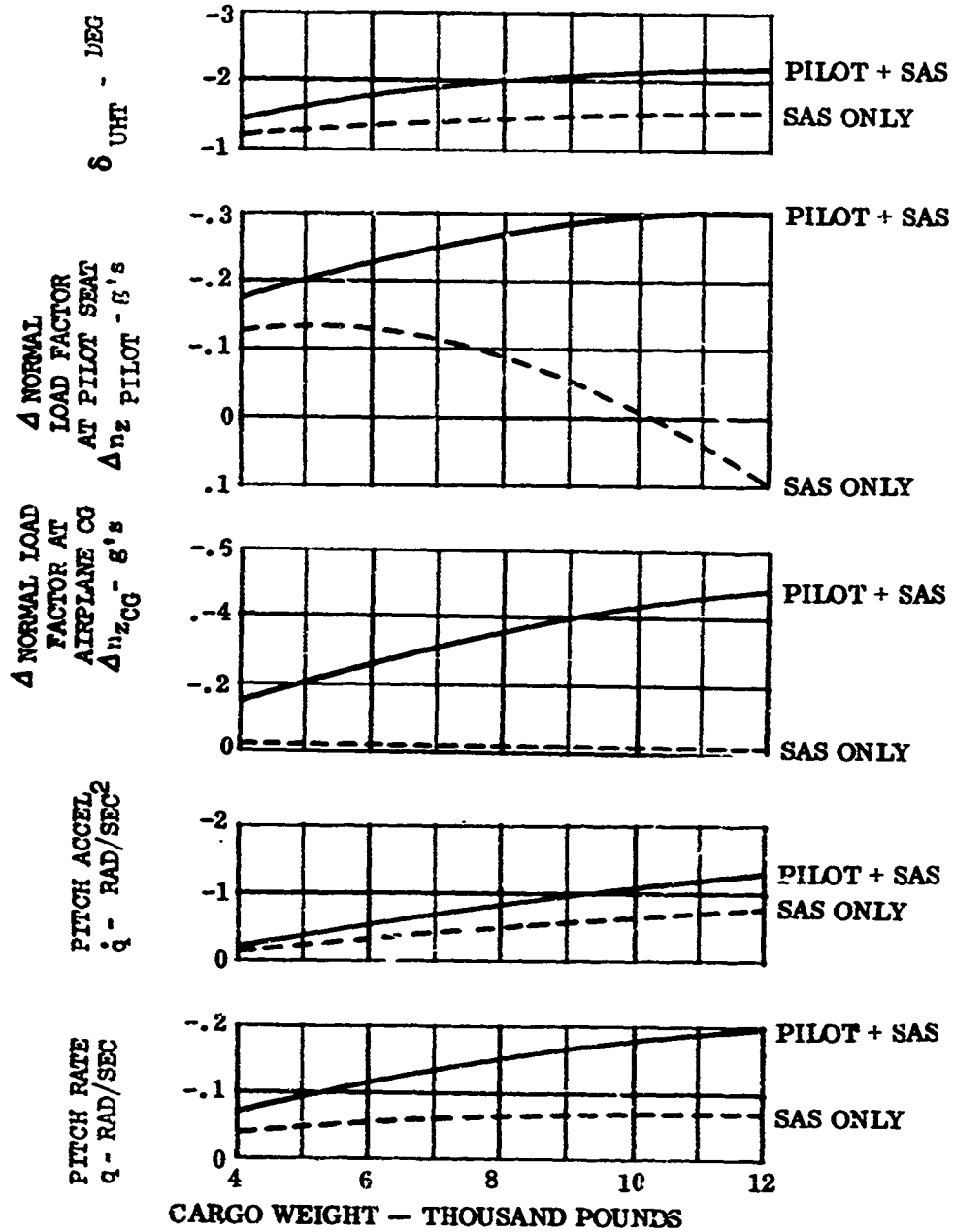


Figure 44. Peak Responses After Cargo Extraction, $i_v/\delta_F = 0/30$
 Parachute Extraction Force = .5 x Cargo Weight,
 $K_G = 2 \times \text{Nominal Value} = -22.78$

AIRPLANE GROSS WEIGHT = 31,300 POUNDS
 INITIAL CG POSITION = 21.6% MGC
 NOMINAL SAS GAINS

———— FLIGHT TEST DATA
 - - - - ANALOG DATA, $K_{P_\theta} = -45$, $\tau_L = 1.0$, $\tau_I = .5$

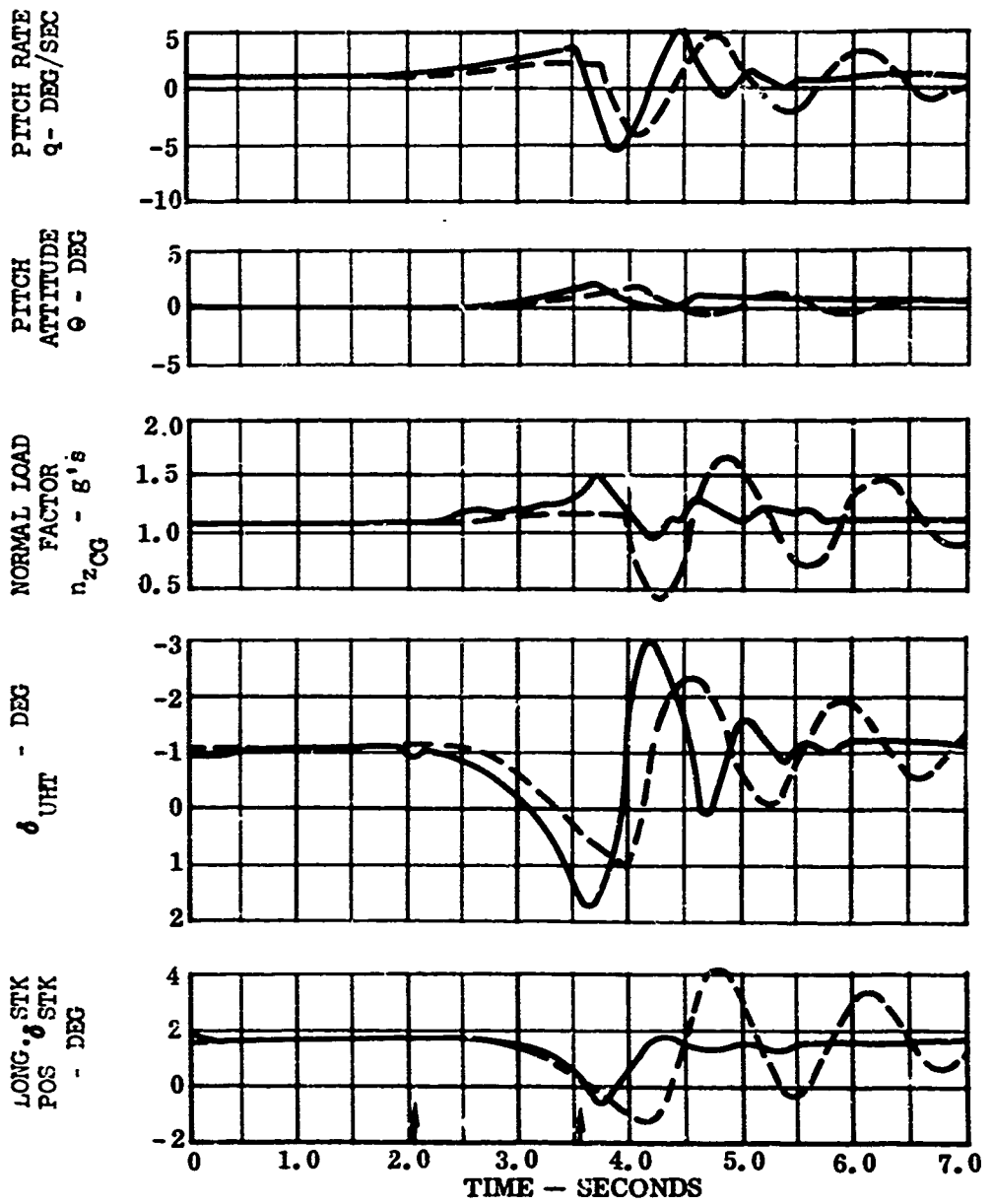


Figure 45. Response Matching, Flight Test Data Versus Analog Simulation Data, $i_w/\delta F = 0/30$, 4,000-Pound Drop, Parachute Extraction Force = .5 x Cargo Weight

AIRPLANE GROSS WEIGHT = 31,300 POUNDS
 INITIAL CG POSITON = 21.6% MGC NOMINAL SAS GAINS

———— FLIGHT TEST DATA
 - - - - ANALOG DATA, $K_{P_\theta} = -35$, $\tau_L = 1.0$, $\tau_I = .5$

NOTE: THE PILOT GAIN, K_{P_θ} , WAS PROGRAMMED TO GO TO ZERO AFTER THE CARGO EXTRACTION ON THE ANALOG DATA

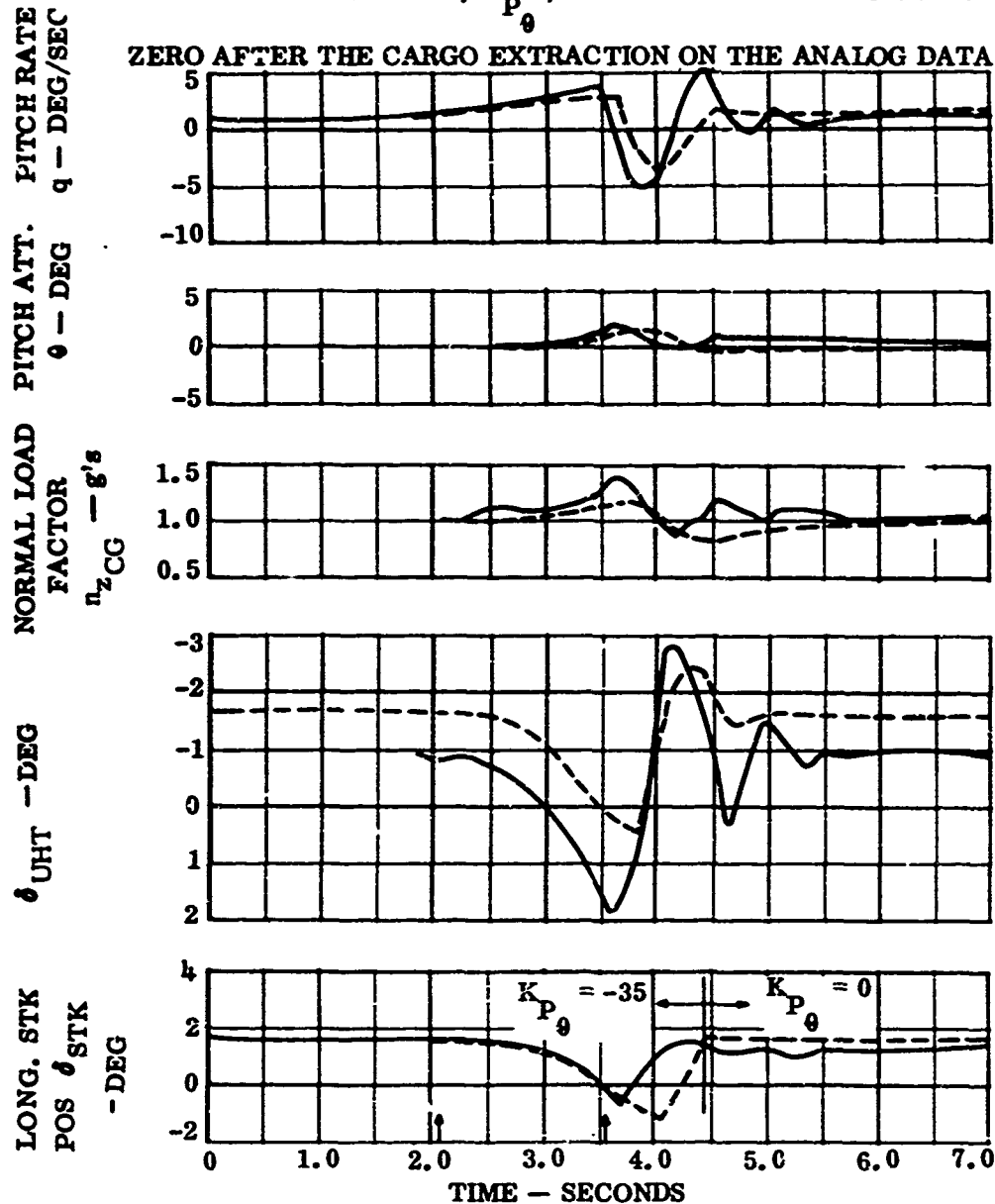


Figure 46. Response Matching, Flight Test Data Versus Analog Simulation Data, $i_w/\delta F = 0/30$, 4,000-Pound Drop, Parachute Extraction Force = .5 x Cargo Weight

AIRPLANE GROSS WEIGHT = 31,300 POUNDS
 INITIAL CG POSITION = 21.6% MGC , NOMINAL K_{θ}

— FLIGHT TEST DATA, NOMINAL K_{θ}
 - - - ANALOG DATA, 2 X NOMINAL K_{θ} , $K_{P_{\theta}} = -35$, $\tau_L = 1.0$, $\tau_I = .5$

NOTE: THE PILOT GAIN, $K_{P_{\theta}}$, WAS PROGRAMMED TO GO TO ZERO AFTER THE CARGO EXTRACTION ON THE ANALOG DATA

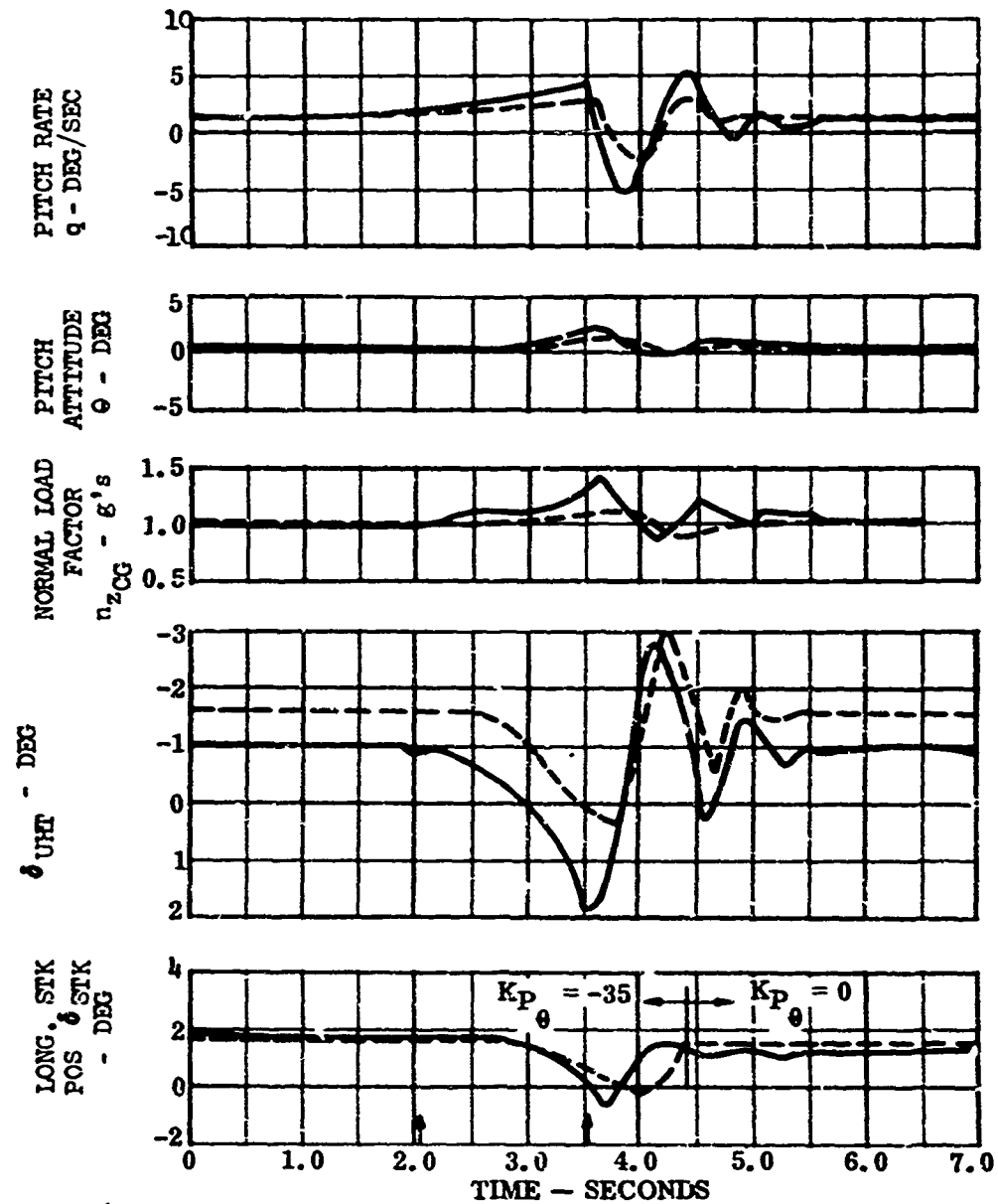


Figure 47. Response Matching, Flight Test Data Versus Analog Simulation Data, $1_v/\delta_F = 0/30$, 4,000-Pound Drop, Parachute Extraction Force = .5 x Cargo Weight

AIRPLANE GROSS WEIGHT = 31,300 POUNDS, CG = 21.6 % MGC

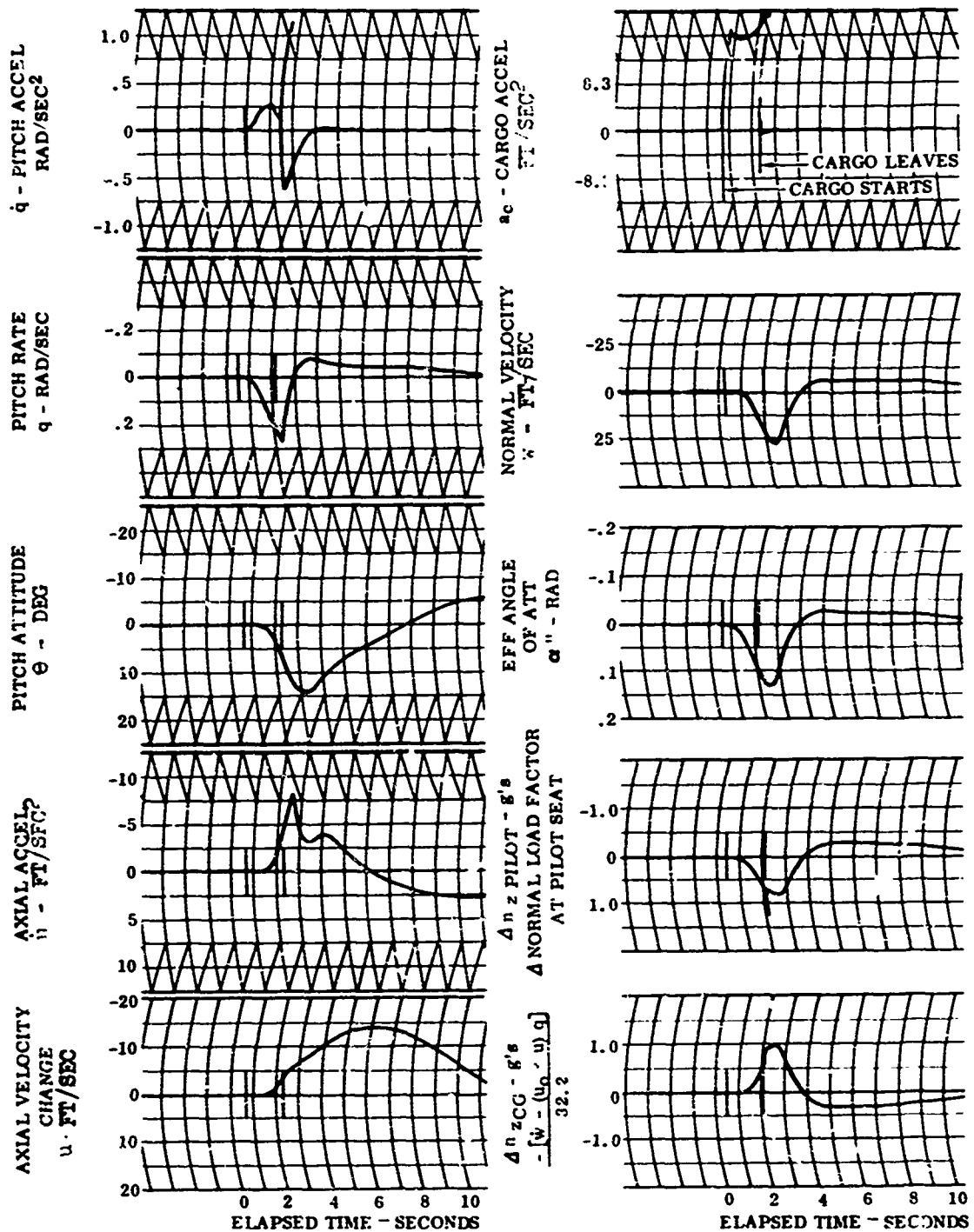


Figure 48. Analog Simulation Time Histories, $i_w/\delta_F = 0/30$, 8,000-Pound Drop, SAS off, Pilot out of Loop, Parachute Extraction Force = .5 x Cargo Weight

AIRPLANE GROSS WEIGHT = 31,300 POUNDS, CG = 21.6% MGC

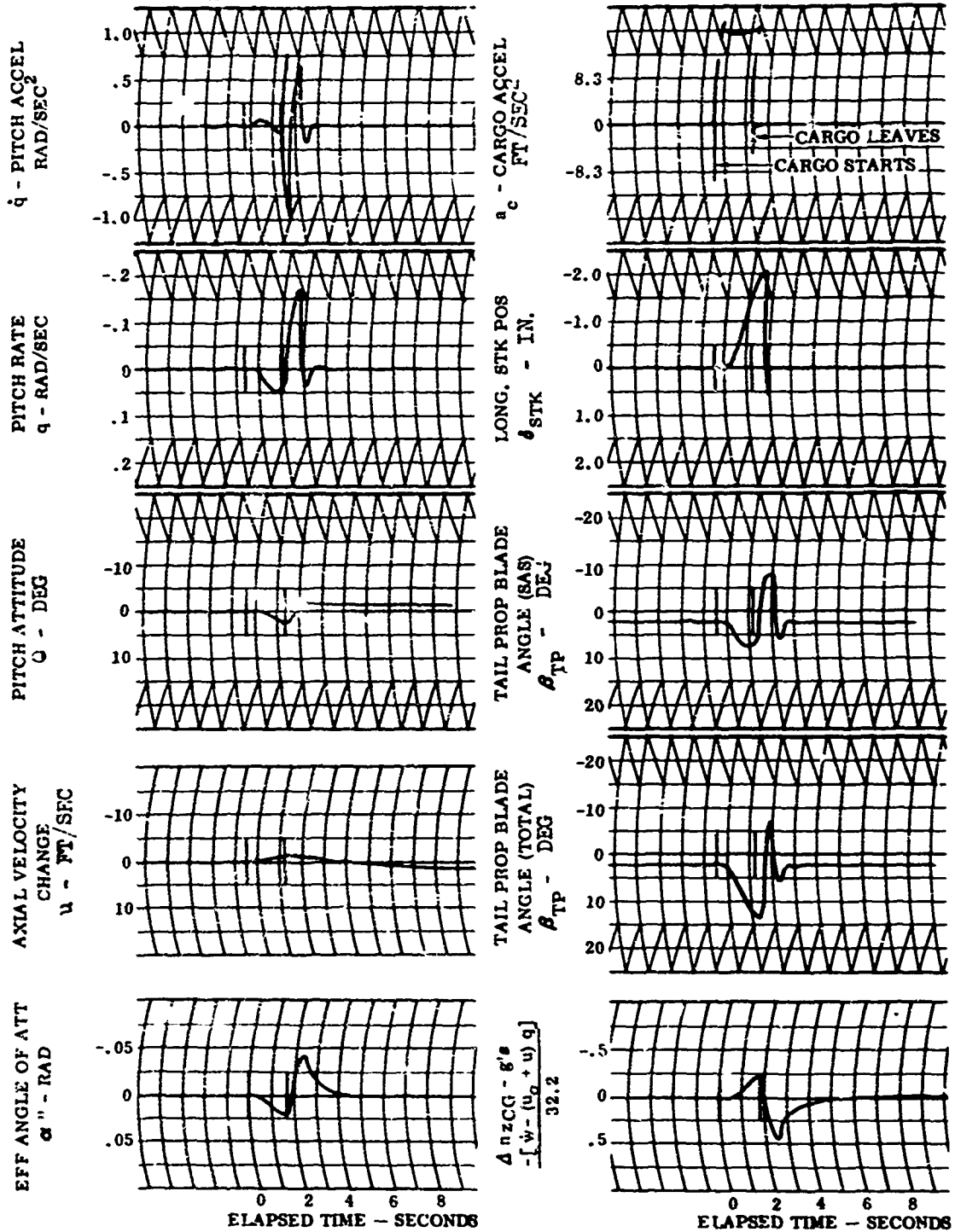


Figure 49. Analog Simulation Time Histories, $i_w/\delta_F = 0/30$, 8,000-Pound Drop, SAS on, Pilot in Loop, Parachute Extraction Force = .5 x Cargo Weight

AIRPLANE GROSS WEIGHT = 31,300 POUNDS, CG = 21.6 % MGC

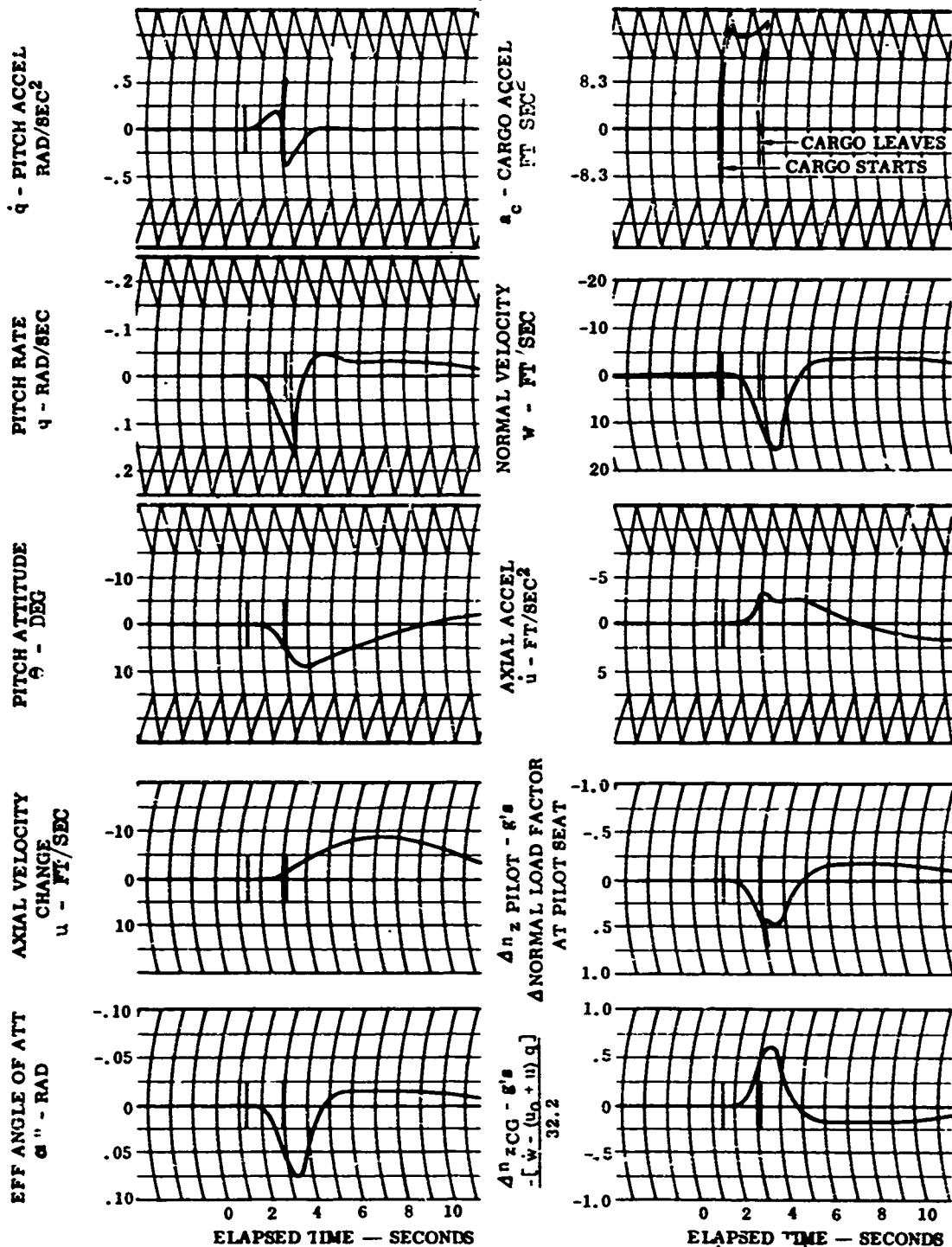


Figure 50. Analog Simulation Time Histories, $1_w/\delta_F = J/30$,
 4,000-Pound Drop, SAS off, Pilot out of Loop,
 Parachute Extraction Force = .5 x Cargo Weight

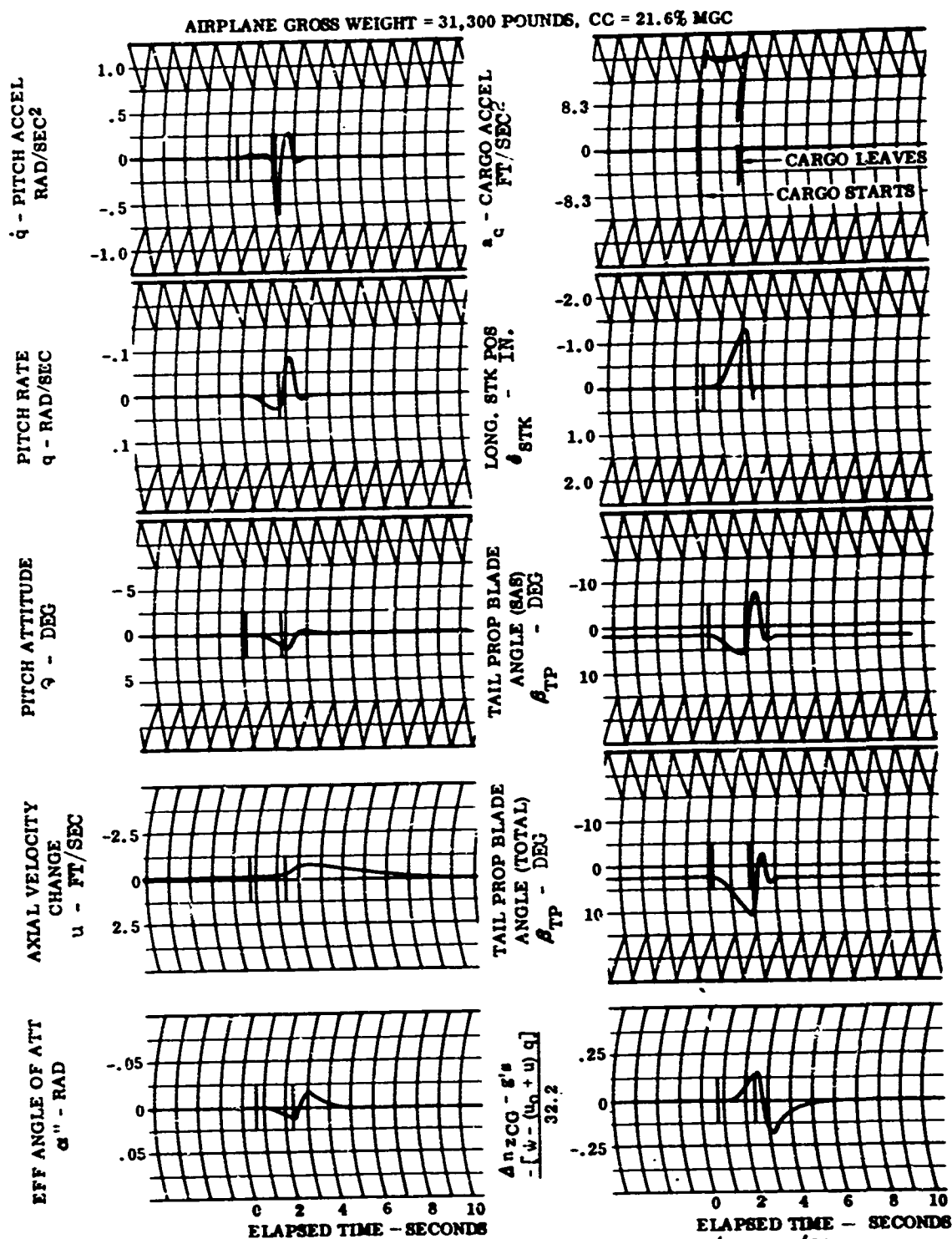


Figure 51. Analog Simulation Time Histories, $i_v/\delta_F = 0/30$,
 4,000-Pound Drop, SAS on, Pilot in Loop,
 Parachute Extraction Force = .5 x Cargo Weight

RESULTS AND DISCUSSIONS

The XC-142A airplane has demonstrated, in flight, its capability to safely air-drop individual cargo weights of up to 3,000 pounds in hover and at 30 knots. There is not enough longitudinal control power at these speeds to statically balance the airplane's maximum payload (8,000 pounds) as it rolls out of the airplane. This study indicates that individual payloads of 8,000 pounds can be air-dropped, but the pilot will have to accept pitch-up after, or while, using the available longitudinal control power. Pitch-up will not be excessive if the cargo leaves the airplane quickly (within 3 seconds from the time it is released). Air-drop demonstrations with the XC-142A airplane proved the feasibility of quick gravity rollout and delivery. A chart of cargo roll-out time versus airplane attitude, from flight tests, is shown in Figure 52. Pictures of air delivery equipment and flight demonstrations from these tests are shown in Appendix III.

Studies of the pilot equation indicate the importance of pilot gains during this type of aerial delivery. During the roll-out portion of a delivery, the pilot should anticipate changes in pitch attitude and react to them strongly in order to hold down pitch-up. To improve stability after the cargo has left the airplane, he should reverse his attitude and allow the SAS and airframe dynamics to dampen the resulting oscillations.

Without SAS, the XC-142A airplane is dynamically unstable in hover and the low-speed portion of transition. SAS gains, displacement, and rate were all optimized during the development of the airplane for desirable flying qualities. The longitudinal SAS plays a strong role in stabilizing and controlling the airplane during an air drop; hence, the effect of individual SAS parameters are considered herein. Increasing the SAS gains K_2 and K_0 tends to reduce the airplane's pitch-up during the roll-out portion of delivery; however, there is little change due to adding gains K_3 and $\int \theta$ to the system. The stick pick-off gain, $K_{\delta_{STK}}$, assists in keeping the SAS from saturating (hitting its stops) during maneuvers resulting from pilot inputs, since in many cases the SAS is damping the motions imposed by the pilot. During an air drop, both the SAS and the pilot are opposing the airplane pitching moment created from the cargo's sliding out; therefore, the stick pick-off gain actually assists in saturation during an air drop. The effect of increasing the longitudinal SAS authority from its design value of ± 1.0 inch of travel is effectively replacing the pilot's control with SAS authority. Increasing the SAS rate capability from its design value of 1.7 inches/second has little effect, as the present rate capability is sufficient to keep up with the pitch rate and attitude gyro commands during an 8,000-pound drop. These studies indicate that the existing SAS parameters are adequate for air-drop missions. Their selection and optimization were based on the complete airplane mission throughout transition, and any change based on air drops would be impractical.

CARGO
WT - LB
2000
3100
1605
1950
3100

2070
500

1000

CARGO STOWED
POS - F S
300
300
350
300

235
350

235

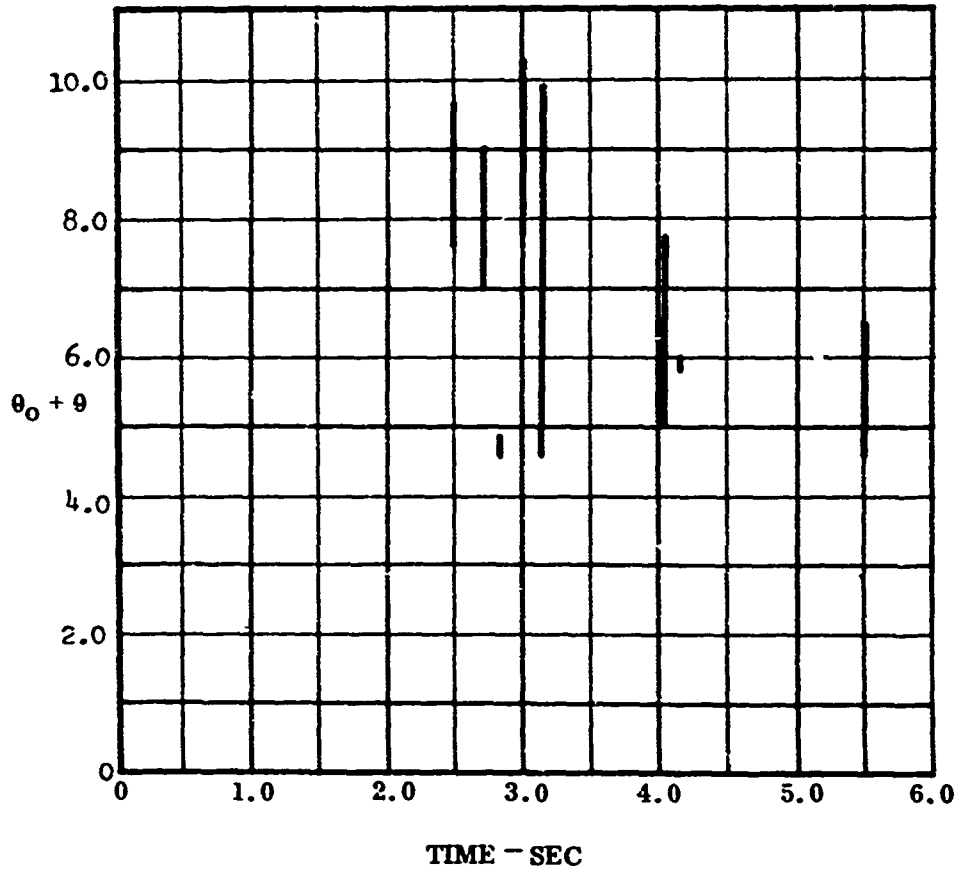


Figure 52. Cargo Roll-Out Time After Release Versus Airplane Attitude During Drop - Flight Test Air Delivery Demonstration

Obviously, the most effective way to improve the airplane's air-drop capability is to increase the total longitudinal control power through increasing the tail propeller total thrust. This study shows beneficial results from percent increases in the longitudinal effectiveness parameter Mg^* , which is obtained by increasing the tail propeller size or by increasing the degrees of blade angle change per inch of control linkage travel.

The peak airplane responses from air-dropping the maximum payload versus velocity are shown in Figures 53 and 54. Also shown are the peak responses of the airplane during the pitch-up during cargo rollout and the pitchdown after the cargo leaves the airplane. These pitch response characteristics with pilot are from the low gain pilot (K_{p0}) established from a response match of the flight test drops. These data indicate that it is feasible with a human pilot (who would be capable of changing his gains readily) to air-drop the 8,000-pound payload throughout the transition flight regime.

The normal operating CG limit of the XC-142A airplane is 15% to 28% MGC. A 31,300-pound airplane (less cargo) with a mid-CG of 21.5% MGC or fuselage station 266.27 could have an 8,000-pound cargo loaded forward to fuselage station 235 or aft to 298 without exceeding these limits. The end of the cargo ramp is at fuselage station 537.5; hence, the cargo will travel approximately 25.2 or 20 feet, respectively, to leave the airplane. Regardless of the initial stowed position, the tail propeller cannot balance an airplane CG aft of approximately 45% MGC in hover and the lower speed flight modes at zero pitch attitude. This CG occurs with an 8,000-pound cargo at fuselage station 378 for the above-mentioned airplane.

The airplane's pitch attitude is the most important parameter in a gravity drop. Flight demonstrations have shown that the pilot will inadvertently permit pitch attitude changes, from not knowing when the cargo starts from its stowed position, by as much as 5° from a 3,000-pound gravity drop. Controlling the airplane's pitch attitude is the pilot's responsibility up until he reaches the forward stick limit, at which time he accepts the pitch-up and controls any wing buffet from high effective angles of attack with the addition of power.

The coefficient of friction between the cargo and type of conveyors, shown in Appendix III, has not been established precisely; however, from flight test results it appears very small, less than the friction that would be overcome by a pitch attitude change of 2.0° .

The parachute and gravity methods of cargo extraction have been demonstrated in flight with a high degree of success. Improvements to these and other ways of extracting cargo, including a short stroke actuator, ground extraction forces, and a conveyor belt extraction system, were simulated. All of these methods are beneficial in helping to get the cargo out quickly and in keeping the pitch attitude down; however, they add weight and complexity to the air-drop system used in the XC-142A.

AIRPLANE GROSS WEIGHT = 31,300 POUNDS
 INITIAL CG POSITION = 21.6% MGC
 TWO-CHANNEL PITCH SAS OPERATION

SYMBOL	TYPE DROP
O, Δ	GRAVITY
\circ , \triangle	EXTRACTION

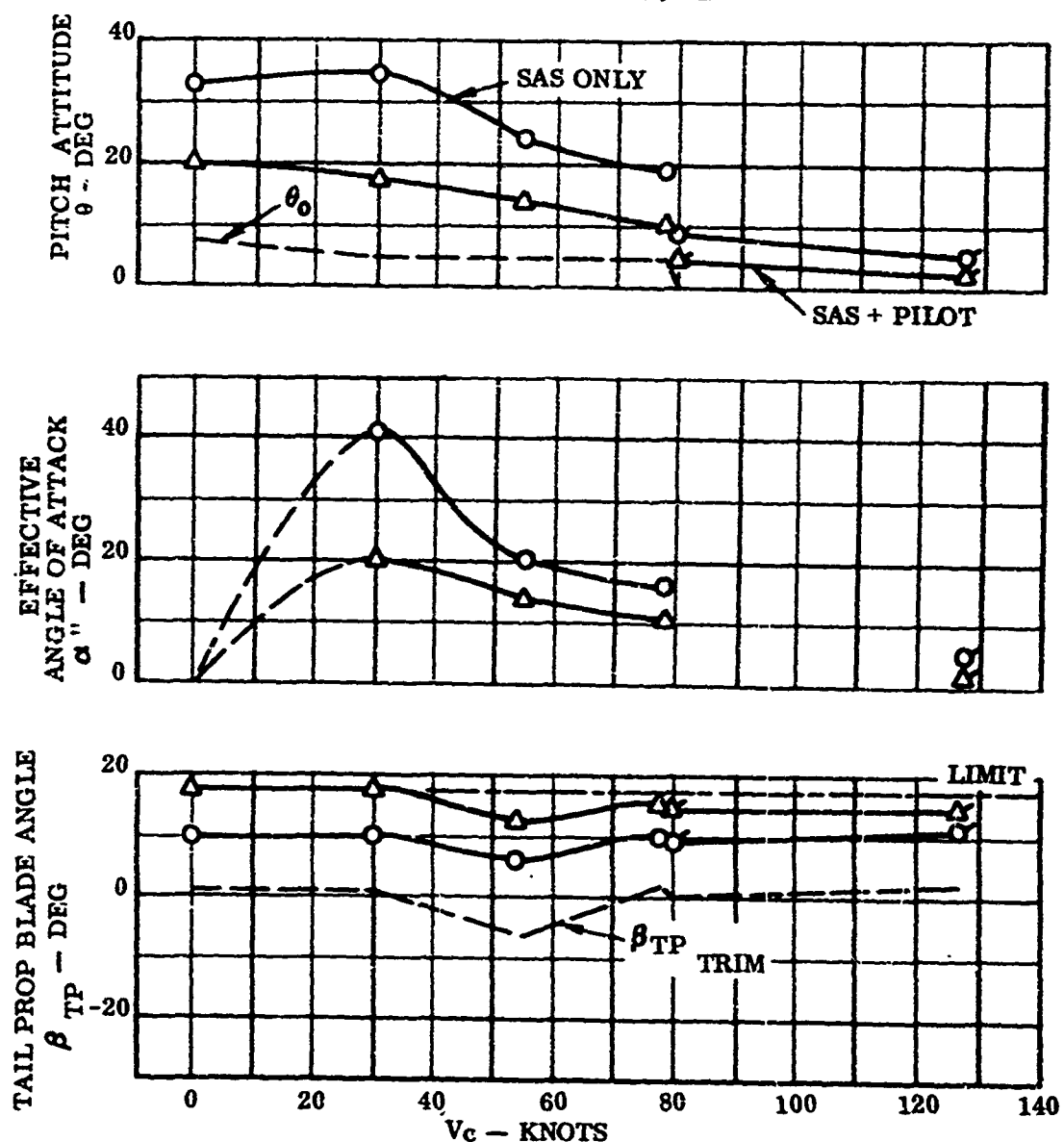


Figure 53. Peak Simulation Response Characteristics During an 8,000-Pound Cargo Drop

AIRPLANE GROSS WEIGHT = 31,300 POUNDS
 INITIAL CG POSITION = 21.6% MGC
 TWO-CHANNEL PITCH SAS OPERATION

SYMBOL	TYPE DROP
○, Δ	GRAVITY
◊, △	EXTRACTION

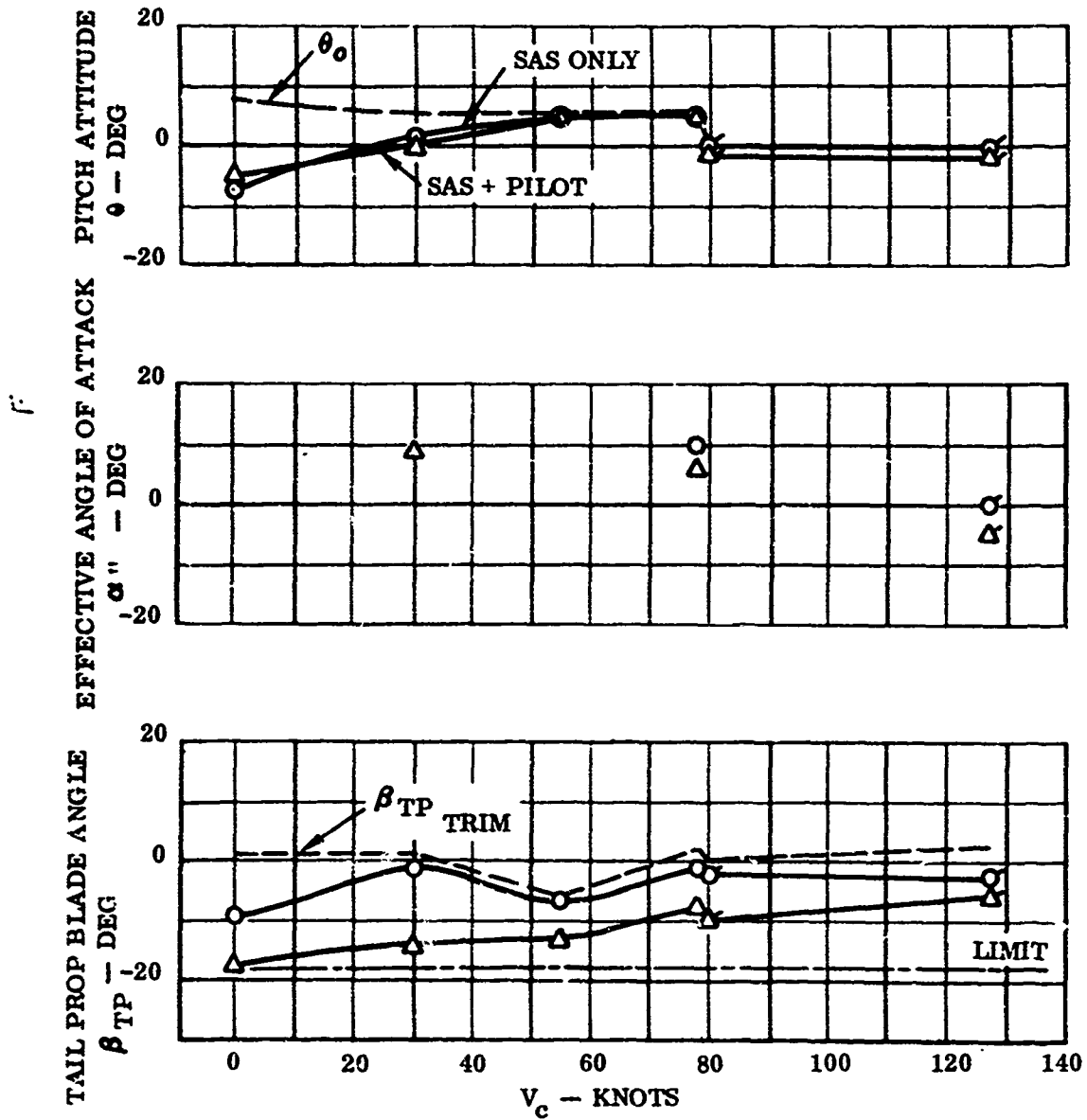


Figure 54. Peak Simulation Response Characteristics After an 8,000-Pound Cargo Drop

CONCLUSIONS

The XC-142A airplane, with proper pilot techniques, has the capability to air deliver the airplane's maximum payload (8,000 pounds) in hover and transition flight. The only restriction is that portion of the operational envelope restricted because of ground effects.

Flight test data from the O/30 configuration (tail prop on) were not matched satisfactorily on the analog computer. Structural dynamics effects should be added to the mathematical model for better simulation. A reduction in the SAS pitch rate gain improves the longitudinal dynamic stability for this configuration.

The XC-142A longitudinal control power is sufficient to statically balance a 4,000-pound cargo weight on the cargo ramp in the hover mode. This analysis is concerned with the dynamic response of the airplane during and after aerial delivery; it is not intended to be a safety-of-flight study concerned with emergency conditions resulting from large cargo weights lodged in the tail of the aircraft. If a criterion for air drops necessitates longitudinal control power to balance aft CG positions with cargo on the tail gate, then more control power is necessary to extend the cargo weight envelope from the recent flight test program.

In consideration of pilot handling qualities for V/STOL-type aircraft, the optimum design for an air drop system is one in which the SAS actuator saturation time equals the cargo extraction time. This can be accomplished with shorter extraction times through use of a different delivery system or by giving the present SAS actuators more authority.

The following conclusions pertain to the pilot model used:

- a. To make the pilot model (Reference 1) move the stick as real pilots did in flight test air drops, it was necessary to vary the pilot gain, $K_{p\theta}$, during the air drop simulation.
- b. Further suggestions for obtaining realistic pilot dynamics include feeding back the normal load factor at the pilot's seat and the longitudinal velocity perturbation, u , to the pilot inputs.
- c. As a servomechanism trying to control air cargo delivery in the XC-142A, the pilot model should possess the following traits: To hold down pitch-up during cargo extraction, the pilot model should anticipate changes in pitch attitude and react to them strongly. To improve stability after the cargo has left the airplane, the pilot model should reverse attitude. The pilot model should not anticipate and should become relatively passive toward pitch attitude perturbations.

The XC-142A airplane propeller slipstream prohibits the aerial delivery of personnel during the hover mode near the ground.

REFERENCES

1. McRuer, Duane; and Graham, Dunstan, "Pilot-Vehicle Control System Analysis," AIAA Paper No. 63-310, 1963
2. Booth, George C., "Flight Control System Simulator Equations for the Computer Simulation," LTV Vought Aeronautics DIR No. 2-53310/210-207 (S&C-77), 18 September 1963
3. Wilson, J. W.; Cartwright, E. O.; and Bialock, D. F., "Model XC-142A Aircraft Category I Aerial Delivery Test Program," LTV Vought Aeronautics Report No. 2-59110/6R-6079, 4 August 1966

APPENDIX I

ENVIRONMENTAL CHARACTERISTICS OF XC-142A PROPELLER SLIPSTREAM IN GROUND EFFECT FOR HOVER AND LOW TRANSITION FLIGHT SPEEDS

This appendix presents the flight test experience on propeller slipstream characteristics relative to man's ability to work and move near the airplane during hover and low-speed transition. During Category II flight tests at Edwards Air Force Base, the XC-142A propeller slipstream characteristics relative to a man (on foot or operating a jeep) and to an H-21 helicopter in close proximity to the airplane were evaluated. Comments of the personnel involved are presented below as a qualitative evaluation of the propeller slipstream environment. Also, during this flight, the initial rescue evaluation was conducted with a line and rescue sling (horse collar) through the airplane forward escape hatch.

Comments by Ground Observer (Major E. Larsen) During Propeller Slipstream-Downwash Evaluation

"The XC-142A initially established a 2- to 5-foot hover over the center of a large concrete apron of at least 500 by 800 feet. The apron was basically clean except for a few pebbles and small rocks. These were immediately blown clear and had no effect during the evaluation. No dust was present during this test in the vicinity of the hovering aircraft. Some slight dust activity was noted off the apron; however, this was negligible at all times.

"The ground observer's outer clothing consisted of a flight suit, combat boots, flight gloves, flight helmet with a cloth dust cover over the visor, and a pair of clear, soft plastic safety/dust goggles. The dust cover on the helmet did not come off during the test, but during portions of the evaluation the front zipper of the flight suit unzipped due to the continual flapping of the suit. The goggles were quite useful and comfortable. Without them, it is felt that maneuvering in this downwash environment would be extremely uncomfortable and possibly even restrictive due to the high velocities. Operations with the flight helmet visor down were not evaluated during this test. This should be the next step in the complete evaluation of downwash environment.

"As the aircraft hovered at 2 to 5 feet, I approached from about a 45° angle to the left of the open cargo ramp. This was done at a walk or a slight trot. Approach from this angle was characterized by turbulence from all directions but mainly from the front of the aircraft. Approach was easier than expected until about 10 feet from the ramp. At this point, downwash from the front of the aircraft became severe and

tended to push me back. Once I had turned my back and started away from the aircraft, it was very difficult to keep my balance and prevent myself from taking many undesired "giant steps." This can be attributed to body position since I would lean forward approaching the aircraft (helping maintain my balance) while I would have to lean backward during departure (hindering my balance). Subsequent departures were generally made either backing away or in a slight "run." An approach from directly aft of the aircraft was attempted and soon given up. Velocities were too strong to allow approach from this direction. It is estimated that I got about 20 to 30 feet from the cargo ramp before I was unable to proceed any further. Body angle during this approach was about 45° to the vertical. Upon departing, the tendency was definitely to be blown down. Crouching minimized this tendency. An approach perpendicular to the fuselage aft of the wing was made and appeared to be the easiest until about 10 feet from the fuselage. At this point, downwash from the front of the aircraft became severe and tended to blow me sideward toward the rear of the aircraft. Once this movement had started, it was almost impossible to stop and definitely impossible to reverse. I believe that if there were something for me to grab (extended bar or railing), I could approach the aircraft from the 45° angle at a slight run and get aboard successfully (providing, of course, the aircraft was in a fairly steady hover). Approaches from any other angle appear to be unsatisfactory. No maintenance or checks could be made on the aircraft by ground personnel while it was hovering at 2 to 5 feet wheel height.

"During the 150-foot hover with the horse collar extended about 50 feet below the aircraft, approach to a position directly underneath was easily accomplished. Downwash turbulence could be felt but nothing severe enough to knock a man off his feet. This was true from any direction. The least turbulent approach was made directly along the wing looking straight up into the exhaust pipes and possibly slightly forward. If approach was made further aft of this, moderate turbulence could be felt. Directly underneath the aircraft, a "calm" area was encountered. Normal movements could readily be made in this area.

"During the 100-foot hover, downwash characteristics were very similar to the 150-foot hover except more pronounced. Approach from aft was difficult, but possible. The best approach again was found to be along the wing slightly forward of the exhaust pipes. The "calm" area was still present but very small and hard to stay in since it varied in locations. If I tended to get too far forward, I would tend to be blown forward; if I got too far aft, I would tend to be blown aft. Turbulence tending to blow me either forward or aft was encountered during approach and departure along the wing. Certain tasks could be performed in this environment, but with difficulty.

"During hover at about 65 feet, approach was more difficult but still possible. I was able to get directly underneath the aircraft and believe I could have gotten aboard a horse collar or rescue hook. While in this

position, the horse collar was still about 10 feet above me and appeared fairly stable. It did move from side to side, but I believe this was due to some mild translations performed by the pilot. As I departed from about 45° aft (4 o'clock position), I planned to circle the aircraft and approach from the front. However, at that time the pilot decided to make a precautionary landing due to the gearcase oil caution light. As the aircraft descended below an estimated 50 feet, with the horse collar in close proximity to the ground, sporadic oscillations by the horse collar commenced. The aircraft continued a slow descent while the crew members very slowly reeled in the dummy. As the aircraft moved forward slightly, the horse collar whipped forward and started flailing around quite violently until it finally swung forward and upward hitting what appeared to be the upper portion of the windshield. At this point it was rapidly hand pulled into the aircraft by the crew instead of using the inefficient, slow, hand-operated winch.

"After the dummy was attached to the aircraft, an unsuccessful attempt was made to turn on the telemetering equipment and calibrate it. The dummy test was continued without telemetering by establishing a hover at about 100 feet. As the dummy was lowered 50 to 60 feet, it was very stable and remained so throughout the aircraft's descent to about 60 feet. I approached underneath the aircraft with some mild difficulty as it was descending. I then varied my position in order to grab onto the dummy. This was accomplished without too much difficulty. No static electrical discharge was felt upon first contacting the dummy. Actually holding onto "him" resulted in a somewhat stabilizing effect for both of "us." At this point, the aircraft climbed to about 75 feet and started a conversion to forward flight (35/30).

"During all three low passes at 35/60 (50 feet), 50/60 (40 feet), and 35/60 (30 feet), no downwash effect was noted until after the aircraft had completely passed by. The effect on all three passes was very mild and would not restrict any movement or prevent running along on the same ground path as the aircraft. It appeared that more downwash effect was noted away from the center line of the aircraft as it passed overhead. This could be seen by small dust clouds building up on the ground outboard of the wing tips, and by the effects on a cameraman occupying this relative position during two of the flybys. Further testing should be conducted to determine the feasibility of a "snatch" pick up using this slow flyby method.

"Generally, the ground environment during hover at 50 feet, or above, was difficult but satisfactory. This situation could completely change without protective goggles and/or hover over a nonstabilized surface. For full evaluation of rescue mission capability of the XC-142A, further testing is required. In my opinion, this test showed that rescue of a human is feasible from the hover mode and could be possible from the STOL mode. The practicality of any of these methods should be determined."

Comments by Jeep Operator (Major J. R. Wing) During Propeller Slipstream-Downwash Evaluation

"Attempts were made to approach the XC-142A from directions in the 3 o'clock to 6 o'clock quadrant (all directions referenced to aircraft) while the aircraft was hovering at each test altitude. In general, downwash increased in intensity as the hover altitudes decreased. In addition, the downwash was greatest when the jeep approached the aircraft from the 6 o'clock direction.

"5-Foot Hover. The jeep was driven to a position approximately 150 feet aft of the tailprop in the 6 o'clock direction. A great deal of debris was blown against the jeep windshield, which probably would have been damaged had the vehicle been driven any closer to the aircraft.

"From the 3 o'clock direction, the jeep was driven to a position approximately 50 feet from the wing tip. The jeep was stopped when the engine hood began to vibrate excessively. The jeep was driven to within 75 feet of the aircraft from the 4:30 o'clock direction. Again the hood began to vibrate excessively, and the jeep was stopped.

"200- and 100-Foot Hovers. The jeep was driven to within approximately 50 feet of the aircraft from the 3:00, 4:30, and 6:00 o'clock directions. It appeared that the jeep could have been driven to a position directly under the aircraft from each direction without sustaining any damage. For safety reasons, however, this was not attempted.

"50-Foot Hover. The jeep was driven to a position approximately 100 feet aft of the tail propeller from the 6:00 o'clock direction. Once again, debris was blown against the windshield and no attempt was made to drive any closer to the aircraft. From the 3:00 o'clock direction, the jeep was driven to a position approximately 25 feet from the wing tip before the hood began to vibrate excessively. The jeep was driven to within 50 feet of the aircraft from the 4:30 direction and the engine stalled at that point."

Comments by Helicopter Pilot (Capt. L. E. Otto, USAF) During Propeller Slipstream-Downwash Evaluation

"Hover Turbulence. Investigation of disturbances in the air caused by the XC-142A to the H-21 were not apparent in hover. The H-21 was flown about 200 feet from the XC-142A in sideward flight and its flight path inscribed a circle about the hovering XC-142A.

"Wake Turbulence. Wake turbulence was investigated upon return from South Base to Taxiway 5. The H-21 initiated the investigation by flying about 5° above and 200 to 300 feet behind the XC-142A and making successive cross-overs gradually lowering from 5° to 0° above the XC-142A.

Little disturbance was noted until 0° was reached. At this time it appeared that the helicopter entered an area of slight suck-down (calm) which was followed by moderate to severe turbulence longitudinally.

"Hoist Observation. The hoist line was extended to 50 feet with the horse collar only while the XC-142A hovered at 200 feet. Stability of the line during extension was excellent. There appeared to be some tendency for the collar and line to shift toward the downwash of the props - perhaps 2° to 5° . This appeared to be true for all until the sling was about 25 feet off the ground. At this point the downwash flow deflected horizontal by the ground caused the sling to oscillate forward. As the XC-142A reeled in the line and prepared for a precautionary landing, the line and sling went almost horizontal when the XC-142A was at a 15- to 25-foot hover. It finally went divergent when approximately 30 feet of the line remained and the sling flipped up and back striking the pilot's windshield. After touchdown the dummy was attached and the hover investigation was again initiated at 100 feet. The dummy was again very stable as the hover altitude was decreased until the dummy was 10 to 15 feet above the ground. At this time the horizontal airflow caused the dummy to start oscillating. This tendency increased as the dummy got closer to the ground. The line and dummy were drawn into the downwash initially 1° to 3° and the tendency disappeared as the dummy felt the ground effects. The various wing angle work was extremely impressive. The dummy was very stable. At the higher airspeed about 40 knots, the maximum line deflection was 10° to 15° . A line instability was noted in the mode of vibration where the amplitude was an estimated 3 feet at about 40 knots. This quickly damped out.

"The low passes made over Major Larsen caused him little difficulty. The downwash velocity appeared very low.

"I was highly impressed by the stability of the dummy in all modes with the exception of the less than 10 feet above the ground with a 60-foot hover height of the XC-142A.

"I strongly recommend the XC-142A utilize conventional size rescue cable and longer cable lengths with associated higher hover altitudes to further investigate the ground effect stability of the sling and dummy."

APPENDIX II

ROOT LOCUS ANALYSIS (0/30 CONFIGURATION)

If the cargo extracting dynamics are considered as an input, a root locus analysis can be made to examine the stability of the response. However, it must be assumed that the input to the airframe, pilot, and SAS combination is such that the system stops are not encountered at any time. If stops are encountered, the system becomes nonlinear and root locus analysis is not applicable.

The configuration selected to be analyzed was 0° wing incidence, 30° flap setting, 31,300 pounds gross weight, and 21.6% MGC center of gravity. The parameters varied on the root locus plot are $K_{p\theta}$, the pilot gain, and K_q , the SAS pitch rate gain.

Figure 8 presents a functional diagram which can be used to obtain a mathematical model for the system. After denoting the output of the feel isolation actuator as δ^*_{pilot} , the output of the scissors linkage gain as δ^*_{stab} , the input to SAS actuator as δ^*_1 , and the output of the actuator as δ^* , five equations can be obtained.

$$\delta_{\text{STK}} = \frac{K_{p\theta} e^{-\tau_D s} (\tau_L s + 1)}{(\tau_I s + 1)} \theta_e$$

$$\delta^*_1 = (K_q s + K_\theta) \theta + K_{\delta_{\text{STK}}} \delta_{\text{STK}}$$

$$\delta^*_{\text{pilot}} = \frac{K_L 15}{s + 15} \delta_{\text{STK}}$$

$$\delta^*_{\text{stab}} = \frac{K_S 21.5}{s + 21.5} \delta^*_1$$

$$\delta^* = \frac{20}{s + 20} (\delta^*_{\text{stab}} + \delta^*_{\text{pilot}})$$

Replacing the pilot transport lag, $e^{-\tau_D s}$, by a standard third order lag approximation,

$$e^{-\tau_D s} \approx \frac{1}{(1 + .6\tau_D s)(1 + .4\tau_D s + .16\tau_D^2 s^2)}$$

and eliminating δ_{STK}^* , δ_{stab}^* , δ_{pilot}^* , and δ_1^* from the above equations results in an expression for δ^* in terms of pitch attitude, θ . This expression is of the form

$$\frac{\delta^*}{\theta} = \frac{K_{P\theta} F_1(S) + F_2(S)}{F_3(S)}$$

and the characteristic equation for the entire linear system becomes the following:

$$G(S) = \begin{vmatrix} S - X_u & -X_w & w_0 S + g & -X_{\delta^*} \\ -Z_u & S - Z_w & (-U_0 - Z_q)S & -Z_{\delta^*} \\ -M_u & -M_w S - M_{\dot{w}} & (S^2 - M_q S) & -M_{\delta^*} \\ 0 & 0 & K_{P\theta} F_1(S) + F_2(S) & -F_3(S) \end{vmatrix} = 0$$

Expansion of the determinant and some more algebra finally results in an equation of the form suitable for factoring by the root locus method of W. R. Evans.

$$-1 = \frac{K_{P\theta} F_4(S)}{F_5(S)}$$

In the pilot gain study, four plots of two pages each have been made, the first page showing all the modes and the second page showing an enlargement of the low-frequency modes. Varying from plot to plot are the pilots' time constants τ_L and τ_I . In Figure 55, $\tau_L = 1.0$ second and $\tau_I = .5$ second, and the troublesome mode goes unstable at a pilot gain, $K_{P\theta} = -55.7$. In Figure 56, τ_L has been increased to 1.5 seconds, making the pilot generate more lead while driving the system unstable at $K_{P\theta} = -37.0$. In Figure 57, $\tau_L = \tau_I = 0.5$ second, and the critical pilot gain is $K_{P\theta} = -92.6$. In Figure 58, $\tau_L = 0.5$ second, and $\tau_I = 1.0$ second, and the critical pilot gain is $K_{P\theta} = -146.1$.

The effect of varying the SAS pitch rate gain with the pilot removed from the system is shown in Figure 59. At nominal $K_q = -11.38$, the period of oscillation indicated in Figure 59 is about 0.75 second, which is in agreement with the period estimated from flight test records on this configuration (see Figure 47). It appears that the damping ratio indicated in Figure 59 is higher than the flight test value. One way to bring the two values into agreement would be to increase the time constants associated with the UHT actuator and the SAS actuator. This would shift the troublesome mode in Figure 59 toward the right, thereby reducing the theoretical damping ratio. To stiffen the airplane response in the 0/30 configuration, SAS on, with the pilot out, this analysis indicates that a reduction in K_q is appropriate.

$I_w/\delta_F = 0/30$, GROSS WEIGHT = 31,300 POUNDS, CG = 21.6% MGC

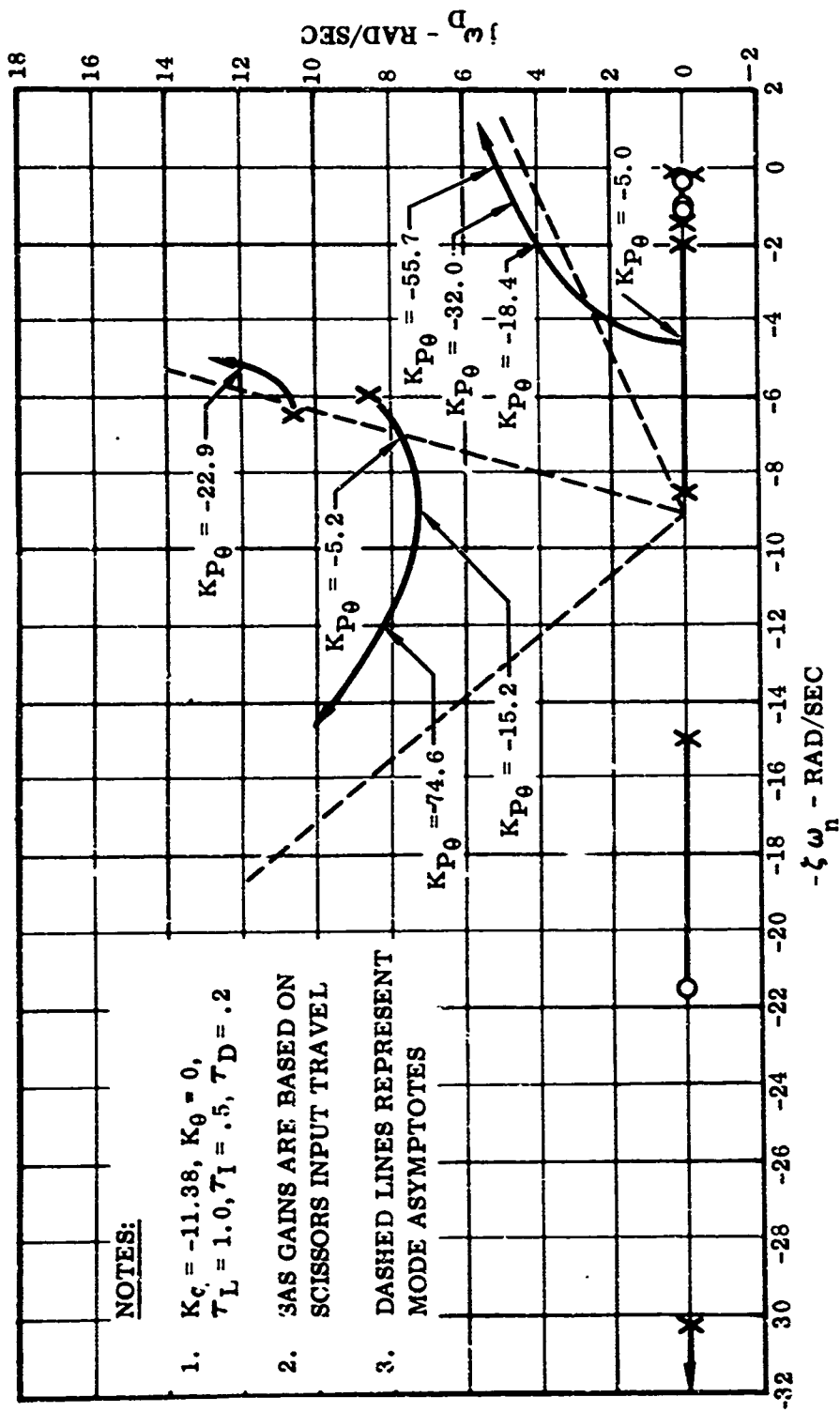


Figure 55. XC-142A Response Modes Versus Pilot Gain,
 $I_w/\delta_F = 0/30$, $T_L = 1.0$, $T_I = .5$, $T_D = .2$

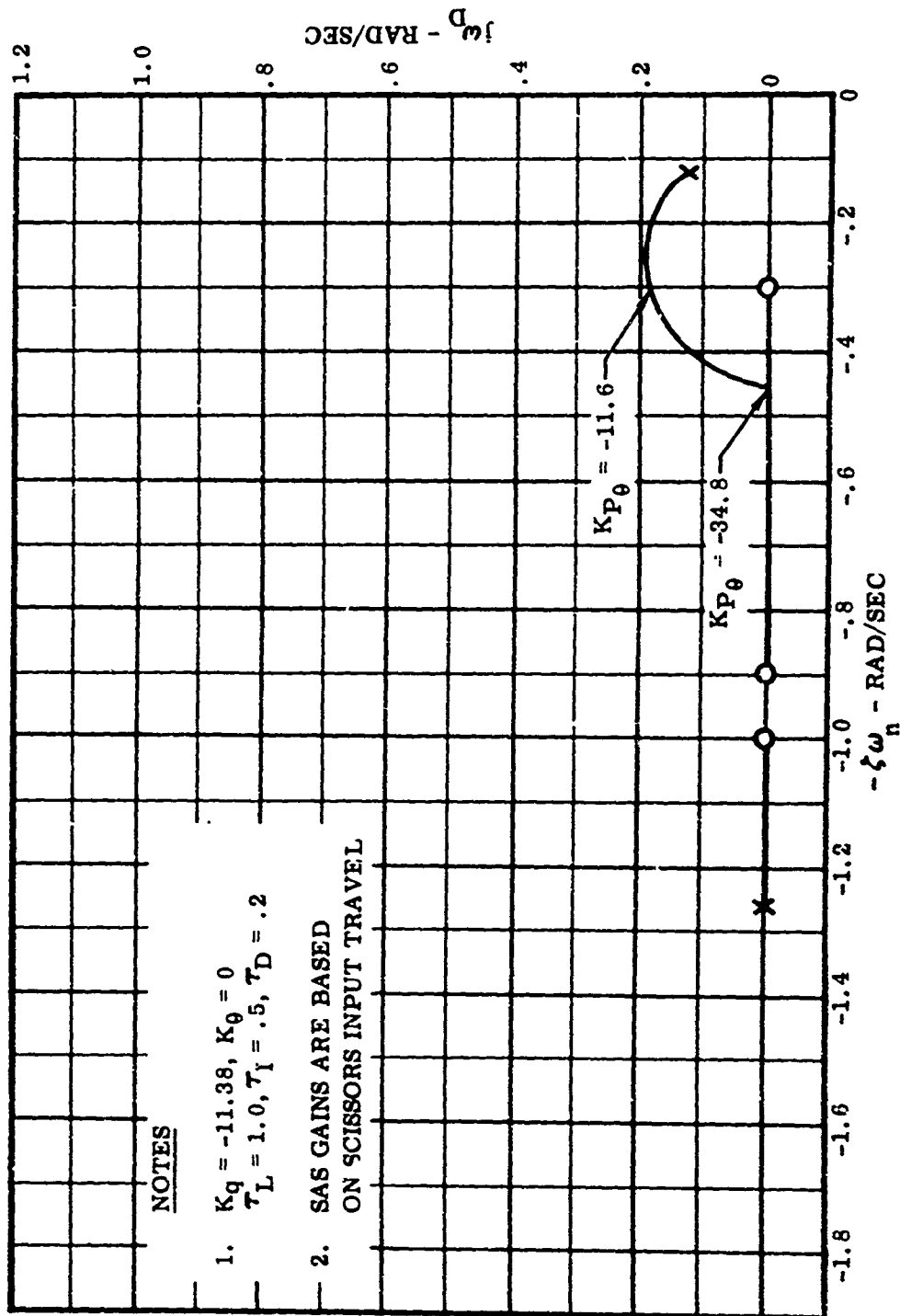


Figure 55. KC-142A Response Modes Versus Pilot Gain, $\tau_w/\delta_F = 0/30, \tau_L = 1.0, \tau_I = .5, \tau_D = .2$ (Concluded)

$i_w/\delta_F = 0/30$, GROSS WEIGHT = 31,300 POUNDS, CG = 21.6 % MGC

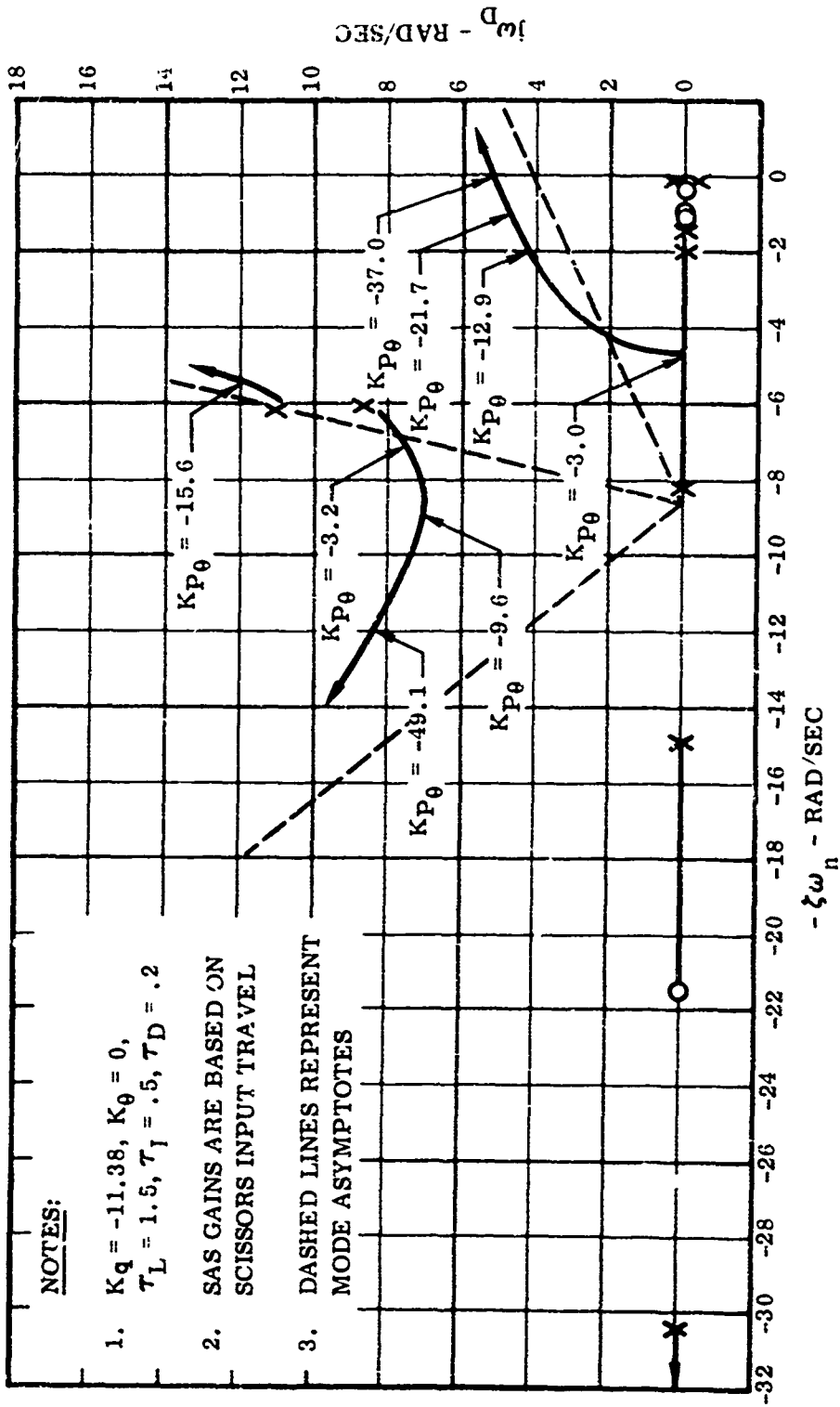
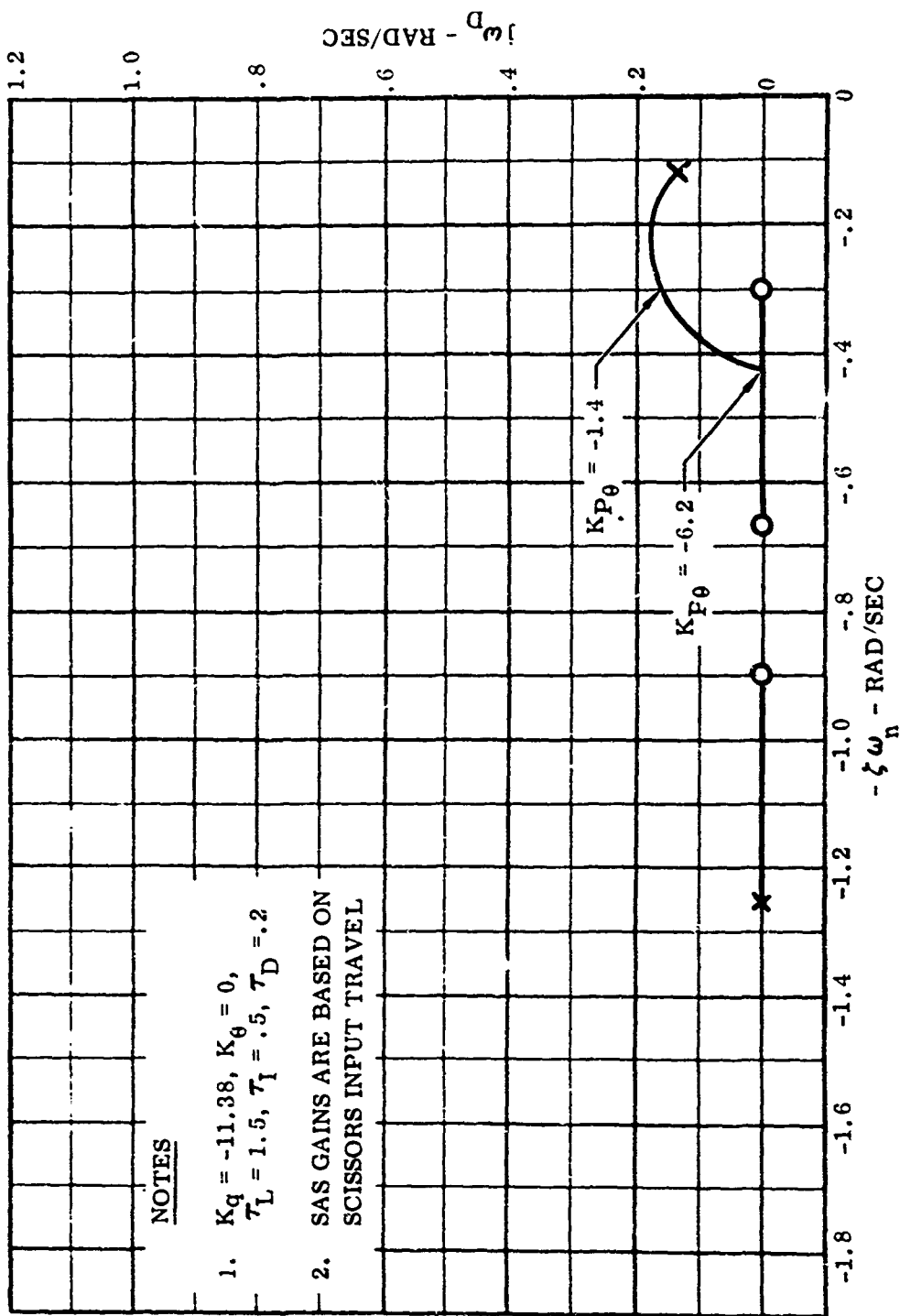


Figure 56. XC-142A Response Modes Versus Pilot Gain
 $i_w/\delta_F = 0/30$, $\tau_L = 1.5$, $\tau_I = .5$, $\tau_D = .2$

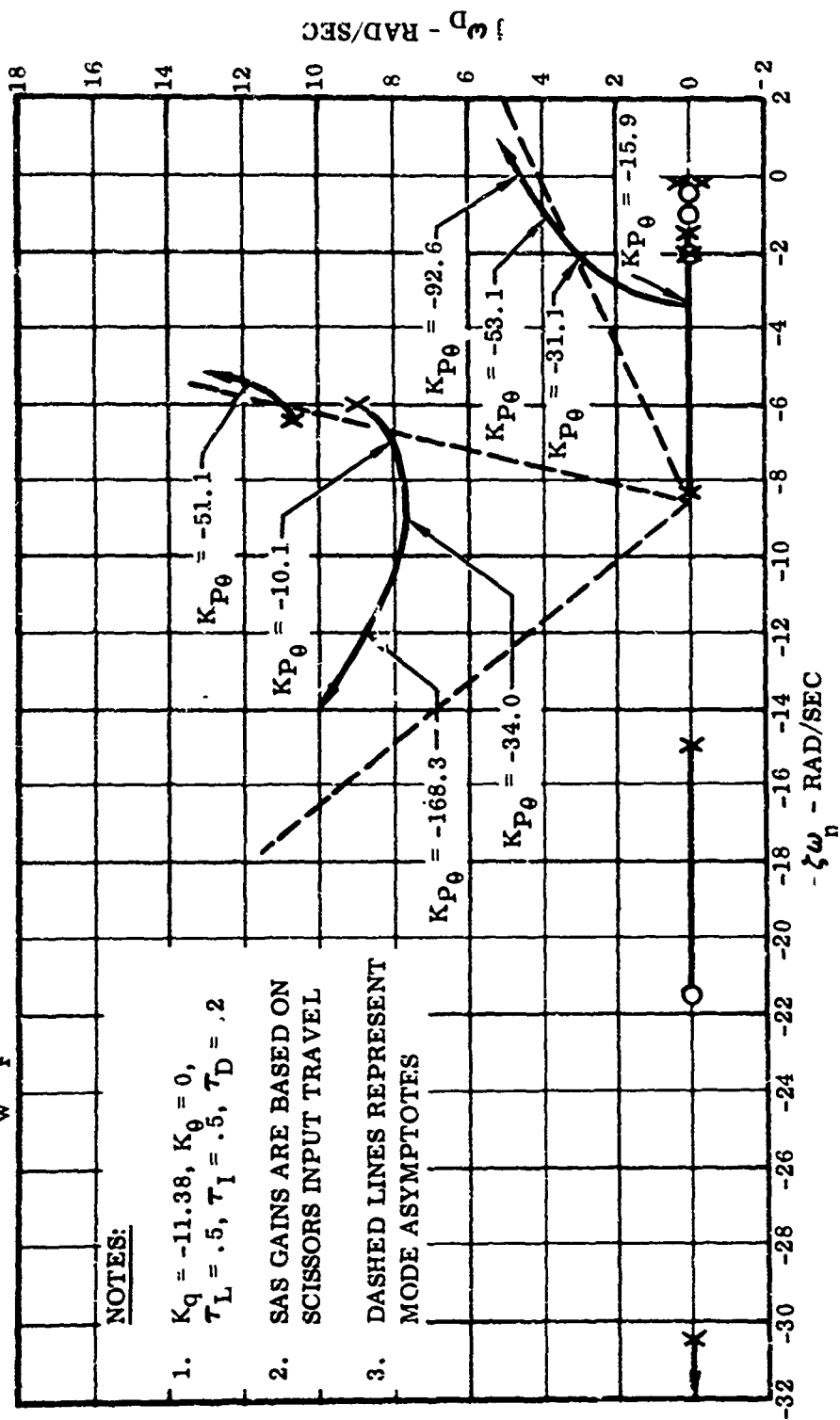


NOTES

1. $K_q = -11.38$, $K_\theta = 0$,
 $\tau_L = 1.5$, $\tau_I = .5$, $\tau_D = .2$
2. SAS GAINS ARE BASED ON
 SCISSORS INPUT TRAVEL

Figure 56. IC-142A Response Modes Versus Pilot Gain, $\tau_L = 1.5$, $\tau_I = .5$, $\tau_D = .2$ (Concluded)

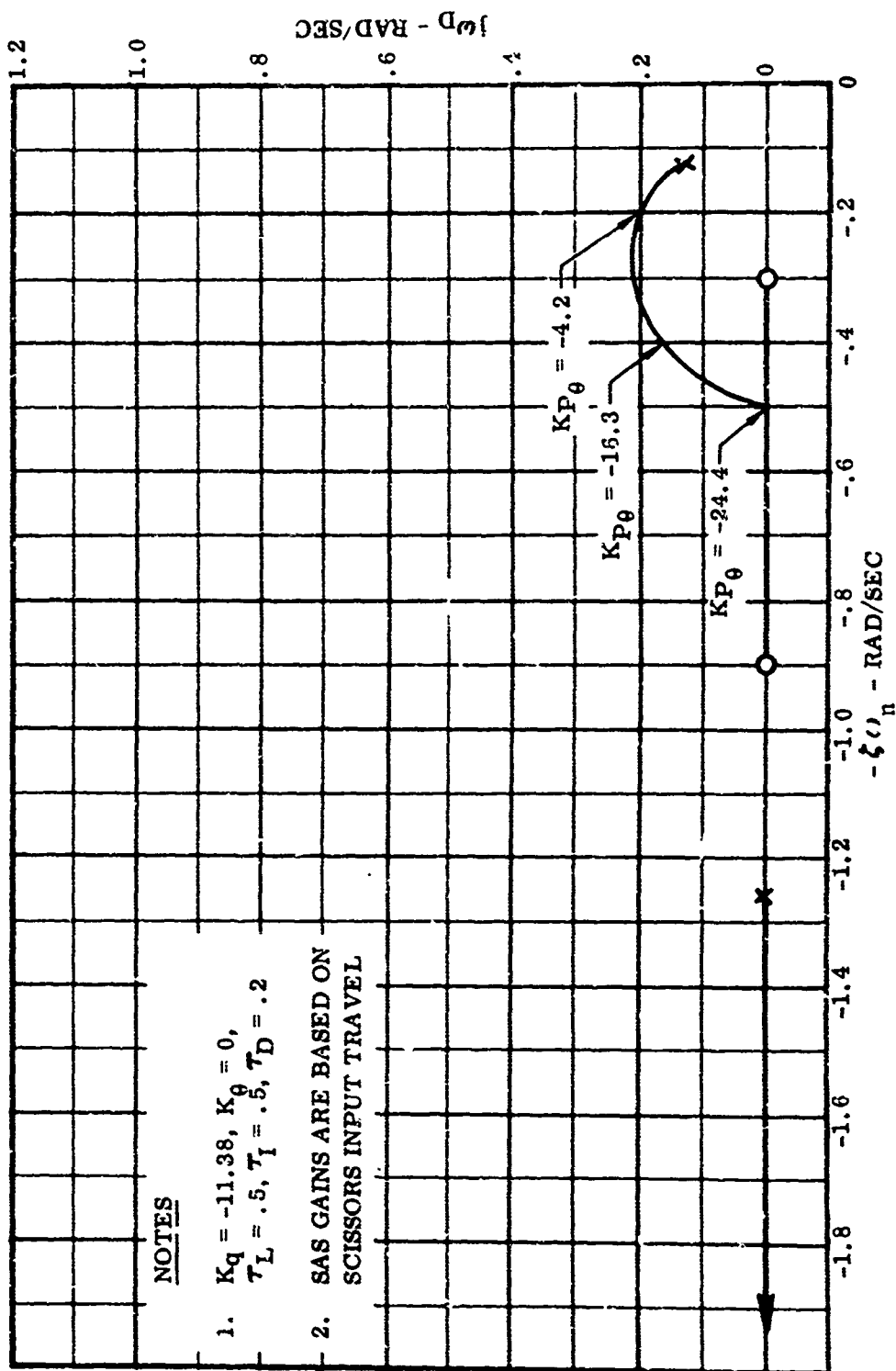
$I_w/\delta_F = 0/30$ GROSS WEIGHT = 31,300 POUNDS CG = 21.6 % MGC



NOTES:

1. $K_q = -11.38$, $K_{\theta} = 0$, $\tau_L = .5$, $\tau_I = .5$, $\tau_D = .2$
2. SAS GAINS ARE BASED ON SCISSORS INPUT TRAVEL
3. DASHED LINES REPRESENT MODE ASYMPTOTES

Figure 57. XC-142A Response Modes Versus Pilot Gain, $I_w/\delta_F = 0/30$, $\tau_L = .5$, $\tau_I = .5$, $\tau_D = .2$



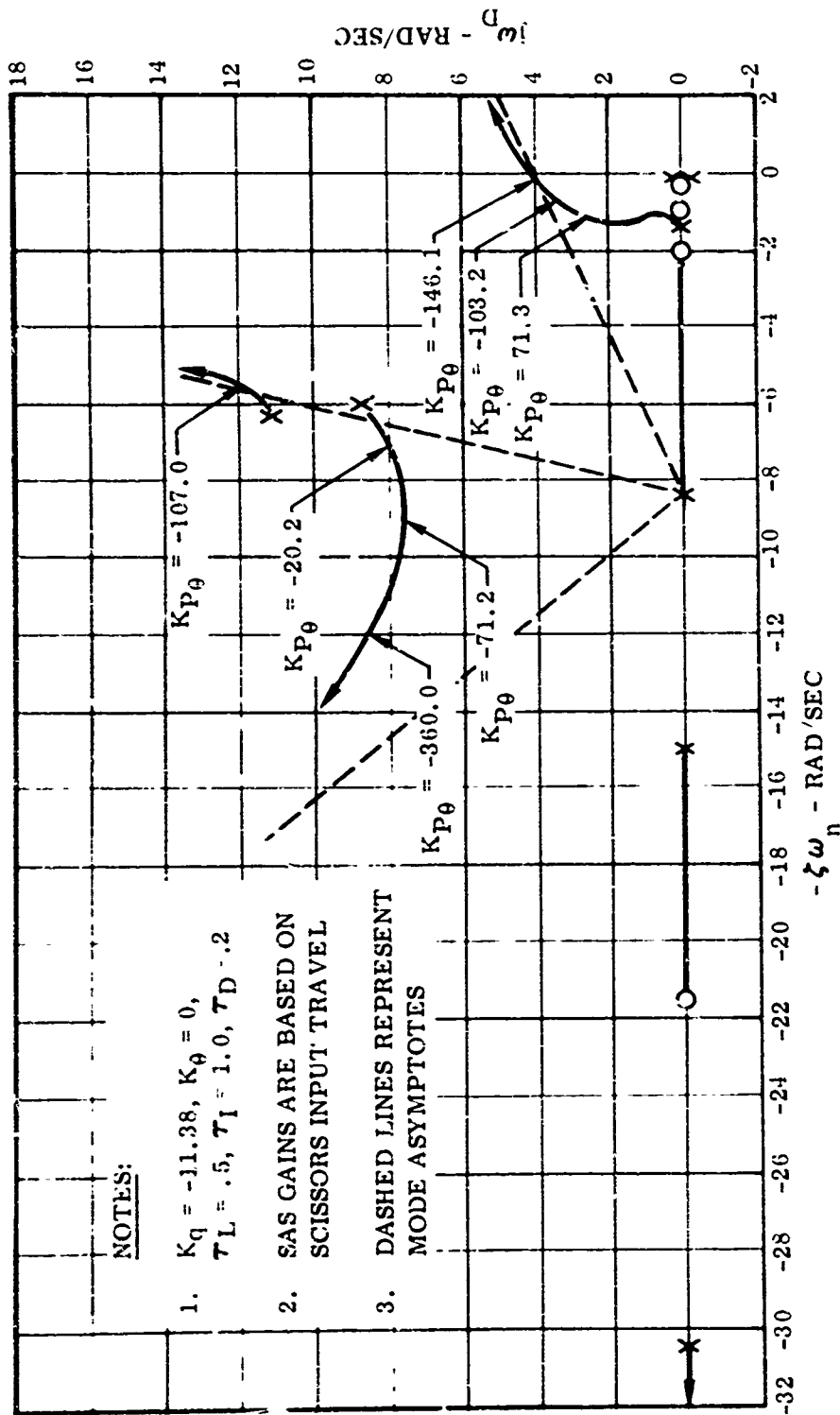
NOTES

1. $K_q = -11.38$, $K_{\theta} = 0$,
 $\tau_L = .5$, $\tau_I = .5$, $\tau_D = .2$

2. SAS GAINS ARE BASED ON
 SCISSORS INPUT TRAVEL

**Figure 57. IC-142A Response Modes Versus Pilot Gain,
 $\tau_w/\delta_F = 0/30$, $\tau_L = .5$, $\tau_I = .5$, $\tau_D = .2$ (Concluded)**

$i_w/\delta_F = 0/30$, GROSS WEIGHT = 31,300 POUNDS, CG = 21.6% MGC



NOTES:

1. $K_q = -11.38$, $K_\theta = 0$,
 $\tau_L = .5$, $\tau_I = 1.0$, $\tau_D = .2$
2. SAS GAINS ARE BASED ON
SCISSORS INPUT TRAVEL
3. DASHED LINES REPRESENT
MODE ASYMPTOTES

Figure 58. XC-142A Response Modes Versus Pilot Gain,
 $i_w/\delta_F = 0/30$, $\tau_L = .5$, $\tau_I = 1.0$, $\tau_D = .2$

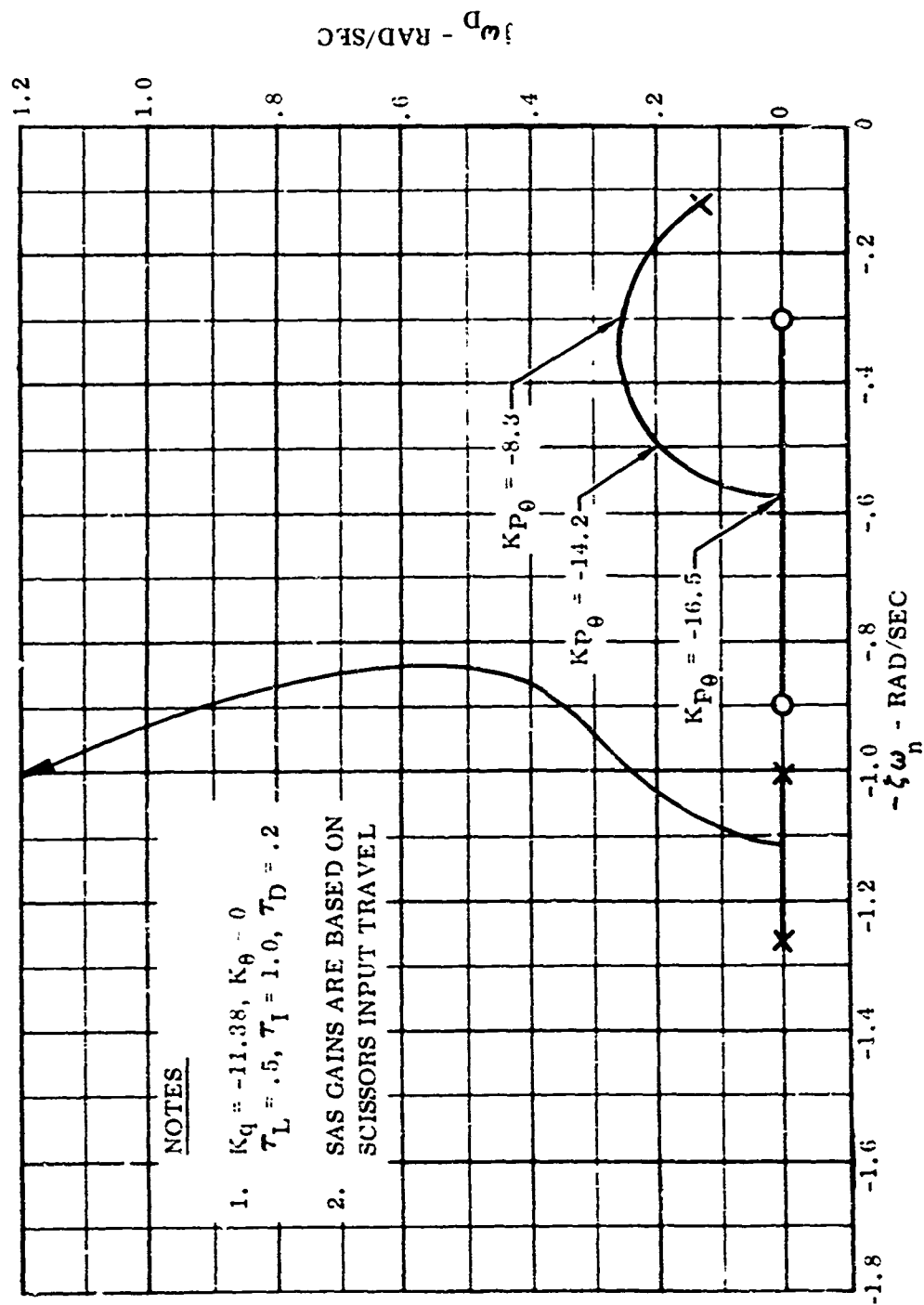


Figure 58. XC-142A Response Modes Versus Pilot Gain,
 $i_w/\delta_F = 0/30$, $\tau_L = .5$, $\tau_I = 1.0$, $\tau_D = .2$ (Concluded)

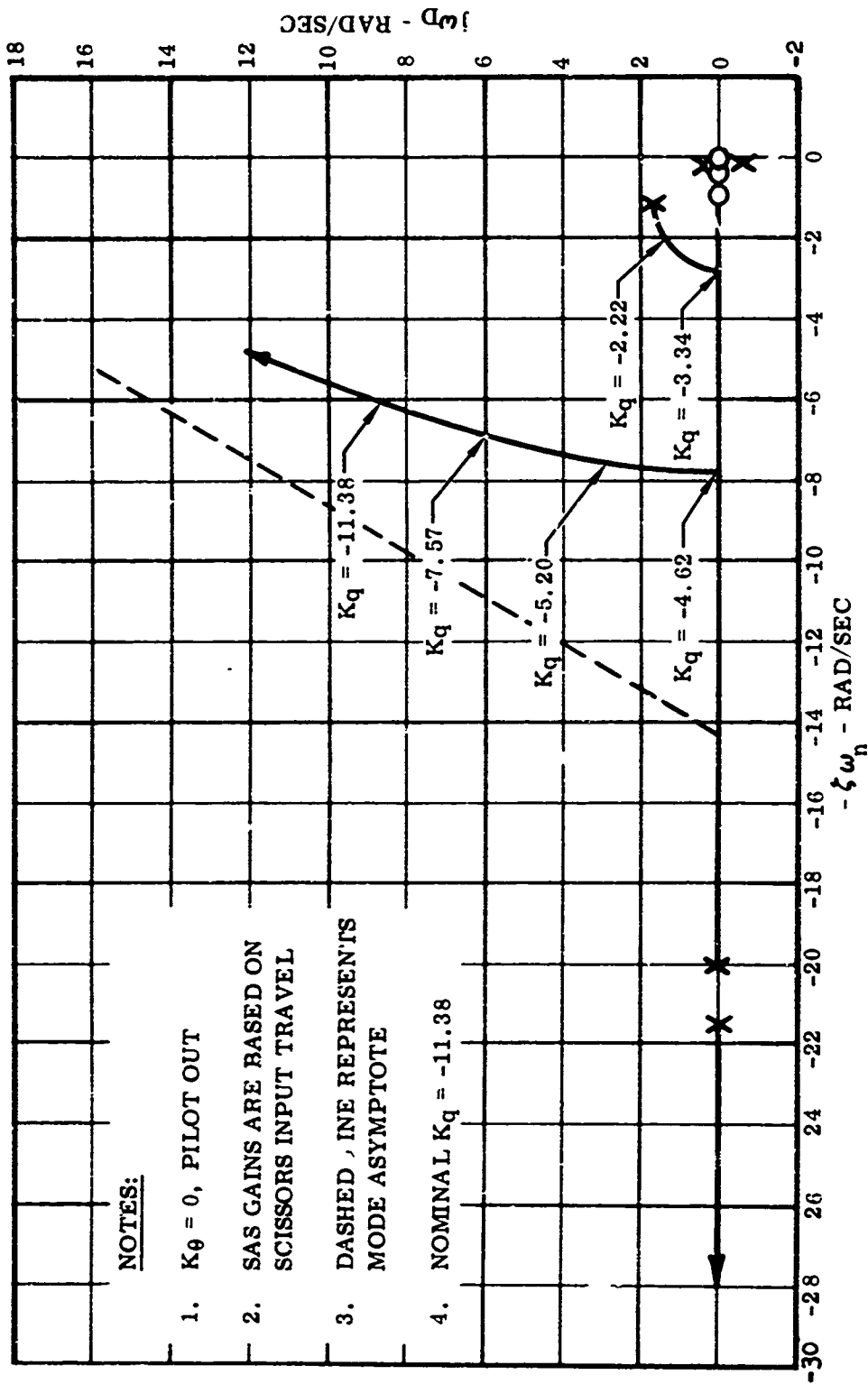


Figure 59. XC-142 Response Modes Versus SAS Pitch Rate Gain, $1/\delta_F = 0/30$, Pilot Out

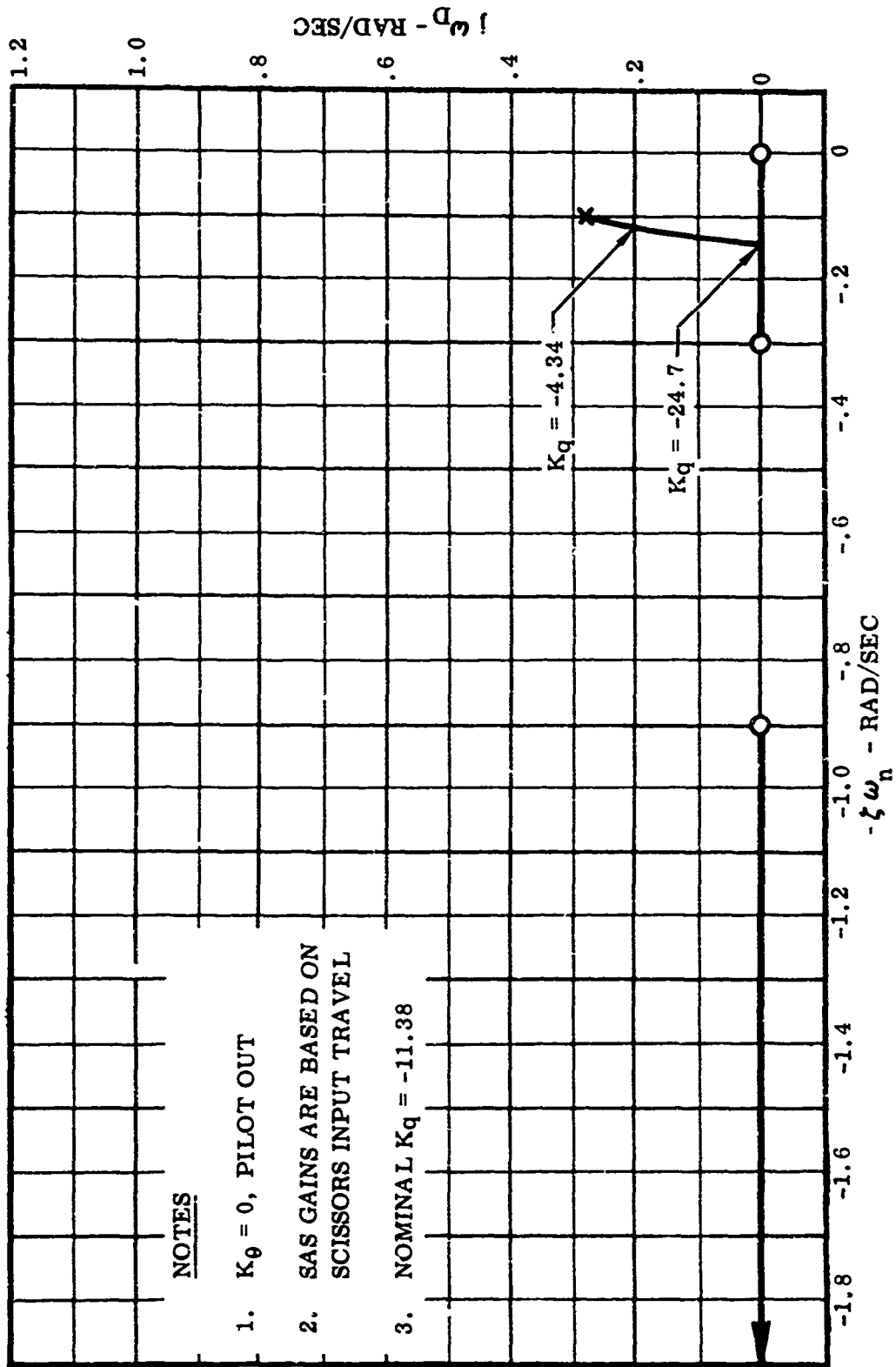


Figure 59. XC-142 Response Modes Versus SAS Pitch Rate Gain, $i_w/\delta_F=0/30$, Pilot Out (Concluded)

A root locus with the pilot out has just been compared with flight test data with the pilot in. Justification for this stems from an examination of the longitudinal stick position trace on the flight test data which shows that the pilot holds the stick essentially constant after the cargo leaves.

Noting the trend on the pilot in plots, it appears that a "laggy" pilot will perform better from the standpoint of stability than will a pilot with a high lead time constant. However, data from the analog simulation runs show that increasing the pilot's lead time constant helps to reduce the initial pitch-up due to the cargo extraction. As is intuitively expected, an increase in pilot gain is stabilizing up to a point where further increases become destabilizing. Figure 60 is a summary of the effect of the pilot lead time constant, τ_L , and the pilot gain, Kp_0 , on stability. This figure is a stability boundary for Kp_0 and τ_L .

In drawing conclusions from the above, it must be remembered that there are some objections to the mathematical representation of the pilot used in this analysis. These objections are pointed out in the section devoted to the pilot. In future analyses, perhaps more root locus work should be done on the system with the pilot out, since a variation in the SAS parameters is not as nebulous as a variation in pilot parameters. It should also be remembered that the analysis carried out in the root locus section is not valid for inputs where the SAS stops are encountered.

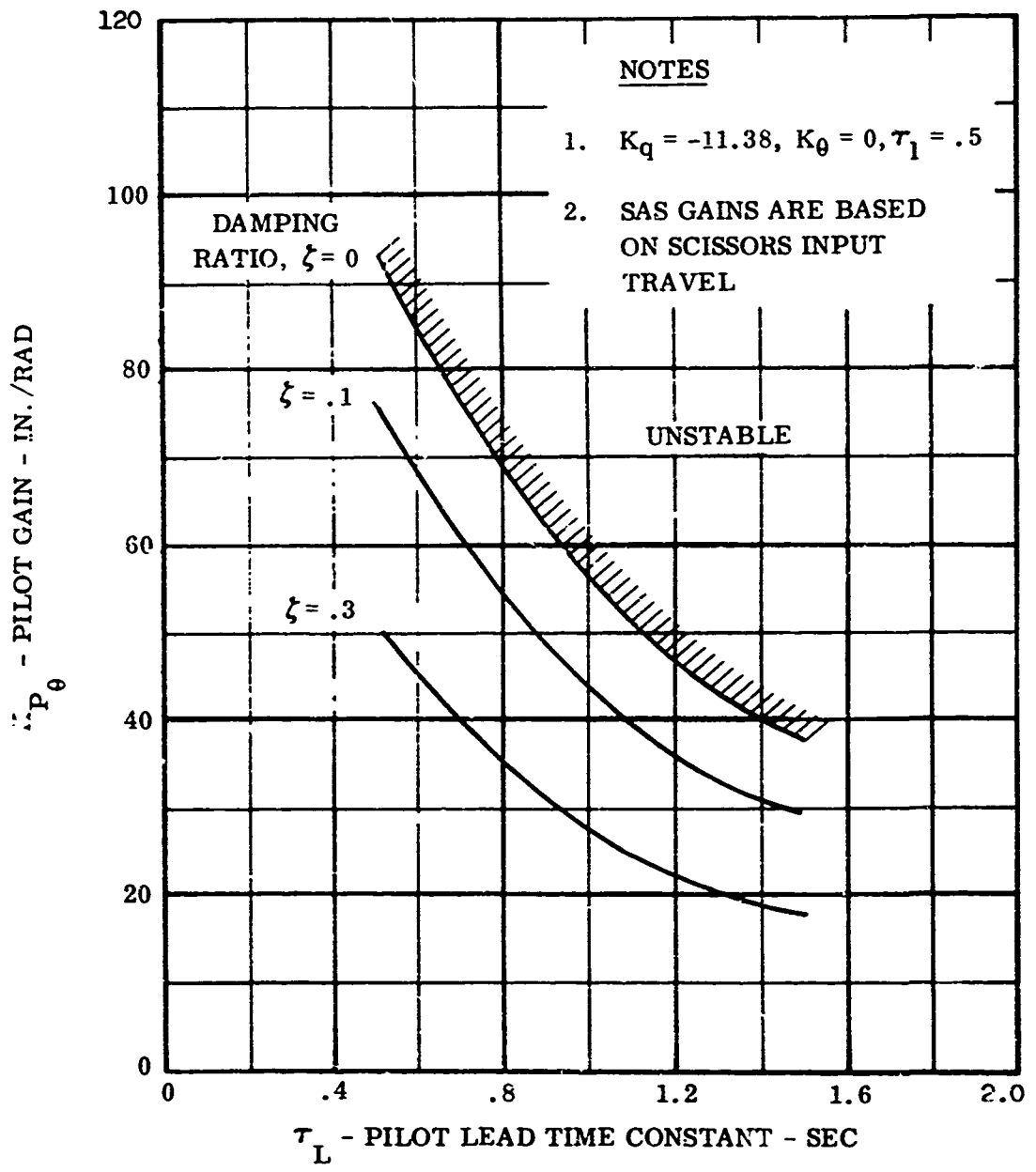


Figure 60. XC-142A Pilot Stability Boundary,
 $i_w/\delta_F=0/30$

APPENDIX III

PHOTOGRAPHS OF THE XC-142A AIRPLANE

AND AIR-DROP DEMONSTRATION

(NO. 4 AIRCRAFT, S.N. 62-5924)



Figure 61. View of Aircraft in Cruise Flight, 0/30 Wing/Flap Configuration



Figure 62. Left-Hand Side View of Aircraft in Static Condition
With the Wing at 90°

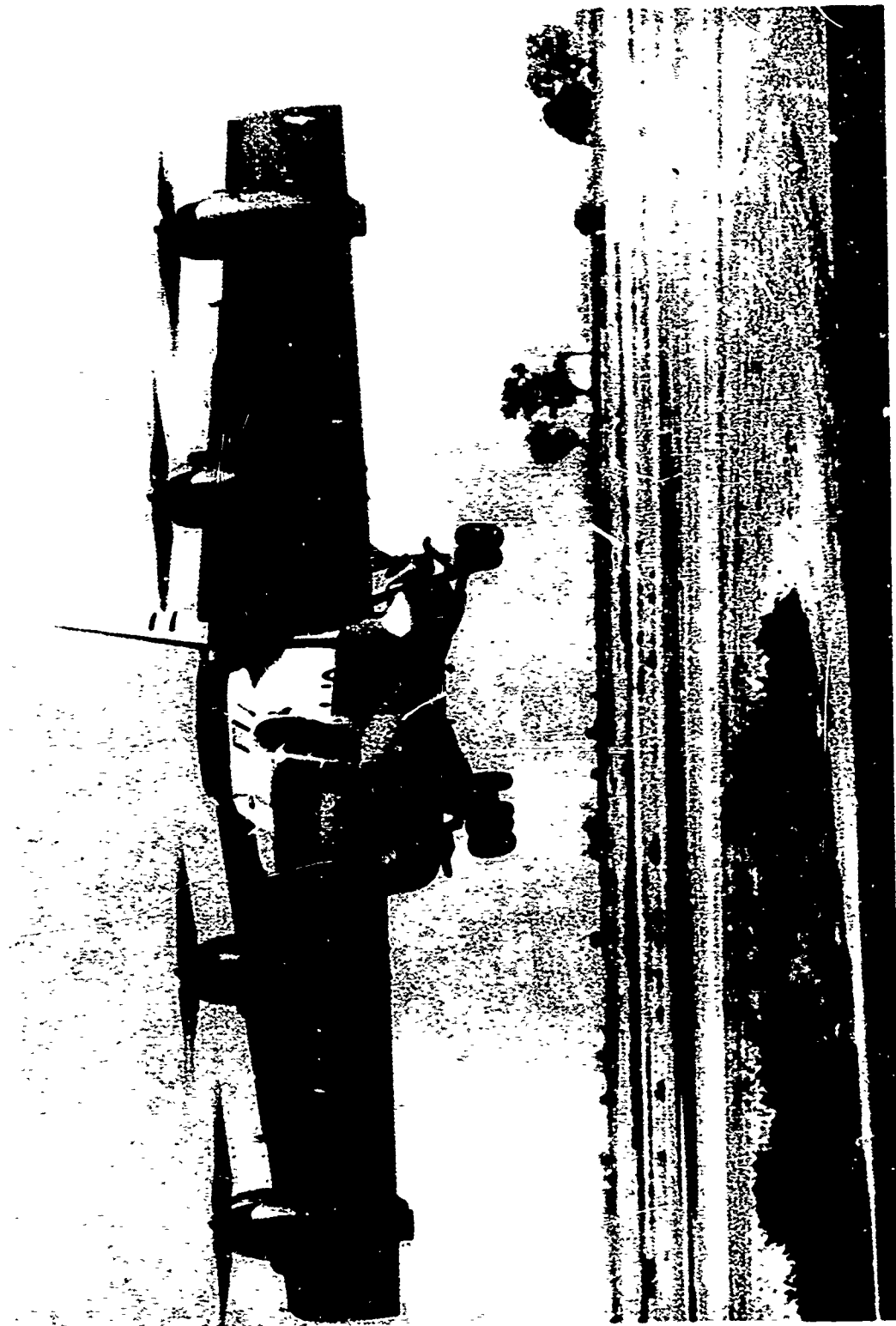


Figure 63. Front View of the Aircraft in Hover Flight with the
Wing at Approximately 90°

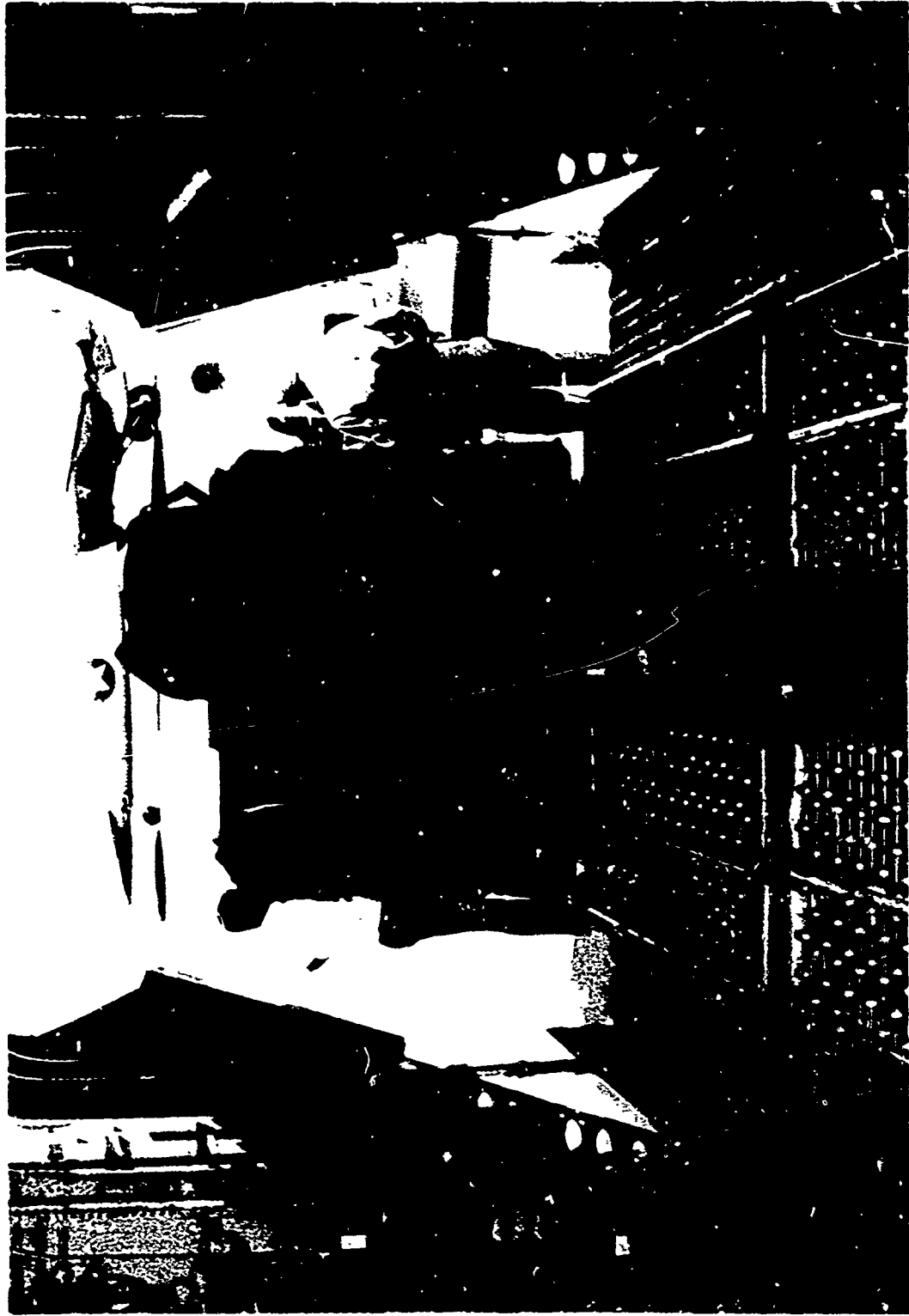


Figure 64. Rearward Looking View of the Cargo Compartment Showing the Skate Wheel Conveyors and an A-22 Container

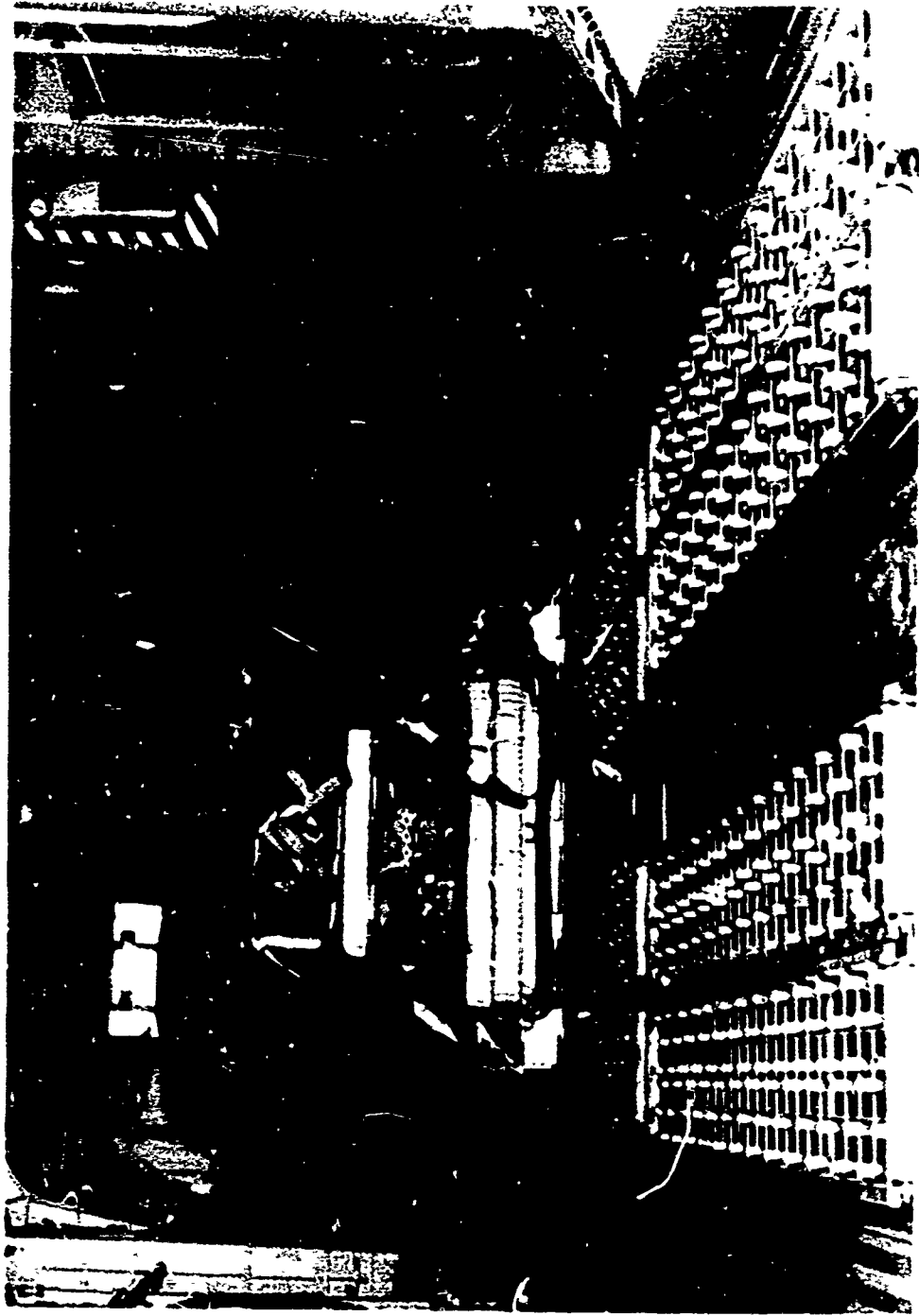


Figure 65. Forward Looking View of the Cargo Compartment Showing the Skate Wheel Conveyors and a Logistics Platform



Figure 66. 500-Pound Gravity Drop - 0/30 Configuration, 5,000 Feet

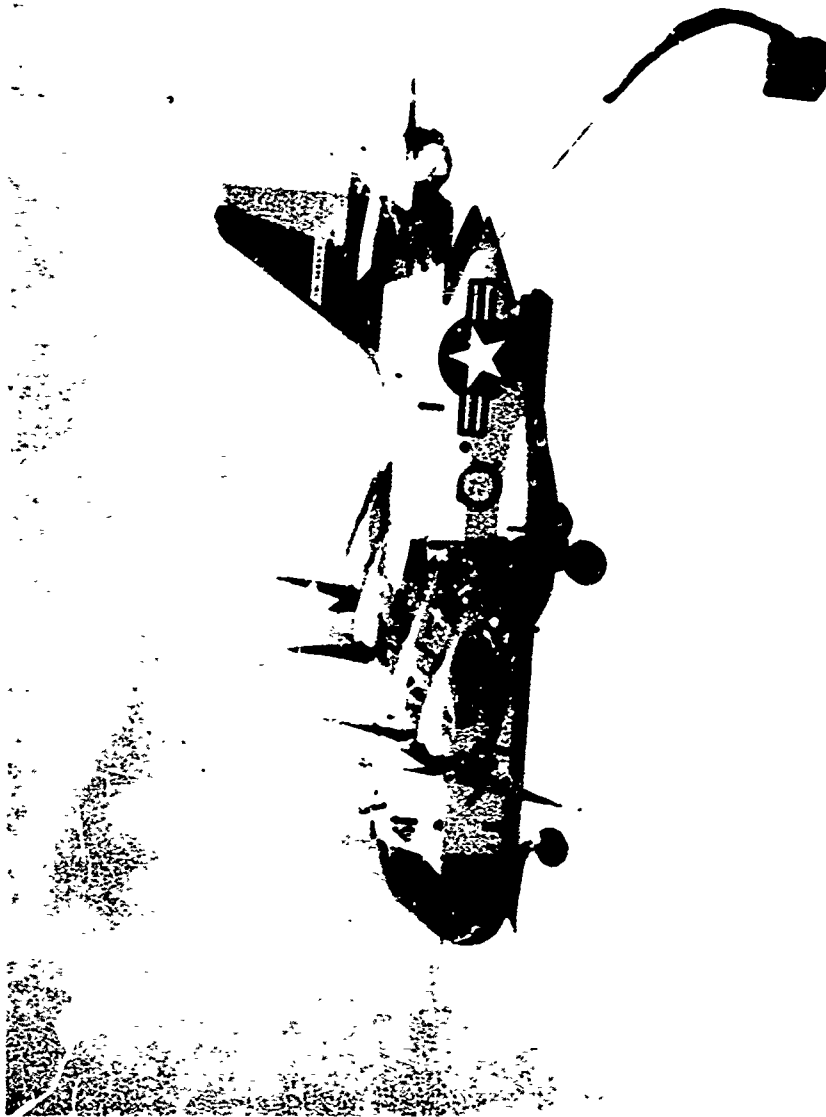


Figure 67. 500-Pound Gravity Drop - 15/60 Configuration, 5,000 Feet

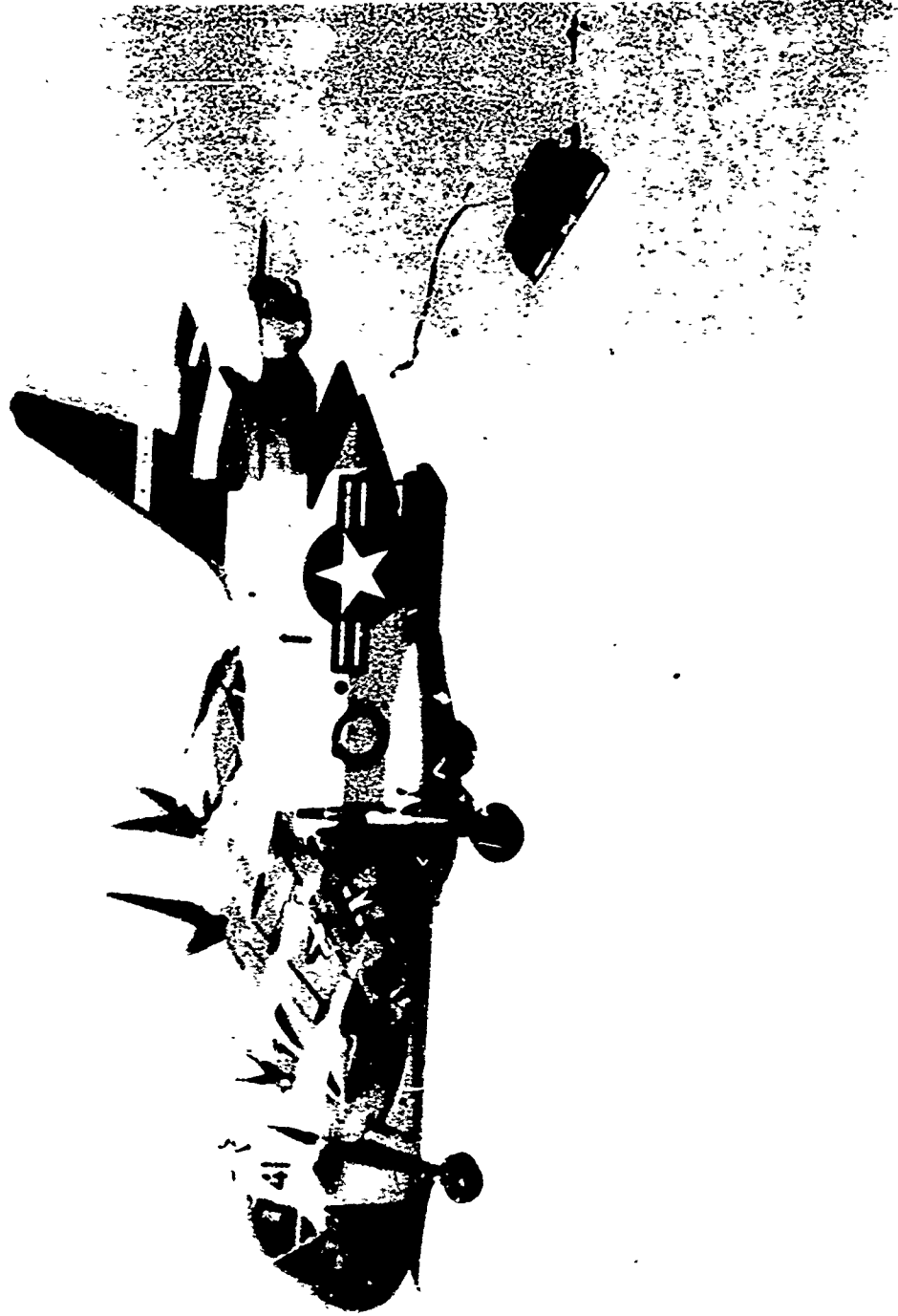


Figure 68. 1,000-Pound Extraction Drop - 15/60 Configuration,
5,000 Feet



Figure 69. Five-Percentile Dummy Drop from Cargo Ramp - 0/30
Configuration, 5,000 Feet

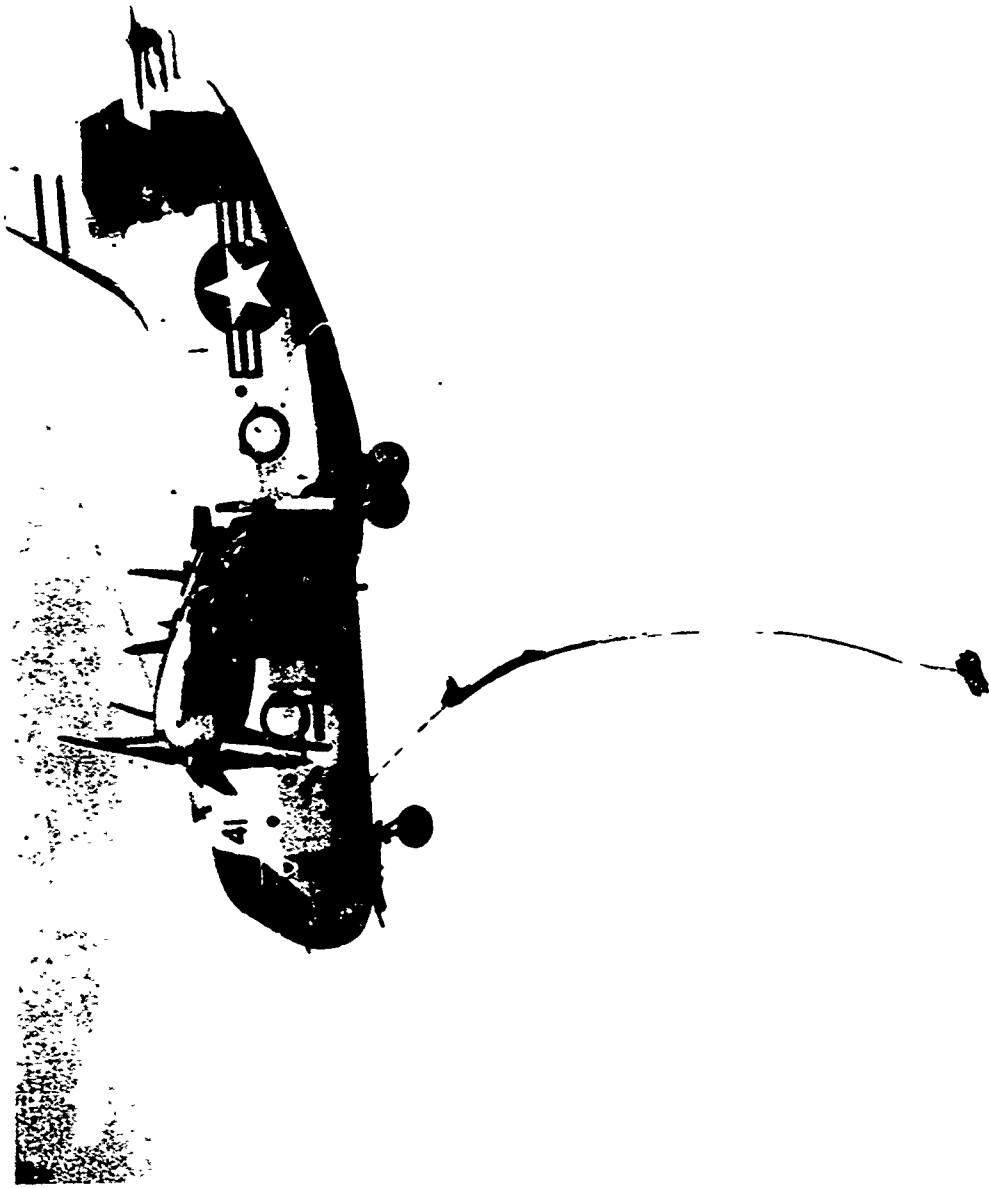


Figure 70. Five-Percentile Dummy Drop from Forward Escape Hatch -
15/60 Configuration, 1,000 Feet

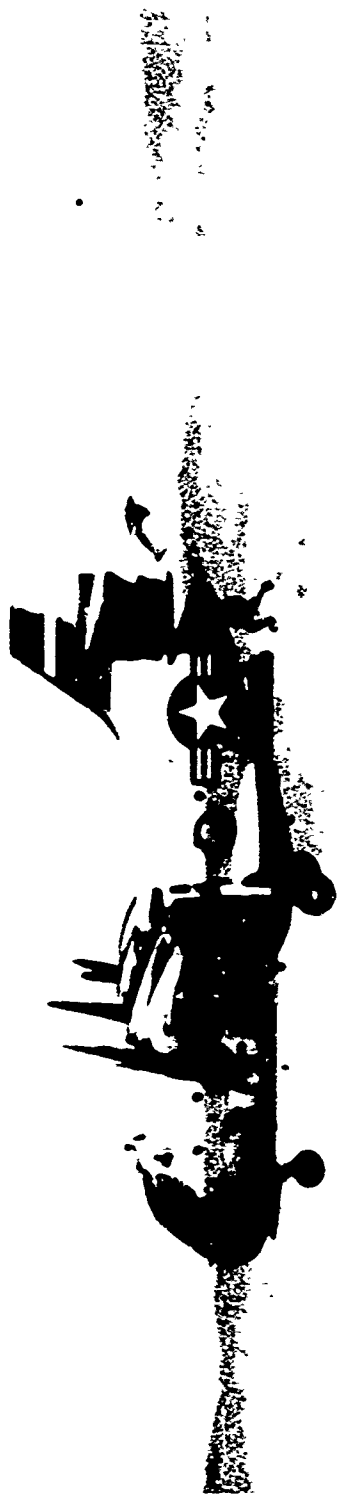


Figure 71. Ten-Man Free Fall Parachute Jump from Cargo Ramp - 15/60
Configuration, 12,500 Feet



Figure 72. 2,000-Pound Dump Truck Drop - 30/60 Configuration



Figure 73. Sequential Drop of Four 500-Pound Cargos - 30/60 Configuration

UNCLASSIFIED

Security Classification

DOCUMENT CONTROL DATA - R & D		
<i>(Security classification of title, body of abstract and indexing annotation must be entered when the overall report is classified)</i>		
1. ORIGINATING ACTIVITY (Corporate author) VOUGHT AERONAUTICS DIVISION LTV AEROSPACE CORPORATION DALLAS, TEXAS		2a. REPORT SECURITY CLASSIFICATION UNCLASSIFIED
		2b. GROUP
3. REPORT TITLE DYNAMIC RESPONSE OF THE XC-142A TILT-WING V/STOL AIRCRAFT TO IN-FLIGHT CARGO DELIVERY AT SLOW SPEEDS		
4. DESCRIPTIVE NOTES (Type of report and inclusive dates) FINAL TECHNICAL REPORT		
5. AUTHOR(S) (First name, middle initial, last name) JERRY W. WILSON MIKE P. SCHIRA J. STEVE DEITERING		
6. REPORT DATE	7a. TOTAL NO. OF PAGES	7b. NO. OF REFS 3
8a. CONTRACT OR GRANT NO. DA 44-177 AMC-327(T)		8b. ORIGINATOR'S REPORT NUMBER(S) USAAVLABS Technical Report 68-4
8c. PROJECT NO. TASK 1F121401A254		8d. OTHER REPORT NO(S) (Any other numbers that may be assigned this report) VAD Report 2-53310/6R-6098
9. DISTRIBUTION STATEMENT This document has been approved for public release; its distribution is unlimited.		
11. SUPPLEMENTARY NOTES		12. SPONSORING MILITARY ACTIVITY U.S. ARMY AVIATION MATERIEL LABORATORIES FORT EUSTIS, VIRGINIA
13. ABSTRACT The potential ability of V/STOL aircraft to perform Army drop missions at various altitudes while flying at speeds from hover to conventional flight could provide a basis for precision in-flight delivery and could overcome major operational restrictions associated with many of the conventional air-drop techniques. This study was partially based on actual air-drop demonstrations at the Naval Air Facility, El Centro, California. Single cargo loads of up to 3,000 pounds were gravity dropped in hover and at 30 knots, and loads of up to 4,000 pounds were extracted by parachute at 127 knots. Using these flight data to set up a realistic simulation, a mathematical model of the XC-142A airplane and a human pilot were used to examine the aircraft's response with cargo weights up to the airplane's maximum payload of 8,000 pounds in the low-speed portion of transition and 12,000 pounds at a 127-knot flight condition. This study shows that the maximum payload could be successfully dropped with proper pilot technique. Means of extending the airplane's air-drop capability through the use of special extraction forces and parameters applicable to the air-drop system have been studied.		

DD FORM 1473

REPLACES DD FORM 1473, 1 JAN 64, WHICH IS
OBSOLETE FOR ARMY USE.

UNCLASSIFIED

Security Classification

UNCLASSIFIED

Security Classification

14. KEY WORDS	LINK A		LINK B		LINK C	
	ROLE	WT	ROLE	WT	ROLE	WT
In Flight Cargo Delivery XC-142A Aerial Delivery Capability V/STOL Aerial Delivery Potential						

UNCLASSIFIED

Security Classification